PhD degree in Molecular Medicine (Curriculum in Molecular Oncology)

European School of Molecular Medicine (SEMM)

University of Milan and University of Naples "Federico II"

Settore disciplinare: Med/04

Role of Ezh2 methyltransferase activity in the maintenance of MYC-driven B cell lymphomas

Valentina Petrocelli

IFOM, Milan

Matricola n. R09858

Supervisor: Dr. Stefano Casola,

IFOM, Milan

Anno accademico: 2014-2015

Don’t be afraid of changes,

be afraid of not changing

Table of contents

1 List of abbreviations

- Ab: Antibody
- AEBP2: AE Binding protein 2
- AID: Activation-induced cytidine deaminase
- ALN: axillary lymph nodes
- AML: Acute Myeloid Leukemia
- ANRIL: Antisense non-coding RNA in the locus
- AP1: Activator protein 1
- BAFF-R: B cell activating factor receptor
- BCL2: B cell lymphoma 2
- BCL6: B cell lymphoma 6
- BCR: B cell receptor
- BL: Burkitt lymphomas
- Blimp1: B lymphocyte induced maturation protein 1
- BM: Bone marrow
- bp: base pair
- BRCA1: Breast and Ovarian Cancer Susceptibility Protein 1
- BrdU: 5-bromo-2'-deoxyuridine
- BSA: bovine serum albumin
- C-terminus: Carboxyl terminus
- CB: Centroblasts
- CBX: Chromobox-domain protein
- CC: Centrocytes
- CDKN2a: Cyclin-Dependent Kinase Inhibitor 2A
- cDNA: Complementary DNA
- ChIP: chromatin immunoprecipitation
- ChIP-seq: ChIP-sequencing
- cKit: CD117
- CRPC: castration-resistant prostate cancer
- CSR: class switch recombination
- D: diversity
- DDR: DNA damage response
- DE: deletion efficiency

- DEG: Differentially expressed gene
- ds: double strand
- DLBCL: Diffuse large B cell lymphomas
- DIPG: Diffuse intrinsic pontine gliomas
- DMEM Dulbecco's Modified Eagle Medium
- DMSO: Dimethyl sulfoxide
- DSB: Double strand breaks
- DZ: Dark zone
- DZNep: 3-deazaneplanocin A
- E2F6: E2 transcription factor 6
- EBV: Epstein Barr virus
- Eed: Embryonic ectoderm development
- ER: Estrogen receptor
- ESC: Embryonic Stem Cell
- Ezh1/2: Enhancer of zeste 1/2
- Eμ: IgH intronic enhancer
- FACS: Fluorescence Activated Cell Sorting
- FBS: fetal bovine serum
- FDC: Follicular dendritic cells
- FL: Follicular Lymphomas
- FO: Follicular B cells
- Fox: forkhead box
- G.o.f.: Gain of function
- GBM: Glioblastoma multiforms
- GC: germinal centre
- GSK: GlaxoSmithKline
- H: Histones
- H2AK119ub1: Histone H2A lysine 119 monoubiquitination
- H3.3K27M: Lysine 27 substitutions with methionine of Histone variant H3.3
- H3K27me: Histone H3 lysine 27 methylation
- HDAC: Histone deacethylase
- HOTAIR: Hox transcript antisense RNA
- Hox: Homeotic genes

- HSC: Hematopoietic Stem Cells
- HS: High sensitivity
- HT: High Throughput
- IFN−γ: Interferon−γ
- IFNGR1: Interferon−γ−receptor 1
- Ig: Immunoglobulin
- IgH: Immunoglobulin heavy chain
- IgK: Immunoglobulin Kappa chain
- IgL: Immunoglobulin Light chain
- Igλ: Immunoglobulin Lambda chain
- Ink4a: Inhibitor of cyclin-dependent kinase 4A
- IP: Immunoprecipitation
- J: joining
- JARID2: Jumonji AT Rich Interactive Domain 2
- JMJD3: Jumonji Domain Containing 3
- Kb: Kilo base
- KDa: Kilo Dalton
- KO: Knockout
- L.o.f.: Loss of function
- LN: lymph node
- loxP: locus of X-over of P1
- LZ: Light zone
- MACS: Magnetic activating cell sorting
- MHC: Major Histocompatibility Complex
- miRNA: micro RNA
- MLL: Mixed-Lineage Leukemia Protein 1
- MLN: mesenteric lymph nodes
- MQ: Milli-Q water
- mRNA: messenger RNA
- MSD/MPS: myelodisplastic syndromes and myeloproliferative neoplasms
- MyoD: Myogenic differentiation 1

- MZ: Marginal zone B cells
- N-term: Amino terminus
- Nanog: Nanog Homeobox
- ncRNAs: non coding RNAs
- NF-κβ: Nuclear Factor Kappa-B DNA Binding Subunit
- NHL: Non Hodgkin lymphomas
- Oct4: Octamer-binding transcription factor 4
- PBS: Phosphate buffered saline
- PC: Plasma cells
- PCA: Principal component analysis
- PcG: Polycomb group Complexes
- PCNA: Proliferating cell nuclear antigen protein
- PCR: polymerase chain reaction
- PI: propidium iodide
- PLZF: Promyelocytic zinc finger
- PLZF-RARα: Promyelocytic leukemia zinc finger-retinoic acid receptor α
- Pol-II: RNA polymerase II
- PRC1/2: Polycomb repressive complex 1/2
- PRE: Polycomb Response Elements
- Pro B/pre B: B cell progenitors
- PTM: Post-translational modification
- qPCR: quantitative PCR
- qRT-PCR: quantitative real time-PCR
- RAG: recombinant activation genes
- RbAp46/48: Retinoblastoma binding protein 46/48
- Ring1a/1b: E3 ubiquitin protein ligase
- RNA-seq: RNA sequencing
- RT-PCR: Reverse Transcriptase PCR
- RT: room temperature
- SAH: S-adenosylhomocystein hydrolase
- SAM: S-adhenosylmethionine
- SET: Su (var) 3-9, Enhancer of zeste, Trithorax
- SHM: Somatic hyper mutation
- Snail 1: Snail Family Zinc Finger 1

- Sox: SRY box
- SPL: Spleen
- ss: single strand
- Suz12: Suppressor of zest 12
- T-ALL: T cell acute lymphoblastic leukemia
- TCR: T cell antigen receptor
- TF: Transcription factors
- TFH: T follicular helper cells
- Tp53: Tumor protein 53
- UTX: Ubiquitously transcribed tetratricopeptide repeat, X chromosome
- V: Variable
- WT: wild type
- Xist: X chromosome specific transcript
- YY1: Yin Yang1

2 Figures Index

3 Tables Index

4 Abstract

The Polycomb group protein Ezh2 catalyzes the Histone H3 lysine-27 trimethylation (H3K27me3) within the Polycomb Repressive Complex 2 (PRC2). PRC2 exerts a critical control over the expression of a large set of target genes controlling important biological functions, including cell proliferation, differentiation and stem cell self-renewal.

Aberrant Ezh2 function is commonly observed in several cancer types and is due to deregulated enzymatic activity and/or expression of the Polycomb protein. Studies in preclinical models have started to reveal the importance of Ezh2 in B cell lymphomagenesis. In contrast, little is known about the effects of Ezh2 deregulated function/constitutive expression in B cell tumor maintenance and progression.

The present study addresses this issue taking advantage of a MYC-driven mouse lymphoma model, featuring high Ezh2 expression as a result of malignant B cell transformation. Conditional, genetic inactivation of Ezh2 methyltransferase activity in aggressive primary Burkitt-like mouse B cell lymphomas led to the identification of two classes of tumors, differentially responding to the loss of Polycomb function. In type-1 lymphomas, Ezh2 inactivation impaired clonal tumor growth starting from single lymphoma cells. Instead, type-2 lymphomas were largely resistant to the loss of Ezh2 catalytic function, giving rise to a substantial number of Ezh2 mutant clones. Transcriptome analyses allowed the identification of a molecular signature discriminating type-1 from type-2 lymphomas, including genes controlling cell cycle progression, DNA replication and cell survival, which were more expressed in type-2 tumors. These results correlated with a more aggressive behavior of type-2 lymphomas when transplantated into immunoproficient hosts.

The growth of rare Ezh2 mutant subclones, established from type-1 lymphomas, was impaired by the treatment with an Ezh1/2 small molecule inhibitor, identifying the Ezh2 paralog, Ezh1, as a determinant of resistance of tumor cells to Ezh2 inactivation. Ezh2 inhibition led to genome wide loss of H3K27me3, which was comparable between

lymphoma types. However, while the loss of H3K27me3 at target genes in type-1 lymphomas failed to alter their expression, in type-2 lymphomas Ezh2 targets were in most cases deregulated following the loss of the histone mark. Based on these results, we propose that Ezh2 mutant subclones from type-1 lymphomas select an H3K27me3-independent mechanism to ensure correct regulation of Ezh2 target genes, which is needed for tumor growth. We also find that residual H3K27me3 is deposited at the promoter of new genes by a non-canonical PRC2/Ezh1, in Ezh2 mutant subclones from type-1 lymphomas. This activity alters the expression of target genes contributing to tumor growth.

We finally report the isolation of clonal variants from type-1 lymphomas that acquire secondary resistance to pharmacological Ezh1/2 inhibition. The latter tumors (together with type-2 lymphomas) will be instrumental to unravel the genetic bases of resistance of MYC-driven lymphomas to PRC2 inhibition.

Anti-Ezh2 inhibitors are currently being tested in phase-1 and -2 clinical trials for the treatment of both solid and blood cancers including B cell lymphomas. Our studies highlight the importance of understanding in more detail the mechanisms of action of Ezh2/PRC2 in tumors, in order to identify those that may benefit from anti-Ezh2 therapies. Our results also provide evidence for mechanisms of lymphoma resistance to Ezh2 inhibition and suggest strategies to circumvent such resistance.

5 Introduction

5.1 Epigenetics

The complexity of multicellular organisms is achieved through the differentiation of several types of cells, with specialized functions. Two principal levels of regulation control the appropriate development of different cell subtypes. The first level of regulation, namely the genetic regulation, relies on the activity of cell-type specific transcription factors (TFs) that establish defined gene expression profiles. TFs act binding to *cis*-regulatory regions of target genes to modulate (promote or repress) their expression, by the recruitment of the transcriptional machinery. The capacity of TFs to bind their targets depends on the local status of the chromatin. The chromatin consists of genomic DNA and histones (H) compacted in basic units, called nucleosomes. Each nucleosome consists of 146 bases of DNA wrapped around two copies each of histones H2A, H2B, H3 and H4 (Kornberg, 1974). Post-translational modifications (PTMs) of histones target the amino (N)- terminus region, thereby causing changes in chromatin compaction. Histone modifications include methylation, phosphorylation, acetylation and ubiquitylation. The deposition of PMTs on histone tails is mediated by the highly dynamic activity of enzymes with opposing function that catalyzes the addition or removal of specific modifications to modulate gene expression and/or the access to chromatin of protein complexes controlling chromosome function. The latter mechanisms contribute to a second level of gene regulation, defined as epigenetics, which is critical to ensure cell identity through subsequent cell divisions (Beck et al., 2010). Epigenetic alterations are commonly associated to inherited disorders as well as sporadic diseases including cancer (Alberghini et al., 2015).

5.2 Polycomb group proteins

The histones PTMs are catalyzed by proteins, commonly acting within macromolecular complexes. Polycomb group (PcG) complexes are epigenetic modifiers whose activity is

thought to promote transcriptional gene silencing. Recent evidences have however challenged this model, associating the function of PcG proteins to active transcription (Scelfo et al., 2015). Polycomb proteins act within two main structural complexes, the Polycomb repressive complex 1 (PRC1) and the Polycomb repressive complex 2 (PRC2) (Levine et al., 2002). Polycomb genes were identified in *Drosophila melanogaster* (Lewis, 1949) as repressor of homeotic (*Hox*) genes, which play a critical role in early embryonic development (Lewis, 1978). In mammals, PRC2 core components are Embryonic ectoderm development (Eed), Suppressor of zest homologue 12 (Suz12) and the catalytic subunit Enhancer of zeste homologue 2 (Ezh2) or its close paralog Ezh1. Ezh2 catalyzes di- and tri-methylation of lysine-27 on histone H3 (H3K27me3). Additional PRC2 components include the zinc finger protein AE Binding protein (AEBP) 2 and the Retinoblastoma binding protein (RbAp46/48). Chromobox-domain (CBX) containing proteins belonging to PRC1 recognize H3K27me3, thereby mediating the recruitment of canonical PRC1 on target genes (Margueron and Reinberg, 2011). As consequence of this targeting, through the E3 ubiquitin protein ligases Ring1a and Ring1b, PRC1 catalyzes the monoubiquitylation of lysine-119 on histone H24 (H2AK119ub1). Concerted deposition of H3K27me3 and H2AK119ub1 histone marks is though to contribute to target gene repression (Morey and Helin, 2010). Recently, alternative, non-canonical PRC1 complexes, lacking the CBX proteins have been described. It has been proposed that non-canonical PRC1 is recruited onto target genes by sequence-specific DNA binding proteins, independent of H3K27me3 recognition (Di Croce and Helin, 2013; Gao et al., 2012) (Figure 1).

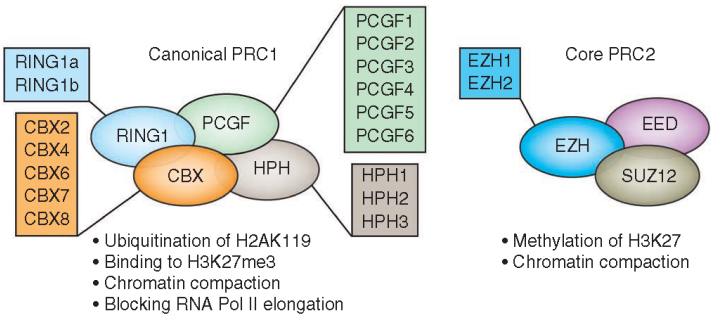

Di Croce L. and Helin K., Nature Structural & Molecular Biology 2013

Figure 1: Polycomb group proteins

Polycomb group (PcG) proteins act within two main multiprotein complexes: PRC1 and PRC2. PRC1 through Ring1a/b proteins promotes H2A lysine-119 monoubiquitylation (H2AK119ub1). The core subunit of PRC2 consists of the EZH1/2 methyltransferases that catalyze Histone H3 lysine-27 trimethylation (H3K27me3). The epigenetic modifications introduced by PRC1/2 facilitate chromatin compaction, thereby contributing to transcriptional repression of target genes.

While in Drosophila, the binding of PcG occurs through the recognition of specific DNA sequences, known as Polycomb Response Elements (PREs) (Schuettengruber and Cavalli, 2009) (Simon and Kingston, 2009), in mammals the modalities of PCR2 recruitment to its target sites is still poorly understood. So far three main mechanisms have been proposed. A first mechanism is based on numerous observations in Embryonic Stem (ES) cells showing a substantial overlap between genome wide PRC2 binding patterns and CpG islands. Although the binding of Polycomb complex to these regions is not direct (Ku et al., 2008), recent findings have unveiled that PRC2 bindings partners, Jumonji AT Rich Interactive Domain 2 (JARID2) and AEBP2 bound to CpG islands, can facilitate PRC2 recruitment to CpG rich regions (Landeira et al., 2010; Li et al., 2010; Pasini et al., 2010; Peng et al., 2009; Shen et al., 2009). A second mechanism involves the interaction of PRC2 with non-coding RNAs (ncRNAs). The X-chromosome-specific 17-kb ncRNA (Xist) is responsible for PRC2-dependent H3K27me3 of the inactive X-chromosome (Plath et al., 2003). In a similar fashion, the recently discovered ncRNA ANRIL, transcribed in the antisense orientation

from the INK4 locus, is able to recruit PRCs to Cyclin-dependent kinase inhibitor 2a (*Cdkn2a*), through the interaction with Cbx7 and Suz12, to promote gene repression (Kotake et al., 2011; Yap et al., 2010). Following a similar mechanism, the antisense RNA *HOTAIR*, transcribed from the *HOX* locus, promotes PRC2 binding in *trans* to repress genes of the *HOXD* locus (Rinn et al., 2007; Tsai et al., 2010).

Finally, it has been proposed that PRC2 recruitment to target sites is mediated by the interaction with specific TFs, including YY1 (Satijn et al., 2001; Wilkinson et al., 2006), E2 transcription factor 6 (E2F6) (Attwooll et al., 2005; Trimarchi et al., 2001), Snail Family Zinc Finger 1 (Snail 1) (Herranz et al., 2008), Promyelocytic zinc finger (PLZF) and Promyelocytic leukemia zinc finger-retinoic acid receptor α (PLZF-RARα) (Boukarabila et al., 2009; Villa et al., 2007).

5.3 Polycomb Repressive Complex 2

Transcriptional repression of PRC2 target genes is achieved through the deposition of H3K27me3. H3K27me3 is catalyzed by the methyltransferase member Ezh2 and critically relies on PRC2 core components Eed and Suz12 (Cao et al., 2002; Cao and Zhang, 2004; Pasini et al., 2004). Ezh2 disposes of the catalytic Su (var) 3-9, Enhancer of zeste, Trithorax (SET) domain (Cao et al., 2002; Rea et al., 2000) (Figure 2) to exert processive di- or tri-methylation (Zee et al., 2010) starting from H3K27me1. Therefore, H3K27me3 is a *bona fide* epigenetic mark. Upon DNA replication, the histone mark gets perpetuated onto newly synthetized histones at the target sites in the daughter cells through the recognition of partially H3K27 methylated nucleosomes by PRC2 component Eed (Campos et al., 2014; Mohn et al., 2008).

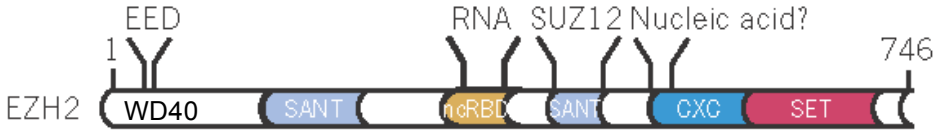

Modified from Reinberg D. and Margueron R., Nature 2011

Figure 2: Schematic representation of Ezh2 protein domains

Ezh2 is a 85 kDa (746 amino acids) protein containing the H3K27 methyltransferase C-term SET domain (purple). Ezh2 binds both Eed (through the WD40 binding domain, white) and Suz12 (through central SANT domain, blue). Moreover, Ezh2 binds histone tails via N-term SANT domain (blue) and RNA molecules through ncRBD1 domain (yellow).

Recent studies on ES cells have shown that around 80 % of the genome is methylated on lysine-27 of histone H3 (Peters et al., 2003). The most representative form of H3K27methylation is the H3K27me2 (50 %), whereas H3K27me3 and H3K27me1 contribute only for 15 % (Peters et al., 2003). The di- and tri-methylated forms of H3K27 are commonly associated with facultative heterochromatin, which plays a critical role during developmental processes. Instead, H3K27me1 is often associated with constitutive heterochromatin (Trojer and Reinberg, 2007), although it can be also found within the body of actively transcribed genes (Cui et al., 2009). H3K27 mono-methylation can occur independently of PRC2 activity, as it is unaffected by the loss of PRC2 core components (Pasini et al., 2004; Schoeftner et al., 2006). It has been proposed that H3K27me1 marking of actively transcribed genes may depend on H3K27 specific demethylases Ubiquitously transcribed tetratricopeptide repeat, X chromosome (UTX) or Jumonji Domain Containing 3 (JMJD3) function, acting on H3K27me2/3 (Swigut and Wysocka, 2007). H3K27me3 can sterically interfere with the binding of chromatin remodeling complexes and/or prevent the establishment of activating histone modifications, thereby enforcing transcriptional silencing (Beisel et al., 2007; Ezhkova et al., 2009; Shao et al., 1999). Indeed, it has been proposed that RNA polymerase II (Pol-II) can directly bind to H3K27me3-rich chromatin regions, resulting in a weak transcriptional activity (Stock et al., 2007). Further studies have

demonstrated that short transcripts, generated from PcG target genes and associated to a paused form of Pol-II, may recruit PRC2 to interfere with Pol-II transcriptional elongation (Kanhere et al., 2010).

5.3.1 The Ezh1 and Ezh2 proteins

In mammals, Ezh2 represents the essential catalytic subunit of PRC2. The Ezh2 close paralog Ezh1 can also be recruited into PRC2, as it is able to bind to the core components Suz12 and Eed, forming an alternative complex. Ezh1 preferentially binds to H3K27me1, but substantially displays weaker methyltransferase activity when compare to Ezh2 (Margueron et al., 2008; Shen et al., 2008). Whereas *Ezh2* knock down results in a strong decrease of H3K27me2/3 levels, the absence of Ezh1 function has a minor impact on global H3K27 di or tri- methylation (Margueron et al., 2008). Importantly, although the two complexes have different chromatin binding properties (Margueron et al., 2008), Ezh1-containing PRC2 shares targets with canonical PRC2 (Shen et al., 2008). Interestingly, Ezh1 and Ezh2 have different expression pattern, pointing to alternative PRC2 functions in different types of cells. Whereas Ezh1 is predominantly expressed in resting cells, Ezh2 function is commonly observed in actively proliferative cells (Margueron et al., 2008; Shen et al., 2008). Together, these data suggest that while Ezh2 is the major player in the regulation of global H3K27me2/3 dynamics in dividing cells, Ezh1 may ensure H3K27me2/3 deposition at target sites in non-dividing cells to counteract H3K27 demethylase activity, to ultimately guarantee stable gene repression.

Recent findings have shown that Ezh1 can compensate for the loss of Ezh2 function during cell differentiation (Ezhkova et al., 2009), somatic cell reprogramming (Fragola et al., 2013) and possibly diseases such as cancer (Mochizuki-Kashio et al., 2015). All together, these data support a model whereby functional compensation by Ezh1 may represent a common

mechanism enabling complex organisms or its components to overcome functional inhibition of the canonical PRC2 complex.

5.4 Mechanisms of action of PRC2

5.4.1 H3K27me3-dependent functions of Ezh2

5.4.1.1 Pluripotency, cellular commitment and differentiation

Studies on ES cells, which express high levels of PcG proteins, have highlighted the relevance of the Polycomb axis in the regulation of stem cell pluripotency and lineage commitment. Data obtained from Polycomb mutant mouse ES cells have indicated that inactivation of PcG components is compatible with pluripotency and self-renewal of the stem cells, due to sustained expression of pluripotency factors, including Octamer-binding transcription factor 4 (Oct4) and Nanog homeobox (Nanog) (Leeb et al., 2010; Pasini et al., 2007; Walker et al., 2010). However, PcG mutant ES cells (*Suz12*$^{-/-}$, *Eed*$^{-/-}$, *Ezh2*$^{-/-}$) showed severe differentiation defects both *in vitro* and *in vivo* (Boyer et al., 2006; Pasini et al., 2007; Shen et al., 2008). The failure of Polycomb mutant ES cells to undergo proper differentiation lies in the property of Polycomb axis to ensure coordinate expression of master regulators (including representatives of the HOX, SRY box (Sox), Forkhead box (Fox) families of TFs) of alternative lineage specific programs (Boyer et al., 2006; Oguro et al., 2010). Indeed, the induction of differentiation of Polycomb mutant ES cells causes concomitant activation of multiple lineage programs, ultimately resulting in aberrant differentiation (Chamberlain et al., 2008). Polycomb proteins also exert fine regulation of self-renewal versus differentiation of stem cells. For example, Ezh2 controls transcriptional silencing of the Wnt-β catenin pathway to avoid premature adipogenesis (Wang et al., 2010). In a similar fashion, in the epidermis Ezh2, on one hand sustains the proliferative potential of basal progenitors by repressing the *Cdkn2a* locus, while, on the other, it

represses the function of Activator protein (AP) 1 transcriptional activator to preclude premature differentiation (Ezhkova et al., 2009). In undifferentiated myoblasts, Ezh2 prevents precocious muscle differentiation by repressing Myogenic differentiation 1 (MyoD) target genes. Upon triggering of muscle differentiation, Ezh2 dissociates from its targets, allowing terminal differentiation of myoblasts (Caretti et al., 2004) (Figure 3).

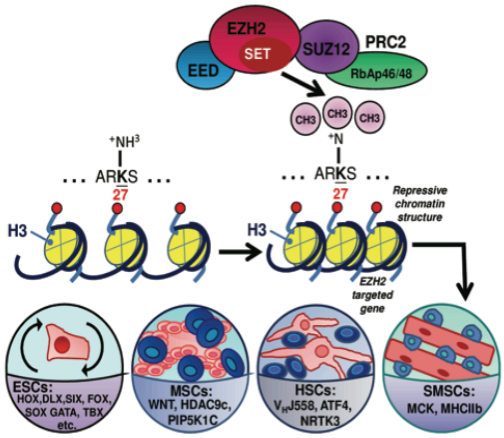

Chen et al., Am J Transl Res 2012

Figure 3: Ezh2 regulation in pluripotency and lineage commitment

H3K27me3-dependent function of Ezh2 regulates embryonic stem cells (ESCs) pluripotency through the repression of developmental genes (HOX: homeobox; DLX: distal-less homeobox; SIX: six homeobox; FOX: forkhead box; SOX: SRY box; GATA: GATA binding protein; TBX: T-box). In addition, Ezh2 controls adult stem cell differentiation (MSCs: mesenchymal stem cells; HSCs: hematopoietic stem cells; SMSCs: skeletal muscle stem cells), targeting genes involved in lineage commitment (WNT: wingless; HDAC9c: histone deacetylase 9c; PIP5K1C: phosphatidylinositol-4-phosphate-5 kinase 1 C; ATF4: activating transcription factor 4; NRTK3: neurotrophic tyrosine kinase receptor3; MCK: muscle creatine kinase; MHC IIb: myosin heavy chain IIb).

5.4.1.2 Cell cycle regulation and cellular senescence

Multiple evidences pointed to a critical role exerted by PRC2 in the control of cell cycle progression. A major focus of investigation has been the influence exerted by PRC2 on the control of the G1-to-S phase transition. The G1-to-S transition is controlled by the

$p16^{Ink4A}$/Rb1 (retinoblastoma1, pRb)-E2F circuitry. In details, hypo-phosphorylated Rb1 interacts with members of the E2F superfamily of TFs repressing their activity and thus blocking G1-to-S progression. Upon mitogen stimulation, Rb1 phosphorylation unleashes E2F factors, which in turn induce transcription of S phase specific genes, allowing cells to replicate DNA and complete cell division (Giacinti and Giordano, 2006). Expression of the Ezh2 gene is induced by E2F proteins (Bracken et al., 2003) and contributes to promote G1-to-S transition through the repression of Cyclin-dependent kinase inhibitor $p16^{Ink4A}$ encoded by the *Cdkn2a* locus (van den Heuvel and Dyson, 2008). The negative regulation imposed by both PRC1 and PRC2 on CDK inhibitors extends beyond the $p16^{Ink4A}$ and includes genes coding for cell cycle inhibitors Cdkn1a/p21/Cip1, Cdkn1b/p27/Kip1 and Cdkn1c/p57/Kip2 (Fan et al., 2011; Fasano et al., 2007; Guo et al., 2011; Itahana et al., 2003; Yang et al., 2009). The contribution of Polycomb proteins to the regulation of cell cycle has an intimate connection with the role of PRC1/2 in the control of cellular senescence. The latter process is an irreversible arrest of the cell in the G_0/G_1 phase of the cell cycle, which is a tumor suppressive mechanisms triggered by excessive telomeric shortening and/or oncogene-induced DNA damage (Campisi and d'Adda di Fagagna, 2007; Di Micco et al., 2011). Senescent cells express low levels of PcG proteins (Jacobs et al., 1999). Studies on mutant mice have unveiled an important contribution of PcG in the prevention of cellular senescence. Inactivation of both PRC1 and PRC2 components facilitates cellular senescence (Guo et al., 2007). In particular, it was shown that PcG proteins inhibit senescence through active repression of the *Cdkn2a* locus (Agherbi et al., 2009; Chen et al., 2009; Miki et al., 2007). Conversely, transgenic mice overexpressing PcG proteins (Ezh2, Bmi1, Cbx2/8) are resistant to age-dependent senescence of tissue and organs (Dietrich et al., 2007; Sasaki et al., 2009).

5.4.1.3 DNA damage response

DNA damage response (DDR) is a safeguard mechanism enabling cells to recognize DNA lesions and ensure their appropriate repair. The DDR is the result of a multistep activation process that involves a substantial number of proteins/enzymes involved in the recognition of the damage, in the recruitment to the site of damage of repair factors and in their active repair of the DNA lesions, respectively. These processes are highly coordinated and intimately connected to the regulation of the cell cycle progression (Sulli et al., 2012). In the past years, several evidences have proposed a role for PcG proteins in the control of DDR. In particular, PcG proteins are recruited in the early phases of the DDR to the sites of DNA damage (Chagraoui et al., 2011; Chou et al., 2010; Facchino et al., 2010; Ginjala et al., 2011; Ismail et al., 2010) PRC2 promotes H3K27 trimethylation at sites of DNA double strand breaks (DSBs), which in turns recruits, through CBX proteins, PRC1. The arrival of PRC1 to sites of DNA lesions promotes ubiquitylation of H2A variant X (H2AX), which ultimately contributes to the recruitment and retention of DSB repair proteins at sites of damage (Ginjala et al., 2011; Ismail et al., 2010). A contribution of Ezh2 in DDR was first proposed studying the cellular response to a genotoxic insult (Campbell et al., 2013). Further evidences supporting a role of Ezh2 in the protection against genotoxic damage has recently come studying the role of the Polycomb protein in the germinal center (GC) B cells (see below). In particular, it was shown that Ezh2 exerts a critical role in protecting B cells, recruited into an immune response, from the genotoxic activity of an endogenous protein called Activation-induced cytidine deaminase (AID) (Caganova et al., 2013). Ezh2 was recently reported to influence the response of cells exposed to a genotoxic stress (Wu et al., 2011). Under these conditions, Ezh2 triggers both a G1/S and G2/M cell cycle arrest, regulating transcriptional repression of F-box protein (FBXO) 32, which directs p21 proteasome-degradation. As consequence, DDR occurred at the sites of lesions to protect cells from undergoing apoptosis (Wu et al., 2011). Recent data have also shown that Ezh2

recruitment to sites of DNA damage depends on Poly (ADP-ribose) polymerase (PAPR) protein, while it is independent on H2AX phosphorylation and PI-3-related kinases ATM and DNA-PKcs (Campbell et al., 2013).

5.4.2 H3K27me3-independent functions of Ezh2

Besides the property to facilitate gene silencing through H3K27me3, recent studies have proposed a role for Ezh2 in mediating post-translational modifications of non-histones substrates (Nolz et al., 2005). First evidence suggesting a role for Ezh2 to modulate the function of cytosolic proteins has come from the Tarakhovsky group (Su et al., 2005). Specifically, a cytosolic pool of Suz12/Eed/Ezh2 was proposed to influence actin polymerization in T lymphocytes in response to T cell receptor (TCR) cross-linking. PRC2 components were shown to interact in the cytoplasm of T cells with the Vav1 signaling protein. Such interaction may influence the proximal signaling events triggered in T cells in response to TCR cross-linking at the immunological synapse (Su et al., 2005). Recent evidences by Su and colleagues have provided further proof for the relevance of the cytosolic Ezh2/Vav1 interaction (Gunawan et al., 2015). Indeed, Ezh2 was shown to methylate the Vav1-binding protein, Talin1, which in turns was critical for its interaction with F-actin. The failure to methylate Talin1 was responsible for the impaired migratory properties of Ezh2 mutant leukocytes as a result of defects in cell adhesion (Gunawan et al., 2015).

5.5 Ezh2 and B cell differentiation

5.5.1 B cell development

B cell development is a highly regulated process, coordinated by the action of a pool of TFs, which ensure specific step-wise maturation of lymphoid cells. B cell lymphopoiesis starts in

the bone marrow (BM), where hematopoietic stem cells (HSCs) commit through multiple differentiation intermediates to become pro B cells, in response to environmental cues and interaction with stromal cells. Pro B cells activate the Recombinant Activation Genes (RAG) 1 and 2 proteins to initiate Variable (V), diversity (D) and joining (J) (VDJ) rearrangement. This process is completed in pre B cells, giving rise to a vast repertoire of variable regions of the immunoglobulin (Ig) Heavy (H) and Light (L) chain polypeptides. Expression of an Ig (also called B cell receptor or BCR) on the surface of pre B cells leads to their differentiation into immature B cells. In the BM, immature cells are subjected to a critical checkpoint that eliminates all cells expressing an auto-reactive BCR. Only immature B cells that succeed to pass this checkpoint are allowed to exit the BM to complete their maturation in secondary lymphoid organs, such as spleen and lymph nodes (Rajewsky, 1996). Here, a small fraction of newly generated immature B cells succeeds to further differentiate to become one of the three major mature B cell subpopulations represented by Follicular (FO), Marginal zone (MZ) and B1 B cells, respectively (Casola, 2007). B1 B cells predominantly reside in the body-cavity sierosa. They belong to the innate immune system, where they contribute to the production of the so-called natural antibodies reacting against common microbial antigens. FO B cells represent the major population of mature B cells. They recirculate among primary and secondary lymphoid organs and actively participate in both T cell-dependent and -independent immune responses. Finally, MZ B cells are restricted to the spleen, where they contribute, together with B1 B cells, to produce antibodies in response to blood born pathogens during T cell-independent immune responses. Occasionally, MZ B cells may contribute with FO B cells to T cell-dependent immune responses (Casola, 2007) (Figure 4).

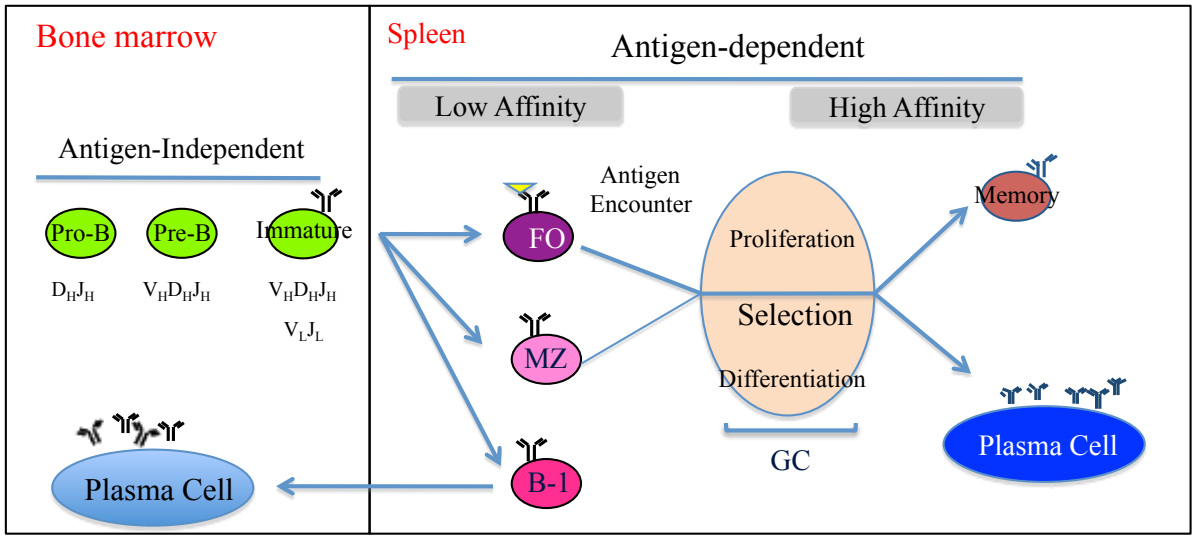

Figure 4: Schematic view of B cell development

B cell development starts in the BM, where HSCs through intermediate steps become B cell progenitors. Upon successful VDJ recombination in B cell progenitors, expression of a functional non auto-reactive Ig receptor drives the formation of immature B cells, which ultimately egress from the bone marrow to home to secondary lymphoid organs, such as spleen and lymph nodes. The three major mature B cell subsets are follicular (FO), marginal zone (MZ) and B1 B cells. The principal role of B1 B cells is the production of natural antibodies and rapid response to T independent antigens by low-affinity antibodies secreting plasma cells. In contrast, FO and MZ B cells, after antigen encounter enter in the germinal center (GC), in a T cell-dependent manner. GC B cells undergo many cycles of division, *Ig* gene mutations and selection to finally differentiate into high-affinity Ig expressing memory B cells and high-affinity antibodies secreting plasma cells.

Upon recognition of T cell-dependent antigens through the BCR, B cells are recruited into the GC reaction. In the dark zone (DZ) of GC, antigen-specific B cells intensively proliferate as so-called centroblasts (CB). Following controlled exit from the proliferation state, GC B cells migrate to a different region of GC, called light zone (LZ), where as centrocytes (CC) they get in close contact with antigen-presenting follicular dendritic cells (FDC) and T follicular helper cells (TFH) (Allen et al., 2007; McHeyzer-Williams et al., 2009; Victora et al., 2010). As CBs, B cells accumulate at high rate mutations within the *Ig V* region genes, through a process catalyze by AID, also called somatic hypermutation

(SHM) process. As a result of SHM, GC B cells express BCRs with a large range of affinities for cognate antigen (Wagner and Neuberger, 1996). GC B cells that are not sustained by BCR-mediated survival signals, resulting by BRC engagement, rapidly undergo apoptosis (Liu and Mullbacher, 1989). In fact, GC B cells express high levels of pro-apoptotic factors (Klein et al., 2003; MacLennan, 1994; Martinez-Valdez et al., 1996), whereas they lack the expression of most anti-apoptotic factors (Klein et al., 2003; Liu and Mullbacher, 1989; MacLennan, 1994). CBs, carrying mutated BCRs, migrate to the LZ becoming CCs. In the LZ, CCs are in close contact with FDCs, which present antigen on their surface in the form of immune complexes (Allen et al., 2007; Schwickert et al., 2007). As a result of an aggressive competition, only few GC B cells, expressing high-affinity BCRs, succeed to bind to the antigen and to receive by the TFH cells the co-stimulatory signals necessary for survival and to proceed in further rounds of expansion and Ig SHM (McHeyzer-Williams et al., 2009; Schwickert et al., 2007). TFH are also important because they release cytokines that instruct the process of Ig class switch recombination (CSR). Ig CSR (also called isotype switching) leads to the replacement of the constant region of IgM with that of another class including IgG3, IgG1, IgG2a, IgG2b, IgE and IgA (Chaudhuri and Alt, 2004). Both Ig SHM and CSR depend on the function of AID, whose expression is strongly induced in GC B cells (Muramatsu et al., 1999). Antigen-driven selection of B cells ultimately promotes their exit from the GC after completing their differentiation into high-affinity, long-lived, memory B cells or antibody secreting-plasma cells (PCs) (Rajewsky, 1996). Whereas PCs represent the endpoint of B cell differentiation, memory B cells provide a pool of B cells expressing high-affinity BCRs, which are preferentially recruited into secondary immune response after antigen re-encounter. GC-derived PCs are long-lived and, after their differentiation, they repopulate the BM representing the source of high-affinity antibodies. Memory B cells represent precursors of GC B cells while retaining the capacity

to directly differentiate into terminally differentiate PCs (Mond et al., 1995; Rajewsky, 1996; Tarlinton and Smith, 2000)(Figure 5).

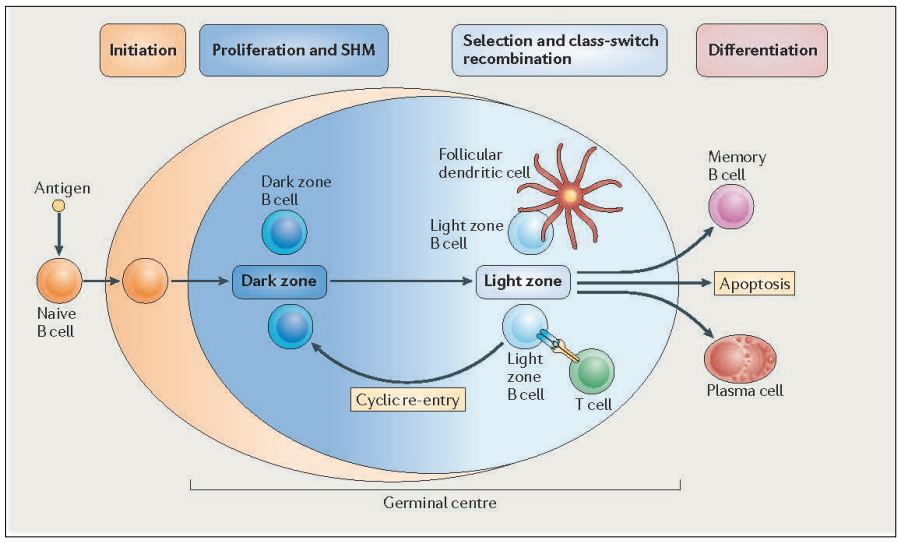

Basso K. and Dalla Favera R., Nature Review, 2015

Figure 5: The germinal center reaction

Upon antigen encounter, activated B cells expressing a fully functional BCR on their surface, enters in the GC reaction. In the dark zone (DZ), centroblast (CB) B cells start proliferating and undergo somatic hypermutation (SHM) of Ig variable region to diversify their immunoglobulin repertoire. After this process CB migrate in the light zone (LZ) of GC and differentiate in centrocytes (CC), which, through class-switch recombination (CSR), produce high-affinity antibodies of different isotype classes. Upon selection in the LZ, CC have three different outcomes: re-enter into the DZ for further rounds of SHM, undergo apoptosis due to low affinity maturation or terminally differentiate into both memory B cells and high-affinity secreting plasma cells.

5.5.2 Effects of Ezh2 inactivation on B cell development

Recently, several studies have assigned to the Polycomb protein Ezh2 a critical function in the control of B cell lymphopoiesis. Ezh2 expression is modulated during B cell differentiation, reaching the highest level in progenitor B cells. In accordance with its expression profile, conditional inactivation of Ezh2 catalytic function starting in pro B cells

causes an early block in B cell development (Su et al., 2003; Su et al., 2005). As result of this defect, conditional Ezh2 mutant mice suffer from a severe B cell lymphopenia (Su et al., 2003) (Caganova and Casola, unpublished results). Mechanistically, Ezh2 mutant progenitor B cells suffer from defects in VDJ recombination, possibly resulting from defects in IgH locus contraction (Su et al., 2003).

In accordance with its low expression in resting B cells, conditional inactivation of Ezh2 in the latter cells caused no over defects in the three mature B cell subsets (Caganova et al., 2013). A rise in Ezh2 expression is observed when resting B cells are recruited into the GC reaction during a T cell-dependent immune response (Caganova et al., 2013). Specific ablation of Ezh2 enzymatic function in GC B cells causes a significant reduction in the number of GC B cells. As consequence of this defect, mutant animals fail to generate high-affinity, long-lived, memory B cells and displaying a substantial reduction in antigen-specific serum antibodies produced by PCs (Beguelin et al., 2013; Caganova et al., 2013). Moreover, conditional Ezh2 inactivation in GC B cells led to strong up-regulation of *Cdkn2a* locus. This evidence suggests that Ezh2 promotes cell cycle progression through the silencing of cell cycle regulator p16 and p19, encoded by the *Cdkn2a* locus. Surprisingly, the loss of *Cdkn2a* is not sufficient to rescue impaired GC responses of Ezh2 mutants, demonstrating that the defects of Ezh2 mutant GC B cells are independent of the regulation that Ezh2 exerts on *Cdkn2a* locus (Caganova et al., 2013). Ezh2 is also critical to prevent B cell terminal differentiation. Ezh2 deficient GC B cells up-regulate the expression of PCs master regulators B lymphocyte induced maturation protein 1 (Blimp1) and Interferon regulator factor (Irf) 4. According to these results, in GC B cells Ezh2 directly modulates Blimp-1 expression, thus preventing a premature exit from GC compartment to guarantee a protective adaptive immune response (Caganova et al., 2013).

5.6 EZH2 function in tumorigenesis

The ability of Polycomb proteins to regulate central aspects of cell biology including stem cell pluripotency, lineage specification, cellular differentiation, cell cycle regulation and DDR, renders deregulation of this regulatory axis a potential determinant of diseases, including cancer. Indeed, expression of PcG proteins, as EZH2, is very often deregulated in aggressive forms of human malignant cancers. Experiments using human cell lines and mouse tumor models have unveiled important contributions of EZH2 to tumor biology (Koppens and van Lohuizen, 2015). In addition, recent advancements in high-throughput genome sequencing have identified common genetic alterations affecting several components of the Polycomb regulatory axis, including EZH2. The picture that has come out from these studies highlights the importance of the cellular context to explain the contribution of Polycomb proteins to malignant transformations. For the interest of this project, following paragraphs will be focused on the evidences linking aberrant EZH2 function to cancer initiation, maintenance and/or progression (Table 1).

Alteration	Cancer type
Overexpression	Prostate, breast, bladder, ovarian, renal carcinoma, lung, liver, brain, gastric, esophageal, pancreatic, melanoma
Activating mutations	Large follicular and B-cell lymphomas
Inactivating/hypomorphic mutations	Myeloproliferative neoplasms Pediatric cancers
H3.3K27M-mediated EZH2 inhibition	Pediatric gliomas

Volkel et al., Am J Transl Res, 2015

Table 1: EZH2 alterations in cancer

Table summarizing the main mutations affecting H3K27 methyltransferase EZH2 in several types of cancers.

5.6.1 EZH2 overexpression in solid cancer

Transcriptome analysis has provided the first evidence indicating recurrent overexpression of EZH2 in malignant prostate and breast cancer (Ku et al., 2008; Varambally et al., 2002). An increase in EZH2 expression levels often correlates with tumor progression, with high EZH2 expression levels commonly observed in metastatic stages and, hence, associated with poor prognosis (Collett et al., 2006; Kleer et al., 2003). In breast cancer, an initial increase in EZH2 expression is already monitored in precancerous lesions, while its levels substantially rise in aggressive metastatic tumors (Collett et al., 2006; Kleer et al., 2003). EZH2 up-regulation has also been described in bladder, ovarian, kidney and lung cancers (reviewed (Yamaguchi and Hung, 2014). Increased EZH2 expression correlates with higher levels of H3K27me3 deposition at its target genes (Tan et al., 2007). Silencing by EZH2 of tumor suppressor genes, including *Cdkn2a* and Breast and Ovarian Cancer Susceptibility Protein 1 (*Brca1*) is thought to contribute to tumor initiation, maintenance and/or progression (Tan et al., 2007; Wilson et al., 2010). In specific circumstances, EZH2 can also act as transcriptional activator. In breast cancer, EZH2 interacts with several partners depending on estrogen receptor status (ER). In ER-positive breast cancer cells, EZH2 was shown to interact with ERα and β-catenin proteins, facilitating their recruitment to promoters of target genes, including *Axin2*, *c-Myc* and *Cyclin D1,* which in turn, become activated (Shi et al., 2007). The interaction between EZH2 and β-catenin was also reported in colon cancer cells, where the two factors form a trimeric complex with the DNA repair protein proliferating cell nuclear antigen (PCNA)-associated factor to promote β-catenin target gene expression. Along the same lines, EZH2 can directly activate *Cyclin D* gene expression, thereby triggering cell proliferation of natural killer/T-cell lymphomas (Yan et al., 2013). Importantly, in all instances, positive regulation of gene expression by EZH2 did not rely on its catalytic activity (Jung et al., 2013; Kim et al., 2013a; Xu et al., 2012). The repertoire of TFs, whose activity is supported by EZH2, is completed by evidences in ER negative breast

cancer cells, where EZH2 was shown to facilitate NF-κβ-mediated gene expression (Shi et al., 2007).

EZH2 can influence the biology of cancer cells acting also on non-histones substrates. Studies on castration-resistant prostate cancer (CRPC) cells, have underlined the ability of EZH2, once phosphorylated by the AKT kinase, to catalyze lysine methylation of the androgen receptor (AR) or AR-binding proteins to promote their expression and ultimately support their transcriptional activity. Interestingly, in the same experimental setting, it was observed that EZH2 cooperated with the AR in activating the expression of target genes, further emphasizing the ability of the Polycomb protein to act either as repressor or activator of gene transcription, depending on the cellular context and repertoire of interacting partners (Xu et al., 2012). The ability of EZH2 to mediate methylation of non-histone proteins has been also confirmed in glioblastoma (Kim et al., 2013a). In the stem cell-like fraction of the latter tumors, serine-21 phosphorylation of EZH2 by AKT can trigger the binding to the transcription factor STAT3, followed by lysine methylation of the latter. EZH2 methylation of STAT3 potentiates the transactivation activity of the TF, thereby contributing to tumor maintenance (Kim et al., 2013a). Finally, EZH2-mediated lysine methylation of the tumor suppressor retinoic acid-related orphan nuclear receptor α (RORα) was shown to contribute to its degradation by the DCAF1/DDB1/CUL4 E3 ubiquitin ligase complex, identifying a novel mechanism through which EZH2 is able to modulate the half-life of interacting partners (Lee et al., 2012).

5.6.2 EZH2 inactivating mutations in myeloid disorders

Whereas a large body of evidences supports a role for EZH2 in promoting tumorigenesis, recent data obtained through whole genome/exome sequencing projects have unveiled possible tumor suppressor function for the Polycomb protein. Indeed, somatic inactivating

mutations in the *EZH2* gene were commonly identified in myelodisplastic syndromes, myeloproliferative neoplasms (MSD/MPS) and acute myeloid leukemia (AML). A first study identified 49 mutations in a total of 614 patients affected by MSD/MPS, chronic myelomonoctyic leukemia and atypical chronic myeloid leukemia. *EZH2* mutations often targeted both alleles, consistent with a tumor suppressor role for the PcG protein (Ernst et al., 2010). A second study performed in 126 patients identified a series of frame-shift, missense and nonsense mutations, in most of the case targeting codons encoding for the methyltransferase SET domain of EZH2 (Nikoloski et al., 2010). Furthermore, in patients displaying heterozygous 7q36.1 deletions, encompassing the EZH2 locus, the EZH2 protein was expressed at very low levels. Importantly, patients with homozygous inactivating *EZH2* mutations had a poorer prognosis, compared to those retaining one functional copy of the Polycomb gene. More recently, a third study on 469 patients with myeloid malignancies identifies EZH2 mutations in 8 % of patients. Decreased EZH2 levels resulted from mutations in splicing factor genes, including U2 Small Nuclear RNA Auxiliary Factor 1 (U2AF1) and Serine/Arginine-Rich Splicing Factor 2 (SRSF2) or from EZH2 loss of heterozygosity (LOH). As consequence of EZH2 haploinsufficiency/loss, tumor-relevant target genes, including *HOXA9* could not be further repressed, possibly contributing to leukemogenesis (Khan et al., 2013). Loss of function (l.o.f) mutations in core PRC2 components have also been reported in T cell acute lymphoblastic leukemia (T-ALL) with a frequency of 18 % for EZH2 and 7 % for SUZ12 (Ntziachristos et al., 2012). Studies in T-ALL mouse models, in particular those driven by increased Notch1 signaling, confirm the pro-tumorigenic effect of Ezh2 inactivating mutations. Furthermore, Ezh2 inactivation rendered T-ALL cells more tumorigenic than control cells, after transplantion into Non obese diabetic/severe combined immunodeficiency (NOD-SCID) mice (Simon et al., 2012).

Recent studies in mouse tumor models have provided unexpected hints on the activation of Ezh2 as tumor suppressor in myeloid malignancies (Lund et al., 2014). Specifically,

inactivation of Ezh2 in HSCs causes the development of myeloid tumors, including MDS and MPN. Combination of transcriptome and genome wide H3K27me3 distribution data allowed the identification of Ezh2 targets that become up-regulated in Polycomb mutant HSCs. Interestingly, the latter set of genes acquired *de novo* H3K27 trimethylation in MDS tumor cells as result of the action of Ezh1 (Mochizuki-Kashio et al., 2015). Hence, occurrence of myeloid malignancies is the result of deregulated Ezh1, whose function is unleashed by the concomitant absence of its paralog Ezh2.

5.6.3 Histone mutations alter EZH2 function in pediatric gliomas

Data obtained from whole genome/exome studies of high-grade pediatric gliomas have unveiled a novel mechanism contributing to the deregulation of Polycomb function in tumor cells. Specifically, it was shown that 70-80 % of high-grade pediatric gliomas, including glioblastoma multiforms (GBM) and diffuse intrinsic pontine gliomas (DIPG) carry a heterozygous mutation causing the substitution of lysine-27 with methionine in the gene coding for the histone variant *H3.3* (Schwartzentruber et al., 2012). The occurrence of this mutation is associated with poor clinical outcome. The mechanism of action of this mutation, affecting a small proportion of histone proteins in the tumor, is yet poorly understood. It has been proposed that nucleosomes containing H3.3K27M stably recruit PRC2, thereby inhibiting genome wide H3K27me3 deposition (Venneti et al., 2013). The exception is represented by genetic loci within chromatin domains containing H3.3, which still appear heavily H3K27 trimethylated. The silencing of the latter genes has been proposed to contribute to tumorigenesis (Lewis et al., 2013). Together, these evidences support a scenario whereby in tumor cells mutations in H3.3 hijack the function of PRC2 onto a selected subset of Polycomb target genes to ensure their stable repression, which is required for tumor growth. This condition unleashes the remaining set of Polycomb targets from epigenetic silencing, possibly contributing as well to sustain the malignant phenotype.

5.7 EZH2 activating mutations in B cell lymphomas

5.7.1 Non Hodgkin Lymphomas

B cell lymphomas represent the 95 % of all yearly-diagnosed lymphoma worldwide. Malignant B cell transformation results from alterations in the complex mechanisms regulating B cell development, identity and function. B cell Non Hodgkin lymphomas (NHL) originate in most of the cases from mature B cells. The most common forms of NHL are represented by Follicular lymphomas (FL), Diffuse large B cell lymphomas (DLBCL) and Burkitt lymphomas (BL) (reviewed in (Shaffer et al., 2012)). Tumor B cells of the three NHL subtypes outlined above display somatic mutation within their *Ig V* genes, pointing to a possible GC origin (Kuppers et al., 1999; Stevenson et al., 2001). GC B cell transformation results from the acquisition of reciprocal chromosomal translocations juxtaposing *Ig* loci to several proto-oncogenes, including *MYC* (in BL), *BCL6* (in DLBCL) and *BCL2* (in FL). The effect of such translocation is the deregulated constitutive action of genes, which promote cell proliferation and/or protect tumor cell precursors from undergoing programmed cell death (Basso and Dalla-Favera, 2015; Klein and Dalla-Favera, 2008). Chromosomal translocation represents the byproduct of Ig CSR triggered in GC B cells by the action of AID (Dorsett et al., 2007; Pasqualucci et al., 2008). Aberrant AID function is also responsible for the acquisition of somatic mutations within non-*Ig* genes, which contribute to lymphomagenesis (Basso and Dalla-Favera, 2015; Dorsett et al., 2007; Pasqualucci et al., 2008) (Figure 6).

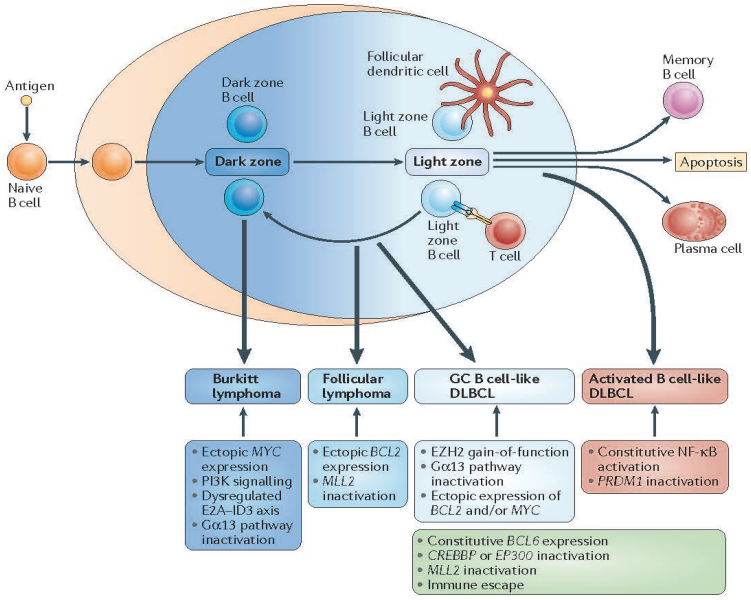

Basso K. and Dalla Favera R., Nature Review, 2015

Figure 6: B cell NHL are commonly derived from GC reaction

Schematic representation of the principal NHLs, which originate from the GC reaction. Genetic alternations consist in most of the cases in chromosomal translocation between Ig genes with different oncogenes including MYC in BL, BCL2 in FL and BCL6 in DLBCL, leading to their constitutive expression.

5.7.2 EZH2 gain-of-function mutations in DLBCL and FL

Expression of PcG proteins, including EZH2, is commonly observed in NHL (Basso and Dalla-Favera, 2015). In particular, tumors of GC origin, including BL, DLBCL and FL express high levels of EZH2 and other components of both PRC1 and PRC2 (Dukers et al., 2004; van Kemenade et al., 2001). Beside augmented expression, whole genome/exome sequencing of DLBCL and FL have revealed the frequent occurrence of EZH2 gain-of-function (g.o.f.) mutations (Lohr et al., 2012; Morin et al., 2010) (Figure 7). As a consequence of such mutations, which preferentially target specific residues of the catalytic SET domain, H3K27 trimethylation is substantially increased in malignant B cells (Morin et al., 2011; Yap et al., 2011). In DLBCL and FL, EZH2 g.o.f. mutations occur always in heterozygous fashion, consistent with their function. Moreover, *in vitro* biochemical studies

have suggested that mutant forms of EZH2 loose the ability to perform H3K27 mono-methylation, becoming therefore dependent on the wild type Polycomb protein to generate H3K27me1, required for the subsequent methylation reactions (McCabe et al., 2012a; Yap et al., 2011; Sneeringer et al., 2010). Whole exome sequencing of cases of indolent FL have revealed the presence of EZH2 g.o.f. mutations starting from the earliest stages of the tumorigenic process (Bodor et al., 2013; Pasqualucci et al., 2014). This result highlights the possible tumor driver function associated with mutant EZH2. Moreover, in DLBCL, EZH2 g.o.f. mutations are commonly associated with the occurrence of IgH/BCL2 translocations, pointing to a possible cooperation between the two proto-oncogenes in driving the tumorigenic process events (Okosun et al., 2014; Pasqualucci et al., 2014; Sungalee et al., 2014). In support to these data, bone marrow reconstitution studies in the mouse model have confirmed cooperation between mutant EZH2 and BCL2 in promoting aggressive B cell lymphoproliferative disorders (Beguelin et al., 2013). Similar results were observed combining the expression of mutant EZH2 with constitutive activation of the MYC proto-oncogene in the EμMYC lymphoma model (Berg et al., 2014). The combination of studies performed *in vivo* on Ezh2 conditional knockout and knock-in (for mutant EZH2) mouse strains, respectively, has pointed to the mechanisms through which deregulated activity of the Polycomb proteins participates to the transformation of GC B cells. First, Ezh2 stably represses through H3K27me3 of the promoter region, the expression of tumor suppressor Blimp1 (Beguelin et al., 2013; Caganova et al., 2013). Second, EZH2 is required to sustain the function of Bcl6 proto-oncogene, which is commonly deregulated in GC derived B cell malignancies (Beguelin et al., 2013). Third, Ezh2 protect B cells from genotoxic damage introduced by AID. In doing so, EZH2 g.o.f. mutations may allow the accumulation, in GC B cells, of exceeding levels of somatic mutations outside the *Ig V* genes (Caganova et al., 2013). Finally, by repressing critical tumor suppressor genes, including *Cdkn2a* and *p21,*

Ezh2 may facilitate cell proliferation and protect B cells and their tumor derivatives from undergoing senescence (Caganova et al., 2013).

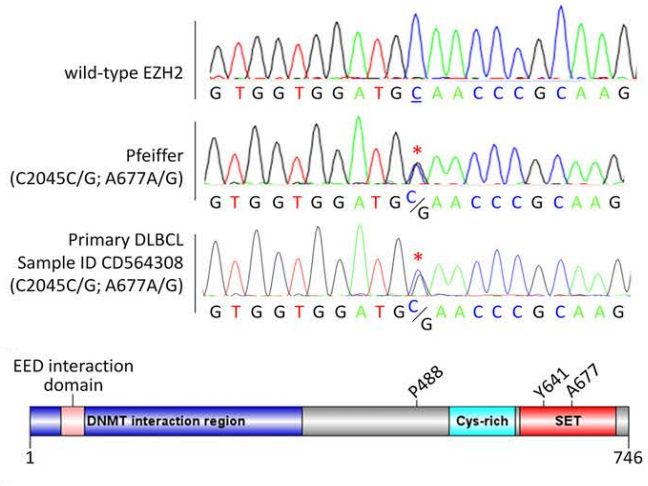

McCabe et al., PNAS, 2012

Figure 7: EZH2 activating mutations are selected in GC-derived DLBCL and FL
Identification by Sanger sequencing of mutations (Y641 and A677) in the catalytic (SET) domain of *EZH2* gene in wild type control sample, Pfeiffer DLBCL cell line and in a primary DLBCL patient sample (sample ID CD564308), harboring EZH2 heterozygous C-to-G missense (red asterisks) mutations.

5.8 EZH2 overexpression and BL

5.8.1 Burkitt lymphoma

BL is an aggressive form of B-NHL, firstly identifies by Dr Burkitt in malarial areas of subequatorial Africa and described as a sarcoma of the jaws of African children (Burkitt, 1958). Together with the endemic form of the disease present in Africa, BL appears as a sporadic disease in the Western world (Burkitt, 1962). Sporadic BL commonly develop in the gut associated lymphoid tissues where it rapidly disseminates to the bone marrow and other organs. The molecular hallmark of BL is represented by the t(8;14) chromosomal

translocation that juxtaposes the *c-MYC* proto-oncogene to IgH *cis* regulatory region locus, leading to constitutive MYC expression in B lymphoid cells. In 20 % of the cases, MYC translocation involves the Igκ or Igλ loci on chromosome 2 and 22, respectively (Dalla-Favera et al., 1982; Hecht and Aster, 2000; Taub et al., 1982). BL tumor cells express somatically mutated Ig V genes and often display ongoing Ig SHM (Chapman et al., 1996; Klein et al., 1995). Recent studies have attempted to define the cell of origin of BL. MYC expression is transiently observed in GC B cells upon T-B cell interaction in the light-zone. The burst in proliferation triggered by MYC in response to CD40/CD40L interaction is followed by the re-entry of B cells in dark zone of the GC. At this point MYC expression is extinguished through the action of repressors, such as BCL6 (Dominguez-Sola et al., 2012). Upon acquisition of a t(8;14) translocation, the negative regulation of MYC expression in CB is lost leading to constitutive expression of the proto-oncogene in these cells. The accumulation of additional genetic events, such as the loss of tumor suppressor Tumor protein (*TP) 53* gene or *CDKN2A* (Evan et al., 1992; Meyer et al., 2006; Schmitz et al., 2012), or deregulated expression of pro-survival factors such as BCL2 (Blum et al., 2004), allow BL precursors to overcome programmed cell death and ultimately acquire a malignant phenotype. BL cells retain a CB transcriptional program, which sustains intense proliferation of tumor cells fuelled by MYC deregulation (Calado et al., 2012; Dominguez-Sola et al., 2012; Victora et al., 2012). Besides recurrent inactivation of tumor suppressor TP53 and CDKN2A, and within the transactivation domain of MYC itself, BL cells display several recurrent mutations interfering with the biology of GC B cells (Schmitz et al., 2012). Mutations in the TCF3 (E2A)/ID3 transcriptional network are thought to potentiate the expression of genes important for BCR function, pointing to a contribution of the antigen receptor to tumor growth. Moreover, BL cells display frequent mutations in the gene coding for the Foxo1 transcription factor that has been shown to play an important role in the GC B cell biology (Chang, 2011). At the histological level, BL have a peculiar “starry sky”

appearance and are characterized by dense clusters of CD10/CD20/IgM-positive cells (Campo et al., 2011; Xie et al., 2015). The high proliferative rate of BL renders this cancer particularly sensitive to cytostatic drugs including cyclophosphamide, vincristine, prednisolone and doxorubicin (CHOP), which are given at doses that are proportional to the stage of the disease. The addition of rituximab (anti-CD20) (or improved variants of anti-CD20 antibodies, such as Veltuzumab or Ofatumumab) to primary therapy (R-CHOP) has been assessed with an overall cure rate of roughly 90 % (Foon et al., 2012). Current therapeutic treatment, based on intensive chemotherapy, has pronounced hematological toxic effects and mucositis, as well as high risk of severe infections. Moreover, relapse of BL, even though uncommon, occurs on average 6 months after the end of the treatment, and has a very poor prognosis, probably because of the selection of particularly aggressive chemo resistant clones (Molyneux et al., 2012).

5.8.2 Models of Burkitt lymphoma

To better understand BL pathogenesis and develop safer/loss toxic therapeutic regimens, several transgenic mouse models recapitulating major aspects of human BL were developed over the past 20 years (Schmitz et al., 2014). The first described *MYC*-driven B cell lymphoma mouse model was the EμMYC model. In these transgenic mice, the c-*MYC* gene was placed under the control of IgH intronic enhancer (Eμ). EμMYC mice develop lymphomas with a latency of 4^{th} to 6^{th} months (Adams et al., 1985). However, given the premature expression of the *c-MYC* transgene starting in B cell progenitors, the majority of tumors developing in EμMYC animals are of pro B/pre B origin. An alternative MYC driven-lymphoma model, called λ-MYC, takes advantage of the Ig Light chain regulatory sequences to postpone constitutive MYC expression to IgM-expressing B cells (Kovalchuk et al., 2000). Indeed, in λ-MYC mice the majority of lymphoma develops from

immature/mature BCR-expressing B cells (Kovalchuk et al., 2000). Tumors in λ-MYC mice resemble human BL in terms of surface phenotype (IgM^+; $CD19^+$; $B220^+$; $CD43^+$; $BAFF\text{-}R^+$; $CD5^-$; $CD23^-$), most common genetic alterations (frequent loss of *TP53* and *CDKN2A*) and histological appearance. The main difference with BL consists in the pre-GC origin of λ-MYC B cell lymphomas, as confirmed by the lack of somatic mutations accumulated in clonal Ig V gene rearrangements. A third BL mouse model, targeting deregulated MYC expression to GC B cells in combination with constitutive activation of the PI3K pathway, has recently been described (Sander et al., 2012). In these transgenic animals the combined action of MYC deregulation and chronic PI3K activation has led to the development of *bona fide* GC B cells-derived BL (Sander et al., 2012). The relevance of this murine tumor model for the study of BL biology is further support by the isolation of recurrent genetic mutations that are shared with human BL (Schmitz et al., 2012), including *Tcf3, Id3* and *Cyclin D3*.

5.8.3 EZH2 overexpression in BL

Regardless of the mutational status, the *EZH2* gene is commonly highly expressed in most forms of aggressive B-NHLs (Dukers et al., 2004; van Kemenade et al., 2001). In particular, in Burkitt lymphoma EZH2 protein levels are substantially incremented when compared to their normal B cell counterparts (Sander et al., 2008). Previous data have linked *EZH2* gene expression to the activation of the E2F1 TF. Since MYC-driven lymphomas display substantial E2F1 transcriptional activity, it is possible that high EZH2 levels reflect sustained function of the E2F1/MYC transcriptional network in tumor B cells. A direct influence of MYC on EZH2 gene has also been suggested. Indeed, several studies have proposed the existence of a positive feedback loop centered on the MYC/EZH2 axis, which is mediated by the action of specific microRNAs (miRNAs) species. In BL cell lines, constitutive high MYC activity results in the deregulation of several miRNAs, including

miR-26a (Zhang et al., 2012). Ectopic expression of miR-26a reduces EZH2 protein levels, interfering with tumor cell proliferation. These data have proposed a model whereby deregulated c-MYC action sustains EZH2 expression through the repression of miR26a (Sander et al., 2008). Conversely, EZH2 together with Histone deacethylase (HDAC) 3 was shown to inhibit miR494, that is capable of down-regulating *c-MYC* expression (Zhang et al., 2012) (Figure 8).

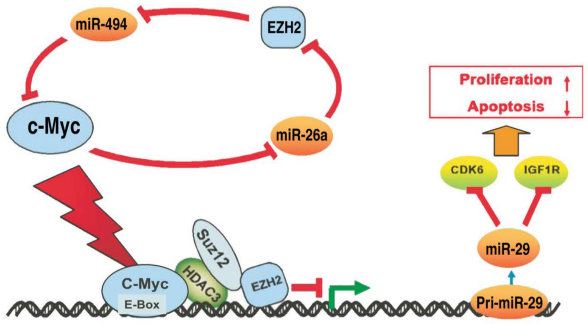

Zhang et al., Cancer Cell, 2012

Figure 8: MYC-EZH2 positive feedback loop

Schematic model displaying the mechanism by which MYC activates EZH2 via repressing EZH2-targeting miR-26a, in c-MYC driven lymphomas. As results, EZH2 induces silencing of miR-494, that suppresses MYC expression, leading to a constitutive expression of both MYC and EZH2 and consequent repression of miR-29.

The strong increase in EZH2 levels observed in BL cells is compatible with the hypothesis that the Polycomb proteins exert pro-oncogenic functions in malignant MYC-transformed GC B cells. However, recent data have challenged this model (Lee et al., 2013). Using the EμMYC lymphoma model, it was shown that haploinsufficiency of Ezh2/Suz12, starting from HSCs and achieved through gene targeting or RNA interference technology, accelerates progenitor B cell tumorigenesis (Lee et al., 2013). The shorter latency in tumor appearance was associated to an expansion of the progenitor B cell compartment as a result

of the interference imposed by PRC2 haploinsufficiency on early B cell development (Lee et al., 2013). The substantial interference with early hematopoiesis caused by the deregulation of PRC2 function in all hematopoietic lineage precursors, combined with a preferential occurrence of progenitor B cell tumors, poses some doubts on the values of these results to understand the function of EZH2 in GC-derived BL. In support of this, works describing the combined effect of *in vivo* EμMYC and a constitutive active form of EZH2 restricted to B cells, have revealed potent cooperation between the two transgenes in promoting B cell tumorigenesis (Berg et al., 2014). All together these results indicate that cellular context plays a crucial role in the regulation by EZH2 on c-MYC driven tumorigenesis. Moreover, whereas many studies have attempted to define the role of deregulated EZH2 in the development of MYC-driven tumors, there are currently no evidences showing the actual requirement for EZH2 in established MYC lymphomas.

5.9 EZH2 as target anti-cancer therapy

5.9.1 Development of anti-EZH2 inhibitors

The recurrent identification of EZH2 g.o.f. mutations in B-NHL as well as the common increase in EZH2 expression in advanced stages of both solid and hematopoietic malignancies, has identified Polycomb protein as possible target of anti-cancer therapies. The first described EZH2 inhibitor is 3-deazaneplanocin A (DZNep) (Tan et al., 2007). It acts to suppress S-adenosylmethionine (SAM)-dependent cellular methylations through the inhibition of the S-adenosylhomocystein hydrolase (SAH) (Miranda et al., 2009; Richon et al., 2011). DZNep is a global inhibitor of histone methylation, which has shown potent anti-tumor activity in breast, colon cancer and melanoma cancers (Fan et al., 2011; Puppe et al., 2009; Tan et al., 2007).

Later generations of SAM inhibitors showed more restricted specificity towards EZH2. The latter class of inhibitors competitively binds to the SAM pocket within the catalytic SET domain of EZH2. The first two described inhibitors were EPZ005687 (Knutson et al., 2012) and GSK126 (McCabe et al., 2012b). Both drugs showed high specificity for their target EZH2. Moreover, studies in preclinical DLBCL models indicated that the inhibitors acted on both the (WT) type and the constitutively active mutant form of EZH2 (Knutson et al., 2012; McCabe et al., 2012b; Qi et al., 2012). EPZ005687 targets selectively EZH2, while largely sparing the activity of its close paralog EZH1. A derivative of GSK126, GSK343, was developed soon after to increase Ezh2 specificity. UNC1999 represents the first described orally bioavailable small molecule inhibitor that is able to inhibit both EZH1 and EZH2 methyltansferase activities (Konze et al., 2013). UNC1999 inhibition results in a global loss of H3K27me3, followed by growth impairment of DLBCL cell lines displaying EZH2 g.o.f. mutations (Konze et al., 2013). Recently, a novel approach was employed to inhibit PRC2 function (Kim et al., 2013b). Specifically, the Orkin laboratory developed a 27-mer hydrocarbon-stapled (SAH-EZH2), that is able to compete with EZH2 binding to the core PRC2 component EED. SAH-EZH2 mimics the α-helical EED binding domain of EZH2. Exposure of DLBCL cells to SAH-EZH2 leads to growth interference resulting from impaired H3K27 methyltransferase activity. Importantly, SAH-EZH2 will inhibit PRC2 regardless of whether EZH1 or EZH2 constitute the catalytic subunit of the complex (Konze et al., 2013) (Figure 9).

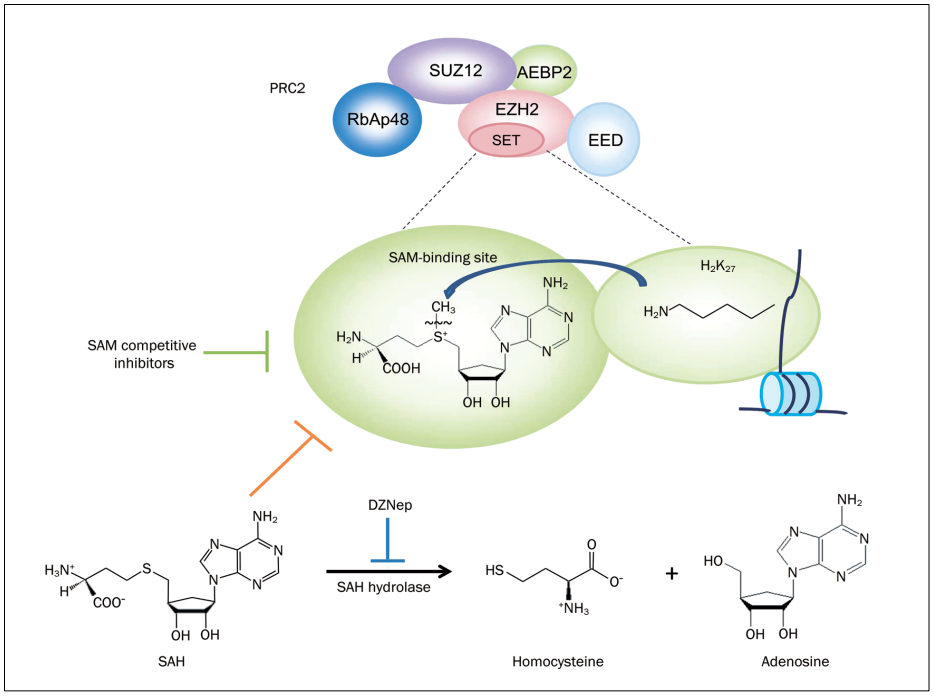

Tan et al., Acta Pharmacologica Sinica, 2014

Figure 9: Principal EZH2 inhibitors

Schematic model displaying three models of action of EZH2 inhibitors targeting the SET catalytic domain of the methyltransferase: SAM competitive inhibitors, DZNep and SAH.

5.9.2 Comparison between EZH2 and EZH1/2 inhibitors

The studies describing the efficacy of anti-Ezh2 inhibitors in DLBCL lines have underlined a heterogeneous response to the drug. Even lymphomas showing EZH2 g.o.f. mutations display in some instance resistance to EZH2 inhibitors (McCabe et al., 2012b). In this context, targeting the methyltransferase activity of both EZH1 and EZH2 may represent a better strategy to inhibit PRC2 function in tumor cells. In support of this, *in vivo* studies on MLL-AF9 driven leukemias have recognized a possible redundancy between Ezh2 and Ezh1 in supporting tumor growth and progression (Neff et al., 2012). Importantly, recent *in vivo* studies on the similar MLL-AF9 driven leukemias have described a potent anti-tumor activity for the EZH1/2 UNC1999, which was not achieved with the EZH2 selective inhibitor GSK126 (Xu et al., 2015a). An alternative to SAM competitors interfering with

both EZH1 and EZH2 is represented by the SAH-EZH2 peptide, which has shown potent anti-lymphoma activity in pre-clinical models (Kim et al., 2013b).

It remains to be seen whether combined EZH1/2 inhibition may exert stronger adverse effects as compared to EZH2 selective inhibitors, as EZH1 is the predominant EZH protein expressed in cell cycle arrested differentiated somatic cells.

5.9.3 Resistance to anti-EZH2 therapies

The successful results achieved by the use of anti-EZH2 inhibitors in preclinical models have led to the rapid translation of the findings into the clinical settings. So far, two clinical trials based on EZH2 inhibitors are currently ongoing. The first trial involves the use of EZH2 inhibitor EPZ-6438 (also known as E7438) by Epizyme. It is a phase-1 study for advanced solid tumors and a phase-2 for the treatment of DLBCL and FL (http://clinicaltrials.gov/ct2/show/NCT01897571). The second trial is based on the use of GSK2816126, from GlaxoSmithKline (GSK). It is presently in phase-1 and is directed to patients with relapsed or refractory DLBCL and transformed FL, solid cancers and multiple myeloma (http://clinicaltrials.gov/ct2/show/NCT02082977).

The effectiveness of anti-EZH2 inhibitors is counterbalanced by emerging reports describing forms of acquired resistance of tumor cells to H3K27 methyltransferase inhibition. Recently, the EZH2 specific inhibitor EI1 from GSK (Qi et al., 2012) has been used to develop a model of acquired resistance using the DLBCL line Karpas, which was shown to be highly sensitive to EZH2 inhibition (Gibaja et al., 2015; Qi et al., 2012). Chronic exposure of lymphoma cells to EI1 led to the selection of clonal variants resistant to the drug. Sequencing of the *EZH2* gene in such cells revealed the presence of two *de novo* missense mutations lysing outside (Tyr111) and within (Tyr661) the catalytic SET domain, respectively (Gibaja et al., 2015). In addition, whereas the Tyr111 mutation mapped to the

WT allele, replacement of Tyr661 occurred on the *EZH2*^{Y641} allele (Gibaja et al., 2015). These data predict that EZH2 inhibitors may select tumor clonal variants resistant to the treatment in patients enrolled in anti-EZH2 therapeutic protocols. A comprehensive understanding of the mechanisms of resistance to anti-EZH2 therapies hence represents a pressing medical need.

5.10 Aim of the study

Aggressive forms of both solid and hematopoietic malignancies display, especially in late stages of the disease, incremented levels of EZH2 expression. Whether tumor cells benefit from increased EZH2 expression in order to sustain their growth and/or to select clonal variants with increased malignancy is yet unknown. Data on DLBCL and FL, showing EZH2 g.o.f. mutations, indicate that inhibition of the Polycomb protein in the tumor cells has a negative impact on tumor growth.

The scope of this research project has been to elucidate the role of Ezh2 in an aggressive form of NHL driven by MYC deregulation, in which expression of Polycomb protein is substantially increased. To achieve this goal, we developed a MYC-driven B cell lymphoma model in which Ezh2 catalytic activity can be inactivated in a time-controlled fashion using the Cre/loxP technology. Using this approach, we succeeded to inhibit the catalytic function of Ezh2 in established, highly aggressive, primary B cell lymphomas. Using a combination of both *in vitro* studies and *in vivo* analyses based on reconstitution of immunoproficient animals with lymphomas undergoing acute Ezh2 inactivation, we determined the effects of inhibition of Ezh2 methyltransferase on tumor growth and established its consequence on the transcriptional program of tumor cells. Another major focus of this study has been to define possible mechanisms of resistance of MYC lymphomas to genetic and/or pharmacological inhibition of Ezh2 catalytic function. Through such investigations, this

study aims to provide novel insights into the regulation by EZH2 of tumor cell biology and establish molecular signatures that may allow to select patients with BL (and possibly other cancer types) that could most benefit from anti-EZH treatments and/or to reveal early stages of disease relapse.

6 Materials and methods

6.1 Mice

6.1.1 Mouse strains

λ-MYC; $Ezh2^{fl/fl}$ mice were obtained crossing λ-MYC and $Ezh2^{fl/fl}$ transgenic mice described in (Kovalchuk et al., 2000) and (Su et al., 2003), respectively. C57BL/6J and C57BL/6J x BALB/c F1 (CB6F1) mice were purchased from Charles River laboratories or Jackson Laboratories. Mice were housed and bred in the animal facility located at the IFOM-IEO Campus in Milan.

6.1.2 Mice monitoring

Mouse experimentations were performed under the protocol number approved by the Italian Ministry of Health and the IFOM IACUC Committee. According to published data, λ-MYC mice spontaneously develop neoplastic lesions of lymphoid origin starting from the 4^{th} month of age. During the study, transgenic mice were monitored for tumor formation once every month between the 8^{th} and 16^{th} week of age and at least once every week from then onwards. Suffering mice were sacrificed when they showed a consistent loss of weight (15%), hair ruffling and reduced motility, always associated with enlarged lymph nodes and splenomegaly, according to guidelines for animal welfare (Workman et al., 2010).

6.2 Molecular biology techniques

6.2.1 Genomic DNA extraction from tail biopsy

Tail biopsies of λ-MYC; Ezh2 compound mutants were incubated in 400 µL of lysis buffer (100 mM Tris-HCl pH 8.5; 5 mM EDTA; 200 mM NaCl; 0.2 % SDS) with Proteinase K (PK) (100 µg/mL) at 56 °C, shaking at 850 revolutions per minutes overnight in

Thermomixer compact (Eppendorf). Lysed material was transferred into a new 1.5 mL tube and 1 mL of isopropanol was added, mixed through inversion and centrifuged at maximum speed for 1 minute in a tabletop centrifuge. The DNA was pelleted by centrifugation, air-dried and dissolved in 300 µL of Milli-Q (MQ) water (Q-POD Element, Merck Millipore) by incubation at 50 °C for 20 minutes.

6.2.2 Genotyping strategy

Genomic DNA extracted from tail biopsies of all mouse offspring was analyzed by polymerase chain reaction (PCR). Primers described in table 2 and PCR reagents in table 3 were used to perform the PCR reaction. PCR conditions are summarized in table 4. PCRs were performed in automatic thermocycler GeneAmp PCR System 9700 (Life Technologies).

Table 2: Genotyping primers, annealing temperature (TA) and amplicons

Primers		TA	Product	
Name	Sequence		Amplicon	Size
Human c-MYC				
Human c-MYC Fw	5'-GAGGCAGGCTCCTGGCAAAAGGTA-3'	58 °C	Tg	400 bp
Human c-MYC Rv	5'-GAAATGAGCTTTTGCTCCTCTGCTTG-3'			
Ezh2 SET				
Ezh2 flox Fw	5'-TTATTCATAGAGCCACCTGG-3'	60 °C	Flox	450 bp
Ezh2 flox Rv	5'-CTGCTCTGAATGGCAACTCC-3'		WT	400 bp
Ezh2 ΔSET				
Ezh2 ΔSET Fw	5'-ACTTCACTGCCAGCCAGTCT-3'	60 °C	Δ	500 bp
Ezh2 ΔSET Rv	5'-ACACACCCGACTGGCTTTAC-3'			
Cdkn2a				
Ink4a/Arf Fw	5'-TTAACAGCGGAGCTTCGTACA-3'	60 °C	Tg	150 bp
Ink4a/Arf Rv	5'-CTGCACCGTAGTTGAGCAGAA-3'			
V_kJ_k				
Vκ Fw1	5'-GCGAAGCTTCCCTGATCGCTTCACAGG-3'	55 °C	$V\kappa J\kappa_1$	800 bp
Vκ Fw2	5'-GCGAAGCTTCCCWGCTCGCTTCAGTGG-3'		$V\kappa J\kappa_2$	550 bp
Vκ Fw3	5'-GCGAAGCTTCCCAKMCAGGTTCAGTGG-3'		$V\kappa J\kappa_3$	250 bp
Jκ5 Rv	5'-CTCAGAGCTCTAGGCCCCTCTTTGAT-3'		$V\kappa J\kappa_5$	100b p

Table 3: Master mix used for genotyping

PCR master mix	µL
5X Flexi Buffer	5
$MgCl_2$ 2.5mM	2
dNTPs 2.5mM	2
Primer Fw (50µM)	0.2
Primer Rv (50µM)	0.2
Go Taq Flexi	0.2
DNA	1-2
H_2O	Up to 25

Table 4: Genotyping PCR conditions

PCR Cycle	
Temperature (°C)	Time (minutes)
94	2:30
95 TA 35x 72	0:30 0:30 0:30
72	5:00
4	Hold

6.2.3 Agarose gel electrophoresis and DNA gel extraction

Size of DNA fragments, amplified by PCR, was defined by electrophoresis agarose (0.7 %-2.5 %) (GellyPhor^{LE}, EuroClone) gel separation in 1 X TAE (Sambrook and Russell, 2001) and 1 X Gel Red™ nucleic acid gel stain (BIOTIUM). As reference marker for agarose gel 1 kilo bases (kb) or 100 base pair (bp) DNA ladder (Promega) were used. The size of amplicons was visualized using UV trans illuminator (EuroClone).

6.3 DNA and RNA extraction

Simultaneous purification of total RNA and genomic DNA from 1 to 5x10^6 cells was performed using All Prep DNA/RNA mini kit (Qiagen) following the manufacturer's protocol. Purified DNA and RNA were quantified by a microvolume UV spectrophotometer (NanoDrop ND-100).

6.3.1 cDNA synthesis

Total RNA was extracted from 1 to 5x10^6 cells, using RNeasy mini kit (Qiagen), following the manufacturer's instructions. Possible DNA contamination was removed through a DNAse (Qiagen) digestion step, before RNA elution in RNase-free water, which was included in the RNA extraction kit. Total RNA was quantified by a microvolume UV spectrophotometer (NanoDrop ND-100). Complementary DNA (cDNA) was obtained by reverse transcription (RT) with the Reverse Transcriptase SuperScript II kit (Life Technologies). RNA (500 ng to 1 μg) was mixed with 50 to 250 ng of Random Primers (Life Technologies) and incubate 5 minutes at 65 °C in the automatic thermocycler GeneAmp PCR System 9700 (Life Technologies). Following this incubation step and a quick chill on ice, a master mix composed of 5 X First Strand (FS) buffer, 0.1 M Dithiothreitol (DTT), 10 mM dNTPs mix, 40 U/μL RNase OUT and 200 U/μL Super Script

II (Life Technologies), included in the kit, was added. Subsequent incubation steps of 2 minutes at 25 °C, 50 minutes at 50 °C and heat inactivation of the enzymatic reaction for 15 minutes at 72 °C were performed in the automatic thermocycler GeneAmp PCR System 9700 (Life Technologies).

6.3.2 Quantitative PCR and quantitative real-time PCR

Ezh2 deletion efficiency (DE) was defined measuring gene copy number by quantitative PCR (qPCR). For gene expression analysis, quantitative Real Time PCR (qRT-PCR) was performed. 500 nM primers mix and 10 µL of LightCycler® 480 SYBR Green I Master containing Hot-start polymerase (Roche) were added to DNA (25 ng) or cDNA (25 ng) in a final volume of 20 µL per reaction in 96-well plates (Roche). Reaction conditions included serial steps at 95 °C for 10 minutes, 45 cycles of 95 °C for 10 seconds, 60 °C for 10 seconds and 72 °C for 10 seconds, followed by a final elongation step for 10 minutes. Accumulation of fluorescent products was monitored using the LightCycler® 480 software, version 1.5 provided along with the LightCycler® 480 Real-Time PCR System (Roche). Specificity of the PCR reaction was controlled through the assessment of the melting temperature profiles of the final products (dissociation curve). *Ezh2* gene copy number analysis was performed using primers annealing within the *Ezh2* SET domain loxP flanked segment to quantify the amount of remaining *Ezh2* SET locus (table 5). To normalize for DNA input, a segment of the *Gapdh* gene was amplified (table 5).

Ezh2 DE was calculated as:

DE (%) = 100% - retained SET domain (%) for $Ezh2^{fl/fl}$

DE (%) = 50% / retained SET domain (%) x 100 for $Ezh2^{fl/\Delta}$

Gene expression levels were normalized to the Ribosomal protein large p0 (*Rplp0*) housekeeping gene expression levels (table 5) (Akamine et al., 2007; Laborda, 1991). Transcript fold enrichment was calculated by ΔΔct method (Livak and Schmittgen, 2001).

Table 5: Primer list for qPCR and qRT-PCR

Primers	Sequence	Target
Gapdh4d Fw	5'-AGCGCTGACCTTGAGGTCTCCTTG-3'	DNA
Gapdh4d Rv	5'-GTTGCCTACGCAGGTCTTGCTGAC-3'	DNA
Ezh2 ΔSET Rv	5'-CAGCAGTGAGCAGGAAGACA-3'	DNA
Ezh2 ΔSET Rv	5'-AGATTTTGTGGTGGATGCAA-3'	DNA
Rplp0 Fw	5'-TTCATTGTGGGAGCAGAC-3'	RNA
Rplp0 Rv	5'-CAGCAGTTTCTCCAGAGC-3'	RNA
Ezh1 Fw	5'-GGAGCAAAGGAGTACGCCAT-3'	RNA
Ezh1 Rv	5'-TTCTGTTTCGTGGGGGTCTG-3'	RNA
p16/Ink4A Fw	5'-GAACTCTTTCGGTCGTACC-3'	RNA
p16/Ink4A Rv	5'-CCAGCGTGTCCAGGAAG-3'	RNA
p21/Cdkn1a Fw	5'-CCACAGCGATATCCAGACATTC-3'	RNA
p21/Cdkn1a Rv	5'-CGGAACAGGTCGGACATCA-3'	RNA

6.4 Cell culture techniques

6.4.1 Preparation of cell suspension from lymphoid organs

Lymphoma cells were obtained from spleen, bone marrow and lymph nodes (mesenteric and axillary) of 8-12 weeks to 2-10 months-old diseased experimental mice. Spleen and lymph

nodes samples were smashed between frosted slide glasses and subsequently filtered through 70 μm nylon meshes (Becton Dickinson, USA). Femurs were flushed using a syringe filled with 10 mL of B cell medium containing Dulbecco's Modified Eagle Medium (DMEM) (Lonza) supplemented with 10 % heat-inactivated fetal bovine serum (FBS) (Sigma-Aldrich), 0.1 mM non-essential amino acids, 1 mM sodium pyruvate, 50 μM β-mercaptoethanol (Life Technologies) and 5 mM L-glutamine (Microtech) to obtain bone marrow cells. Erythrocytes lysis from spleen and bone marrow preparations was achieved incubating cell suspensions in 1 mL of a 9:1 (v/v) solution of 0.15 M NH_4Cl and 0.17 M Tris-HCl pH 7.65 for 3 minutes on ice. Red blood cell lysis reaction was inactivated adding 10 volumes of B cell medium. Cells were centrifuged at 290 g at 4 °C and resuspended in B cell medium before counting. Cell density was adjusted to $2x10^5$ cells/mL and medium was refreshed every 48 hours.

6.4.2 B cell purification

Primary B cells were isolated from spleen of C57 BL6/J mice by magnetic activating cell sorting (MACS) purification. Spleens were processed as described in section 6.4.1 and single cell suspensions were magnetically labeled using anti-CD19 conjugated MicroBeads, according to the manufacturer's protocol (Miltenyi Biotec, Germany). Subsequently, cell suspensions were purified using LS column (Miltenyi Biotec, Germany), loading the cells under the magnetic field of a MACS separator (Miltenyi et al., 1990). Magnetically labeled $CD19^+$ B cells were retained in the column, whereas the $CD19^-$ fraction was removed through washing steps with MACS buffer (1X PBS, 0.5% BSA, 2mM EDTA). Columns were then removed from the magnetic support and $CD19^+$ cells were eluted as selected B cell fraction. Purified B cells were used as control for further experiments.

6.4.3 Establishment of cell lines from λ–MYC lymphomas

Primary lymphomas were cultivated in 25 mm^2 or 75 mm^2 cell culture flasks at 37 °C in a humidified cell culture incubator (Galaxy S RSBiotech, Scientific Laboratories) with 5 % CO_2. On average two weeks after initial seeding over 50 % of primary lymphomas gave rise to tumor cell lines adapted to grow under *in vitro* experimental conditions.

6.4.4 TAT-Cre transduction of primary lymphoma cells

Primary lymphoma cells were washed twice in serum-free media (Hyclone, USA) at a density of 10^7 cells/ml and incubated for 45 minutes at 37 °C with 37.5 μg/mL (final concentration) of recombinant TAT-Cre. Transduction was inactivated adding 10 volumes of B cell medium to the samples. Cells were centrifuged at 290 g, resuspended in B cell medium and cultured at a density of $2x10^5$ cells/mL. Deletion efficiency of *Ezh2* was measured 48 hours later by qPCR on genomic DNA purified from transduced cells.

6.4.5 Isolation of Ezh2 mutant cells by limiting dilution

48 hours following TAT-Cre transduction, tumor cells were plated by limiting dilution at final cell density of 1.5 cells/mL in 96 well plates in a final volume of 100 μL. Cells were incubated at 37 °C, 5 % CO_2. After one week, additional 100 μL of fresh B cell medium was added to the 96 well plates. Plates were monitored for clone formation during the following two to three weeks until colonies derived from single cells were visible. *Ezh2* genotype was defined by PCR analysis on genomic DNA extracted from each colony.

6.4.6 Growth curve analysis and lymphoma treatment with small molecule inhibitors

Cell growth analysis was performed plating lymphoma cells at cell density of $2x10^5$ cells/mL in triplicates at 37 °C, 5 % CO_2. Cells were counted and medium was refreshed every two days. Growth curve experiments were also performed to test the effect of Ezh1/Ezh2 dual inhibitor UNC1999 (Konze et al., 2013) treatment on established lymphomas. Cells were treated every two days with UNC1999 at a final concentration of 2.5, 1.25 or 0.6 μM in B cell medium. Drug vehicle, DMSO, was used as treatment control. Parallel experiments were performed using the Mdm2 inhibitor nutlin (Tovar et al., 2006). Cells were treated every two days with increasing doses (2.5, 5 or 10 μM) of nutlin in B cell medium or with DMSO, used as vehicle for the drug.

6.4.7 Lymphomas transplantation

Lymphoma cells derived from λ-MYC; Ezh2 mutant or control mice, once established as cell suspension, were transplanted via tail vein injection in immunoproficient syngenic mice. Before transplantation into recipient animals, lymphoma cells were washed twice in 1 X PBS, resuspended at $5x10^7$ cells/mL and 100 μL of cell suspension was injected into the tail vein of 16-20-weeks old immunoproficient CB6F1 or C57BL/6J mice. Animals were monitored for tumor formation performing abdominal palpation to reveal splenomegaly and increased size of superficial lymph nodes. Recipient mice developed tumors after 15-26 days on average. Tumors were isolated and stabilized in culture as described previously.

6.5 Imaging techniques

6.5.1 Immunostaining for flow cytometry

For flow cytometric analysis aliquots of 10^6 cells were stained for 20 minutes at 4 °C in the dark in 50 μL FACS buffer (PBS 1 %, BSA 0.01 %) containing the appropriate mixture of

fluorescently labeled antibodies (Abs) (table 6). Stained cells, resuspendend in FACS buffer, were acquired on a FACSCalibur (BD Pharmingen, USA). Dead cells were excluded from the analysis by propidium iodide (PI) labeling or based on forward and side scatter parameters. Data were analyzed using the FlowJo software (Tree Star, USA).

Table 6: List of antibodies used for flow cytometry

Antibody and antigen (clone)	Source	Dilution Factor
Anti mouse IgM (R33.24.12)	Home-made	1/400
Anti mouse IgM (R331.12)	Home-made	1/400
Monoclonal Rabbit anti-mouse H3K27me3 (C36B11)	Home made	1/1000
Monoclonal Rat-anti mouse CD138 (281-2)	eBiosciences	1/200
Monoclonal Rat-anti mouse CD19 (eBio1D3)	eBiosciences	1/400
Monoclonal Rat-anti mouse CD21/CD35 (eBioD89)	eBiosciences	1/1000
Monoclonal Rat-anti mouse CD23 (B3B4)	eBioscience	1/100
Monoclonal Rat-anti mouse CD25 (PC61.5)	eBiosciences	1/200
Monoclonal Rat-anti mouse CD38 (90)	eBiosciences	1/600
Monoclonal Rat-anti mouse CD43 (eBioR2/60)	eBiosciences	1/400
Monoclonal Rat-anti mouse IgD	eBiosciences	1/3000
Monoclonal Rat-anti mouse/human CD45R (B220) (RA3-6B2)	eBiosciences	1/400
Monoclonal Rat-anti mouse BP-1 (6C3)	eBiosciences	1/100
Monoclonal Rat-anti mouse CD24 (HSA) (30-F1)	eBiosciences	1/1000
Monoclonal Rat-anti mouse CD117 (c-Kit) (2B8)	eBiosciences	1/200
Monoclonal Rat-anti mouse CD93 (AA4.1)	eBiosciences	1/400
Monoclonal Rat-anti mouse MHC II (M5/114.15.2)	eBiosciences	1/200
Monoclonal Rat-anti mouse CXCR4 (2B11)	eBiosciences	1/200
Monoclonal mouse-anti BrdU (PBR-1)	BD	1/5
Monoclonal Rat-anti mouse CD268 (BAFF-R) (7H22-E16)	BD	1/400

6.5.2 Intracellular immunostaining for flow cytometry

Intracellular staining for H3K27me3 was performed on 10^6 cells. Cells were permeabilized and fixed in U-bottom 96 well plates for 20 minutes at room temperature (RT), shaking, with 100 µL of Cytofix/Cytoperm™ solution (BD Bioscience). Fixed cells were washed with 100 µL of 1 X Perm/Wash™ buffer (P/W) (BD Bioscience). After centrifugation at 4 °C, 340 g for 3 minutes, cells were refixed with 100 µL of Cytofix/Cytoperm™ solution (BD Bioscience) for 20 minutes at RT, shaking. Cells were then incubated with the primary Ab (Alexa647-labeled monoclonal rabbit anti-mouse H3K27me3 C36B11, Cell Signaling, working dilution 1/1000 in 1 X P/W) for 1 hour at RT, shaking. Cells were then washed twice with 100 µL 1 X P/W buffer and resuspended in FACS buffer. Samples were acquired and analyzed using FACSCalibur (BD Pharmingen, USA) and FlowJo software (Tree Star, USA), respectively.

6.5.3 Cell cycle analysis

10^6 B cell lymphomas (mouse λ-MYC and human Ramos) were pulsed with 33 µM of BrdU (Sigma Aldrich) for 10 minutes at 37 °C, 5 % CO_2. After two rounds of washing with cold 1 X PBS, cells were transferred in U-bottom 96 well plates. Cells were fixed in Cytofix/Cytoperm™ buffer (BD Bioscience) for 20 minutes, washed with 1 X P/W Buffer and re-fixed in BD Cytofix/Cytoperm™ Plus buffer (BD Bioscience) for 10 minutes, at RT, light protected. Cells were washed with 1 X P/W and incubated 5 minutes with BD Cytofix/Cytoperm™ buffer, at RT, protected from light, and washed again with 1 X P/W. Fixed cells were treated with 300 µg/mL DNAse for at least 1 hour at 37 °C, washed with 1 X P/W, and stained with FITC-labeled anti-BrdU Ab (BD Bioscience), for 30 minutes at RT. Stained cells were washed two times, resuspended in 1 ml of cold 1 X PBS containing PI (50 µg/mL, Sigma) and RNase (250µg/mL) and incubated overnight at 4 °C. Samples

were acquired by FACSCalibur (BD Pharmingen, USA) and analyzed using FlowJo software (Tree Star, USA). PI staining coupled with immunoflorescent BrdU staining allowed to characterize cells according of their distribution into the different phases of the cell cycle, namely the G_0/G_1, S and G_2/M phases.

6.6 Biochemical techniques

6.6.1 Immunoblot analysis

Cells were harvested by centrifugation for 5 minutes at 290 g and washed with cold 1 X PBS. Protein extraction was performed on whole cell extracts with RIPA buffer (10 mM Tris-HCl, pH 8.0; 1 % Triton-X-100, 0.1 % SDS; 0.1 % Sodium Deoxycholate, 150 mM NaCl; 1 mM EDTA; 1 mM DTT; 1 mM PMSF and protease inhibitor cocktail Set III (EDTA-free, Calbiochem,) and incubate 1 hour on ice. Sonication consisted of 3 cycles, 15-20 seconds each (Bioruptor^{TM} Next Gen, Diagenode). Lysates were centrifuged at maximum speed for 1 minute in a tabletop centrifuge to remove cell debris. Proteins were quantified with DC^{TM} protein assay (BioRad Laboratories) using a bovine serum albumin (BSA) standard curve as reference. Absorbance at 595 nm was measured using Wallac VICTOR^3 1420 Multilaber Counter (Perkin Elmer). 20-50 μg of proteins in Laemmli loading buffer (62.5 mM Tris−HCl, pH 6.8; 2 % SDS; 0.001 % Bromophenol Blue and 10 % glycerol) and 10 μL of NOVEX Sharp Pre Stained protein standard (Life Technologies) were run onto 7-10 % polyacrylamide gels. Gels were run in an XCell Surelock^{TM} Mini-cell apparatus (Life Technologies) in NuPAGE MOPS SDS running buffer (ThermoFisher Scientific) and transferred to nytrocellulose membranes (iBLOT gel transfer stack, Life Technologies) by iBLOT dry blotting system (Life Technologies) in 6 to 10 minutes. After transfer, nitrocellulose membranes were stained with Ponceau S staining solution (0.1 % Ponceau S and 5 % acetic acid) to verify equal loading and appropriate transfer. Membranes were briefly washed in water and blocked for 1 hour at RT in blocking solution 5 % BSA or 5 %

milk in 1 X TBS-T (20 mM Tris-HCl, pH 7.4; 500 mM NaCl, 0.1 % Tween). Membranes were incubated with primary antibodies (table 7), diluted in blocking solution for 1-2 hours at RT or overnight at 4 °C. After 5 washes of 5 minutes each in TBS-T, membranes were incubated with the appropriate horseradish peroxidase (HRP)-conjugated secondary antibody (table 7), diluted in blocking solution for 1 hour at RT. Membranes were washed 5 times for 5 minutes each in 1 X TBS-T and the bound secondary antibody was revealed with SuperSignal™ West Pico Chemiluminescent Substrate (ThermoFisher Scientific) or SuperSignal™ West Dura Extended Duration Substrate (ThermoFisher Scientific). Membrane stripping was performed with Restore™ PLUS western blot stripping buffer (ThermoFisher Scientific). Immunoblot images were acquired using the ChemiDoc system (Bio-rad). Protein levels quantification was performed using the ImageJ software tool.

Table 7: List of antibodies used for immunoblot protein detection

Primary Abs	Clone	Dilution Factor	Source
Mouse α–Ezh2	AE25-13	1/100 (milk)	Home-made
Rabbit α–H3K27me3	C36B11	1/10000 (BSA)	Cell Signaling
Rabbit α –H3 tot	07-690	1/25000 (milk)	Millipore
Mouse α–Vinculin	h-VIN-1	1/20000 (milk)	Sigma Aldrich
Secondary Abs			
Goat α–mouse Ig	170-6516	1/2000	BioRad
Gaot α–rabbit Ig	170-6515	1/2000	BioRad

6.6.2 Chromatin immunoprecipitation

6.6.2.1 Cell fixation

H3K27me3 Chromatin Immunoprecipitation (ChIP) was performed from λ–MYC; Ezh2 proficient or mutant lymphoma cells. Cells were washed twice with cold 1 X PBS and fixed (10 mL/10^7 cells) with freshly prepared 1 % formaldehyde in 1 X PBS for 10 minutes at RT, on rotation. Fixation was stopped by adding glycine to a final concentration of 0.125 M (1 mL of 1.37 M/10^7 cells) for 5 minutes at RT, on rotation. Cells were centrifuged at 290 g at 4 °C for 10 minutes, washed with cold 1 X PBS and transferred to 1.5 mL tubes. After centrifugation at 4 °C, 3300 g for 5 minutes, cells were resuspended in 1 mL SDS buffer (0.5 % SDS; 50 mM Tris-HCl pH 8.1; 100 mM NaCl; 5 mM EDTA pH 8; 0.02 % NaN_3), 1 mM PMSF and protease inhibitor cocktail Set III (EDTA-free, Calbiochem,). Fixed cells were stored for least one overnight at -80 °C.

6.6.2.2 Sonication

Before sonication step, cells were gradually defrosted in a water bath, centrifuged at 15 °C, 1500 g for 10 minutes and resuspended in Immunoprecipitation (IP) buffer (1mL IP buffer/2x10^7 cells) composed by two volumes of SDS buffer and one volume of 1X Triton buffer (5 % Triton-X100; 100 mM Tris-HCl pH 8.6; 100 mM NaCl; 5 mM EDTA pH 8; 0,02 % NaN_3), 1 mM PMSF and protease inhibitor cocktail Set III (EDTA-free, Calbiochem,). Cells were resuspended in IP buffer at a density of 2x10^6/mL. To share the DNA, a maximum of 130 μL of cell suspension was transferred to microTUBE (Covaris) for sonication, which was performed in the S220 Focused ultra-sonicator (Covaris). To obtain 200 bp fragments, machine parameters were set to a duty factor of 10 %, peak incidence power (W) of 175 and 200 cycles per busts, according to manufacturer's guidelines. Each sonication round was performed for 180 seconds. Sonicated material was centrifuged at

maximum speed (16100 g) at 4 °C for 10 minutes and transferred to a new 1.5 mL tube to remove cellular debris. An aliquot (10 μL) of sonicated chromatin was decrosslinked to serve as sonication control. Final 1 % SDS, 0.1 M NaHCO3 and water up to 100 μL was added to the aliquot of sonicated materials and incubated for 1 hour at 30 °C, shaking. After 1 hour, 0.2 M NaCl and 0.025 μg/μL RNase A were added to the mix and incubated overnight at 65 °C. The following day, final 10 mM EDTA; 40 mM Tris-HCl pH 6.5; PK 0.5 μg/μL were added to the same mix and incubated for 1 hour at 45 °C. DNA purification was performed by adding 600 mL PB buffer (Qiagen) to the decrosslinked material. The mix was subsequently loaded onto Qiagen column provided by Qiagen Gel extraction Kit and DNA purification was performed according to the manufacturer' protocol. DNA was eluted in 20 μL of MQ water and quantified using Qubit double strand (ds) DNA high sensitivity (HS) assay (range: 0.2-100 ng) (ThermoFisher Scientific) with Qubit 2.0 Fluorometric quantitation (Life Technologies). Quality of DNA shearing was controlled using High sensitivity DNA assay (concentration range: 100-10000 pg/mL) (ThermoFisher Scientific) with Bioanalyzer 2100 (Agilent Technologies). Bioanalyzer profiles provide information on size distribution of DNA peaks (between 150-200 bp), as a result of an appropriate sonication.

6.6.2.3 Immunoprecipitation

After sonication control, protein quantification was performed using Biorad DC™ protein assay, according to guidelines of DC protein assay instruction manual. BSA dissolved in IP buffer was used as standard protein reference, starting from a BSA concentration of 2 μg/μL, through a 7-points two-folds dilutions standard curve. Following protein quantification, 40 μg of chromatin were used for immunoprecipitation and the final reaction volume was adjusted to 1 mL with IP buffer. An aliquot of 10 μL (1 %) of chromatin before immunoprecipitation (Input) was used as baseline for further analyses. 10 μg of primary Ab

(monoclonal rabbit anti-H3K27me3, C36B11, Cell Signaling) were added to 40 μg of chromatin and immunoprecipitation was carried out overnight at 4 °C, on rotation. The following day, an aliquot of 20 μL protein G dynabeads/sample (Life Technologies) was equilibrated with 1mL of IP buffer, transferred to tubes containing chromatin and Ab and incubated for 3 hours at 4 °C on rotation. Following incubation, tubes containing beads-Ab-chromatin were fitted onto an ice-cold magnet (Life Technologies) to wash off excess beads. Beads washing included 3 steps with 1 mL ice-cold 150 mM Wash Buffer (1 % Triton-X 100; 150 mM NaCl; 20 mM Tris-HCl pH 8; 0.1 % SDS; 2 mM EDTA pH 8), 1 step with 1 mL ice-cold 500 mM Wash Buffer (1 % Triton-X100; 500 mM NaCl; 20 mM Tris-HCl pH 8; 0.1 % SDS; 2 mM EDTA pH 8) and a final step with 1 mL 1 X Tris-EDTA (TE) Buffer.

6.6.2.4 Decrosslinking

Final 1 % SDS, 0.1 M NaHCO3 and water up to 100 μL were added to the beads and to Input samples and incubated for 1 hour at 30 °C. After 1 hour, immunoprecipitated samples were fitted onto the magnet at RT to remove the beads. Eluted DNA was then transferred to a new 1.5 mL tube. Following a 1 hour incubation, 0.2 M final NaCl and 0.025 μg/μL final RNase A were added to the mix and incubated overnight at 65 °C. The following day, final 10 mM EDTA; 40 mM Tris-HCl pH 6.5; PK 0.5 μg/μL were added to the same mix and incubated for 1 hour at 45 °C. DNA purification was performed by adding 600 mL PB buffer (Qiagen) to the decrosslinked material. The mix was subsequently transferred onto Qiagen column provided by Qiagen Gel extraction Kit and DNA purification was performed according to the manufacturer' protocol. DNA was eluted in 25 μL of MQ water and quantified at Qubit Fluorometric quantitation (ThermoFisher Scientific). 10 ng of input and immunoprecipitated materials were used for sequencing analyses.

6.7 Next generation sequencing techniques

6.7.1 ChIP-sequencing

To evaluate genome wide distribution of H3K27me3 in λ-MYC; Ezh2 control or mutant lymphoma cells, 10 ng of sonicated chromatin before (input) and after immunoprecipitation with H3K27me3 Ab (C36B11, Cell Signaling) were used for construction of libraries using a High Throughput (HT) ChIP-sequencing (ChIP-seq) protocol optimized by Italian Institute of Technology (IIT) Genomic Unit, in Milan. DNA concentration of ChIP-seq libraries was quantified with Qubit HS ds DNA assay (ThermoFisher Scientific). Bioanalyzer 2100 (Agilent Technologies) run was performed to assess the size distribution of ChIP-seq libraries and possible contaminations by adapter dimers. Sequencing reactions were performed on HiSeq2000 instrument (Illumina), in collaboration with Italian Institute of Technology (IIT) Genomic Unit, in Milan.

6.7.2 RNA-sequencing

To perform transcriptome analysis of λ-MYC; Ezh2 control and mutant lymphomas, total RNA purified from tumor cells was quantified by a microvolume UV spectrophotometer (NanoDrop ND-100). RNA quality was controlled using RNA 6000 Nano kit (Agilent Technologies) with Bioanalyzer 2100 (Agilent Technologies). Profiles generated by the instrument provide information on RNA integrity and generate ribosomal ratio of 18S and 28S ribosomal subunits, to exclude nucleic acid degradation. 500 ng/sample of total RNA was used for library construction. First, total RNA was processed using Dynabeads mRNA direct micro kit (ThermoFisher Scientific) to isolate intact polyadenylated (polyA) mRNAs. Purified polyAmRNAs were then used to prepare cDNA libraries for strand-specific RNA sequencing on an Ion Proton^{TM} instrument with Ion Total RNA Seq kit v2 (ThermoFisher

Scientific). Construction of libraries and sequencing reactions were performed with an Ion Proton™ instrument, in collaboration with IFOM Genomic Unit, in Milan.

6.8 Bioinformatic analysis

6.8.1 Bioinformatic analysis of ChIP-sequencing data

After filtering for artifacts with FASTX Toolkit 0.0.13.2, reads with a minimum median base quality score greater than 20 were aligned, -end-to-end, to the mm9 genome using Bowtie 2 version 2.2.1 (Langmead and Salzberg, 2012). ChIP-seq provided an average of 30 millions of uniquely mapped reads for each profiled sample (both Input and H3K27me3-immunoprecipitated samples). To identify genomic regions enriched for H3K27me3 (Peaks) in Immunoprecipitated samples relative to the Input samples was used Macs14 (version 1.4.2) (Zhang et al., 2008) with default parameters ($p<10^{-5}$). Peaks calling was assigned to genes by assessing for each RefSeq transcript whether a peak laid within a +/−5 Kb region around the transcription start site (TSS). Read density heat maps in a window of +/− 5 Kb around the transcriptional start site (TSS) were generated with ngs.plot.r function of the ngs.plot software (Shen et al., 2014).

Venn diagrams displaying overlaps among different list of genes were produced using BioVenn tool (http://www.cmbi.ru.nl/cdd/biovenn/).

6.8.2 Bioinformatic analysis of RNA-sequencing data

Quality control of raw reads was performed using the FASTX Toolkit 0.0.13.2 software, to remove the adapters and low quality sequences. Reads with a minimum median base quality score greater than 15 were aligned to the mouse mm9 transcriptome using TopHat version 2.0.11 (Trapnell et al., 2009). The aligned reads were used as input for Cufflinks version 2.1.1, to estimate the relative abundances of transcripts in each sample.

The Cuffmerge script of Cufflinks merged together the Cufflinks assemblies. Running the Cuffdiff program of Cufflinks eventually assessed differential gene expression between groups. Only genes with a Fold discovery rate (FDR) q value < 0.05 were defined as differentially expressed genes (DEGs). To select genes more homogeneous expressed in each groups, R analysis was performed to identify genes satisfying the following conditions: a) minimum value of first group was grater than maximum value of second group: b) maximum value of first group was less than minimum value of the second group.

Unsupervised hierarchical clustering and heat maps for the expression values were generated in R using the heatmap.2 function of the gplots library. ChIP-enrichment analyses and pathways analyses were performed using the EnrichR software tool. Gene lists provided by EnichR were ranked based on the combined score (log of the p-value computed with the Fisher exact test multiplied by the z-score of the deviation from the expected rank (http://amp.pharm.mssm.edu/Enrichr/)

6.8.2.1 B cell subsets signature

To evaluate whether DEGs identified in the comparison between Ezh2 dependent or independent λ-MYC lymphomas relied on a B cell specific signature, microarray raw data of murine B cell subsets were retrieved from Gene Expression Omnibus (GEO, Query DataSets for GSE15907). Data analysis was performed using R software version 3.1.3. Data were normalized using robust multichip analysis (RMA) algorithm. To identify DEGs among the B cell subsets, the makeContrasts function of the limma package of Bioconductor (www.bioconductor.org) was applied. Expression of B cell specific subsets genes was evaluated in the transcriptome profiles obtained from 6 independent λ-MYC; $Ezh2^{fl/fl}$ lymphomas.

6.9 Statistical analysis

6.9.1 Student's t test

Statistical analysis of normally distributed values (Gaussian) was performed by two-tailed unpaired Student's t-test. Differences were considered significant at p-value<0.05.

6.9.2 2-Way-Anova test

Statistical analysis to compare two independent variables in grouped samples was performed using 2-way-ANOVA test. Differences were considered significant at p-value<0.05.

7 Results

7.1 Conditional inactivation of Ezh2 in a mouse model of MYC-driven B cell lymphoma

7.1.1 Malignant transformation is associated with Ezh2 up-regulation

Previous reports have described high levels of EZH2 expression in human BL cell lines and primary tumors (Dukers et al., 2004; Sander et al., 2008; van Kemenade et al., 2001). In order to study the function of Ezh2 in the maintenance of MYC-driven lymphomas, we employed the λ-MYC transgenic mouse model (Kovalchuk et al., 2000). λ-MYC transgenic mice express a mutant/stabilized form of the human c-MYC proto-oncogene (c-MYC), originally isolated from a BL cell line (Battey et al., 1983). The transgene is placed under the control of its endogenous promoter. Robust cell-type (B cells) specific expression of the λ-MYC transgene is achieved juxtaposing the c-MYC mini-gene to Ig-lambda (Igλ) light chain *cis* regulatory sequences, mimicking the t(8;22)(q24;q11) translocation present in a fraction of BL (Figure 10). λ-MYC transgenic mice spontaneously develop aggressive B cell lymphomas that resemble human BL in terms of surface phenotype of the malignant B cells, mode of dissemination of the disease (BM and secondary lymphoid organs) and histological appearance (Kovalchuk et al., 2000).

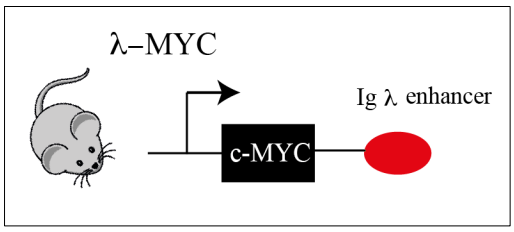

Figure 10: The λ-MYC transgene

Cartoon depicting the structure of the λ-MYC transgene. The MYC gene was cloned from a BL line and placed under the control of its own promoter and mouse Igλ light chain regulatory sequences.

We measured the expression of the Ezh2 protein in B cell lymphomas of λ-MYC animals at different stages of tumorigenesis. Robust expression of transgenic MYC was detected in λ-MYC B cells of young (8-to-10 weeks old) transgenic mice, before the appearance of overt signs of disease (Figure 11). The levels of Ezh2 substantially rose in λ-MYC B cells isolated from diseased animals, when signs of systemic dissemination of lymphoid cells suggested the occurrence of malignant transformation (Figure 11). The significant rise of Ezh2 expression, observed in the transition from the pre-tumoral to the tumoral stage, supports the hypothesis that Ezh2 contributes to the transformation process and/or to sustain the growth of the malignant B cells.

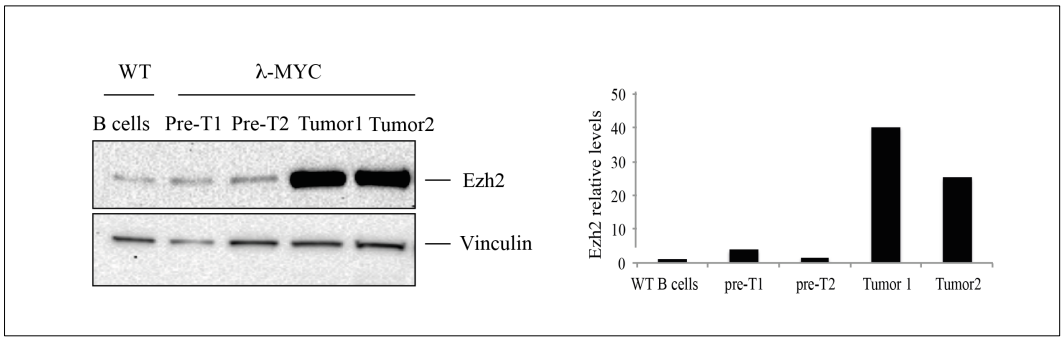

Figure 11: Ezh2 expression in λ-MYC B cells increases from the pre-tumoral to tumoral stage

Immunoblotting analysis of Ezh2 levels in splenic WT C57BL/6J B cells and in pre-tumoral (pre-T) and tumoral B cells isolated from two (Tumor 1 and Tumor 2) representative λ-

MYC transgenic mice. Bar graph displays Ezh2 protein levels after normalization of protein input measuring vinculin expression.

7.1.2 Development of a mouse model to study Ezh2 function in MYC-driven lymphomas

The strong induction of Ezh2 expression in aggressive full-blown λ-MYC lymphomas renders this transgenic model particularly suitable to study the role of Ezh2 in lymphoma maintenance. To achieve this goal, λ-MYC transgenic mice were crossed to animals carrying a conditional knockout allele for the *Ezh2* gene (*Ezh2*^{fl}) (Su et al., 2003). In conditional Ezh2$^{fl/fl}$ mice, the exons coding for the catalytic SET domain are flanked by loxP sites, allowing inactivation of the methyltransferase activity of the Polycomb protein through Cre-mediated recombination (Su et al., 2003) (Figure 12).

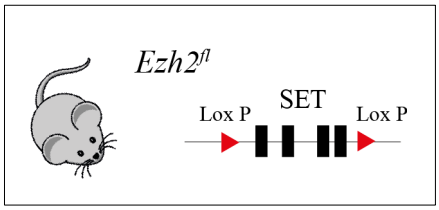

Figure 12: The *Ezh2* conditional allele
Cartoon depicting the structure of the *Ezh2* conditional knockout allele (*Ezh2*^{fl}), in which the exons coding for the catalytic SET domain are flanked by two loxP sites.

These animals developed aggressive B cell lymphomas resembling the λ-MYC tumors previously described by Kovalchuk and colleagues (Kovalchuk et al., 2000). The only exception consisted in the longer tumor latency observed in λ-MYC; Ezh2$^{fl/fl}$ compound mutants, which may result from the different genetic background of the animals (the mice employed for our studies were on the pure C57BL/6J genetic background).

Tumors arising in λ-MYC; Ezh2$^{fl/fl}$ animals were preferentially located in the bone marrow and peripheral lymph nodes. The spleen of diseased animals was often enlarged due to the

conspicuous infiltration of the organ by malignant B cells. So far, we were able to established lymphomas cells from a restricted, but yet consistent number (6) of λ-MYC; $Ezh2^{fl/fl}$ compound mutant mice. Lymphoma B cells, taken from enlarged lymphoid organs of diseased mice, could be successfully transplanted into immunoproficient syngenic hosts, confirming their malignant nature (Table 8). *In vitro* culture of λ-MYC; $Ezh2^{fl/fl}$ primary lymphomas gave rise, in most cases, to primary cell lines that rapidly adapted to *in vitro* growth conditions. Tumor cell lines were established from either primary lymphomas or after one passage of malignant B cells into syngenic immunoproficient animals (Table 8).

Tumor ID	Tumor latency (Month)	Degree of tumor infiltration (% of tumor B cells)				Serial passages (#)	Organ of origin
		SPL	BM	MLN	ALN		
#73664	10	22	10	31	27	1	MLN
#95379	6	35	52	59	61	1	MLN
#123617	10	10	18	5	60	1	ALN
#160887	2.5	50	63	/	/	-	BM
#126803	10	23	13	5	80	1	ALN
#142291	9	15	13	/	44	-	BM

Table 8: Summary of λ-MYC; $Ezh2^{fl/fl}$ lymphomas used for the study

The table summarizes data relative to 6 different primary λ-MYC; $Ezh2^{fl/fl}$ lymphomas that have been used throughout the study. Mouse identification (ID) and survival time are reported in the first two columns, respectively. In addition, the table displays the degree of tumor infiltration represented by the percentage of tumor B cells, assessed by flow cytometry in the indicated lymphoid organs (SP: spleen, BM: bone marrow, MLN: mesenteric lymph nodes and ALN: axillary lymph nodes). The number of serial passages (Serial TP) prior to the establishment of primary cell lines is indicated. Organ of origin refers to the lymphoid organ from which primary cultures were successfully established.

To assess the clonal status of λ-MYC; Ezh2$^{fl/fl}$ lymphoproliferative disorders, we performed immunoglobulin Igκ V gene rearrangement analysis on primary lymphoma cell lines established from 6 λ-MYC; Ezh2$^{fl/fl}$ primary tumors, using a genomic PCR approach. Specifically, a mixture of degenerate primers annealing to most Vκ genes was used in combination with an oligonucleotide annealing downstream of the Jκ5 gene segment, to amplify VκJκ rearrangements from *ex vivo* isolated tumor B cells. Purified splenic WT B cells representing a polyclonal population of B cells were used as comparison. Whereas PCR amplification from the latter cells gave rise to 4 distinct PCR products representing polyclonal VκJκ rearrangements, that respectively consist of Jκ1, Jκ2, Jκ4 and Jκ5 gene segments (Jκ3 is a pseudogene and hence not involved in IgL chain V gene rearrangements), genomic DNA amplified from λ-MYC B cells gave rise in most cases to a single PCR band, indicative of a monoclonal IgL chain V gene rearrangement (Figure 13). Although the presence of genomic DNA in all samples was assessed by the amplification of *Gapdh* gene (data not shown), tumor #95379 resulted negative for Vκ gene rearrangements. This result, combined with the lack of surface Ig expression in the malignant B cells of this lymphoma (Figure 14) suggests a pro B cell origin of this particular tumor.

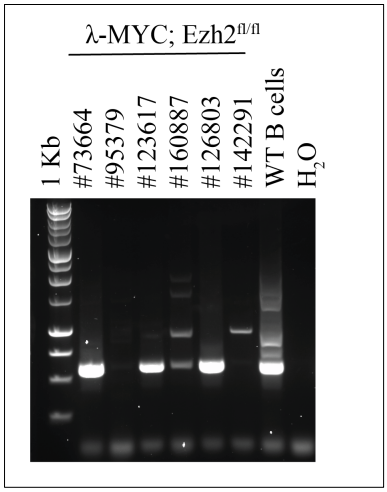

Figure 13: Clonal assessment of λ-MYC; Ezh2$^{fl/fl}$ B cell lymphomas

Genomic PCR analysis to assess the status of VκJκ gene IgL gene rearrangements in splenic WT C57BL/6J B cells and 6 independent primary λ-MYC lymphomas. The four PCR bands amplified in the control sample identify VκJκ rearrangements using Jκ1, Jκ2, Jκ3 and Jκ5 segments, respectively. The 1 Kb ladder was used as reference to determine the size of PCR products.

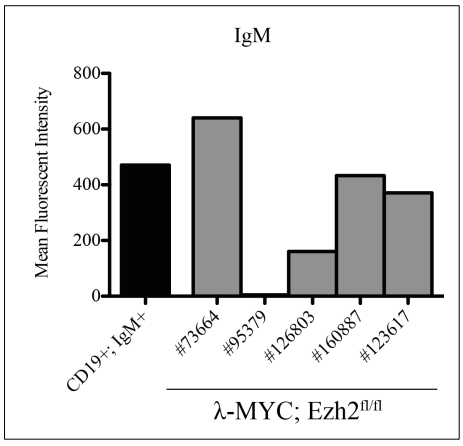

Figure 14: Surface IgM expression levels in λ-MYC; Ezh2$^{fl/fl}$ tumors

Histograms display average expression of surface IgM in 6 primary λ-MYC; Ezh2$^{fl/fl}$ B cell lymphomas (grey filled bar), assessed in a representative flow cytometric analysis. Splenic CD19^{+}; IgM^{+} C57BL/6J B cells were used as comparison (black filled bar).

7.1.3 λ-MYC; Ezh2$^{fl/fl}$ mice develop IgM^{+} B cell lymphomas

To investigate the cell of origin of λ-MYC; Ezh2$^{fl/fl}$ lymphomas, we performed a comprehensive immunophenotypic analysis on the 6 primary tumors (Figure 15A, B). All lymphomas expressed the pan B cell markers B220 and CD19. As previously shown, except for tumor #95379, all lymphomas expressed surface Ig receptor/BCR in the form of IgM (Figure 14). This result indicates that malignant transformation of λ-MYC; Ezh2$^{fl/fl}$ B cells occurred in most cases in an immature/mature B cell that had completed Ig V gene rearrangements. Further immunophenotypic characterization of lymphomas revealed the recurrent expression of markers highly expressed in progenitor B cells (c-Kit, CD43, AA4.1 and in one instance CD25) (Figure 15B), whereas markers of mature B cell identity (CD21, CD23, CD38 and IgD) were largely missing on the surface of malignant B cells (Figure 15B). Tumor cells expressed low levels of histocompatibility class-II molecules (MHC-II), suggesting that tumor cells may select a way to evade the immune system. Finally, all λ-MYC; Ezh2$^{fl/fl}$ lymphomas expressed normal/high levels of the BAFF-R, pointing to a possible dependence of the tumors on the pro-survival factor BAFF/BlyS (Kayagaki et al., 2002) (Figure 15B). All together these results are compatible with a scenario whereby in λ-MYC; Ezh2$^{fl/fl}$ mice deregulated action of MYC transforms a newly generated IgM-expressing B cell, leading to substantial reprogramming of its cell identity.

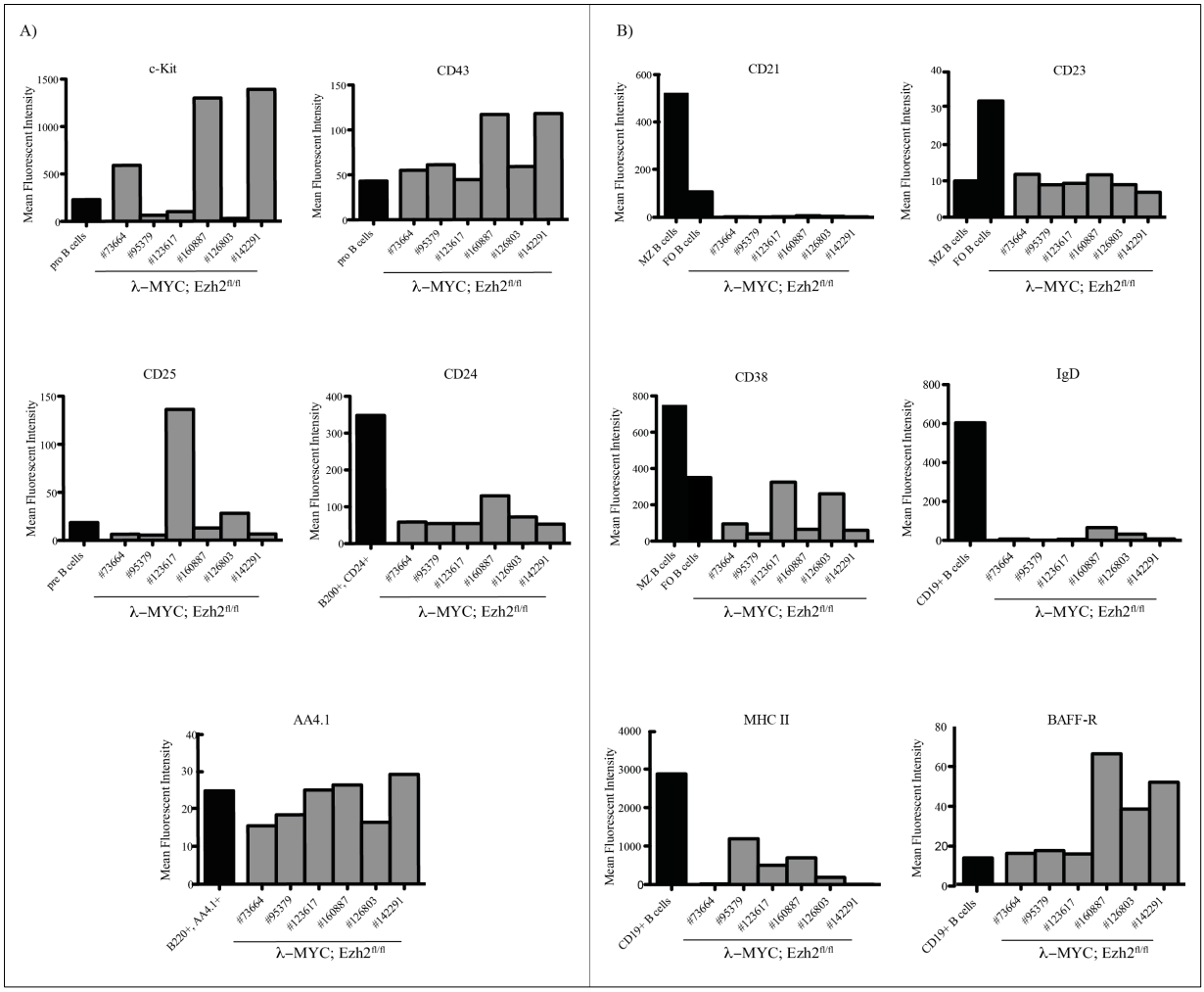

Figure 15: Immunophenotypic characterization of primary λ-MYC; Ezh2$^{fl/fl}$ B cells

Histogram representation of the average expression level of the indicated markers on the surface of 6 primary λ-MYC; Ezh2$^{fl/fl}$ B cell lymphomas (grey filled bar), assessed by flow cytometric analysis. As comparison, we used the indicated B cell subsets of C57BL/6J control mice (black filled bar). The control B cell population expressing the highest levels of the indicated markers was chosen for the comparisons (bone marrow B cell progenitors: A) (splenic mature B cells: B). For IgD, BAFF-R and MHC class II determination the total population of CD19^{+} splenic B cells was chosen as they predominantly consist of resting mature B cells (B).

7.1.4 Molecular heterogeneity of λ-MYC; Ezh2$^{fl/fl}$ lymphomas

In an attempt to define a common cell identity of λ-MYC; Ezh2$^{fl/fl}$ lymphomas using a molecular approach, the 6 tumors were subjected to whole transcriptome analysis by RNA-sequencing. To understand whether tumors developed from a specific subset of B cells, we

established a dedicated “B cell subset (BCS)” transcriptional signature, which included around 70 genes whose expression is mostly (if not only) associated to a specific stage of B cell development. The BCS signature consists of genes differentially expressed between progenitor, immature/transitional, FO, MZ and GC B cells, respectively (Figure 16). Applying the BCS signature to whole transcriptome data of λ-MYC; $Ezh2^{fl/fl}$ tumors, we failed to recognize patterns of gene expression associated to specific B cell subsets (Figure 17). This result, which is in accordance with the immunophenotypic data, highlights: i) the substantial loss of stage-specific B cell identity resulting from malignant transformation and ii) the strong molecular heterogeneity of λ-MYC tumors, which are possibly fuelled by genomic instability imposed on tumor cells by deregulated activity of the MYC oncogene (Kuzyk and Mai, 2014).

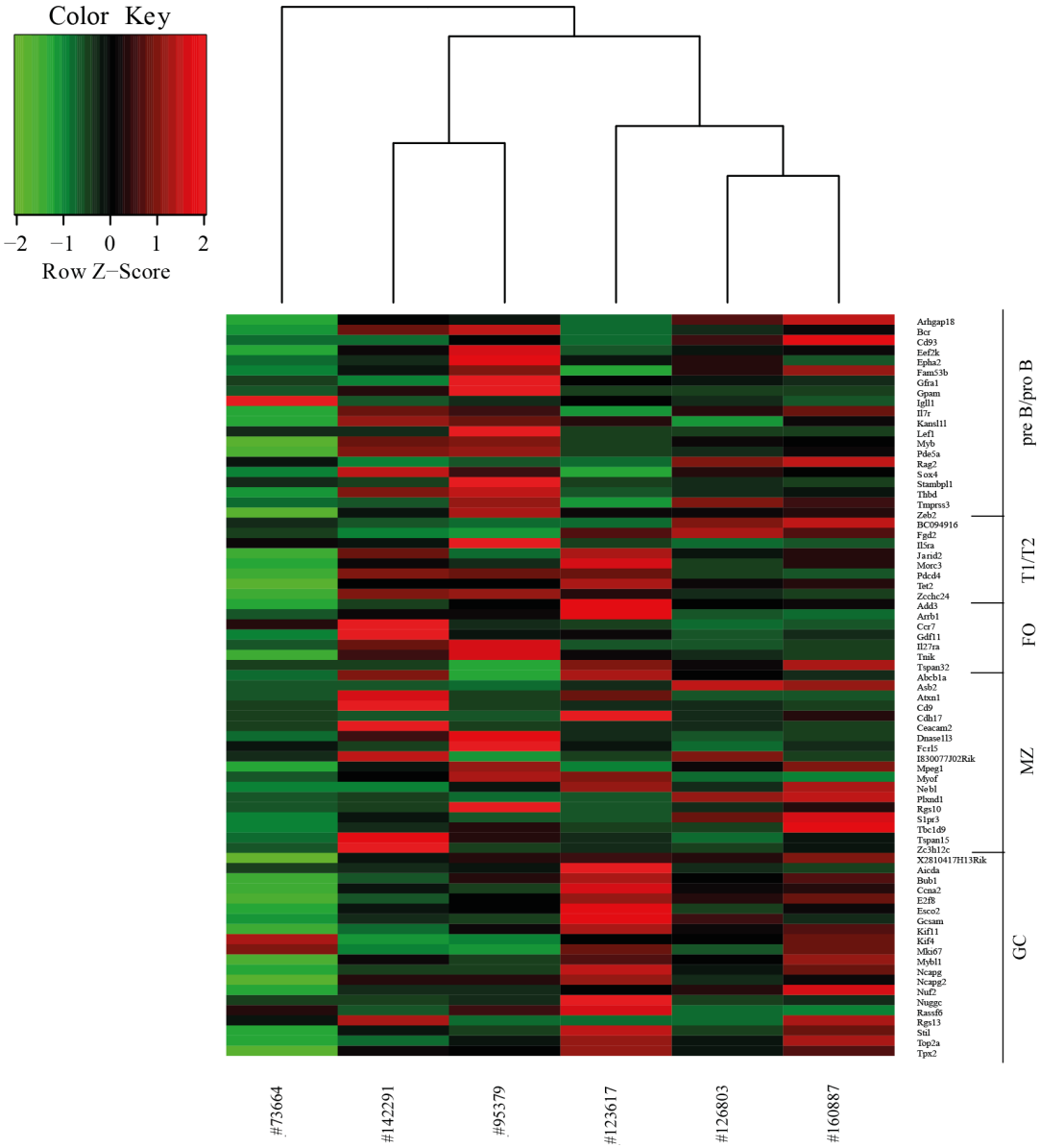

Figure 16: Expression of stage-specific B cell markers in λ-MYC; Ezh2$^{fl/fl}$ lymphomas

Color-coded heat map displaying the expression pattern in the 6 representative λ-MYC; Ezh2$^{fl/fl}$ lymphomas of genes selected for their restricted expression in one of the indicated B cell subpopulations (pre B/pro B: B cell progenitors; T1/ T2: immature/transitional B cells; FO: Follicular B cells; MZ: Marginal zone B cells; GC: germinal center B cells). The stage-specific B cell signature revealed differentially expressed genes from microarray trascriptome data of murine B cell populations obtained from the IMMGEN consortium, through the Gene Expression Omnibus (GEO) database.

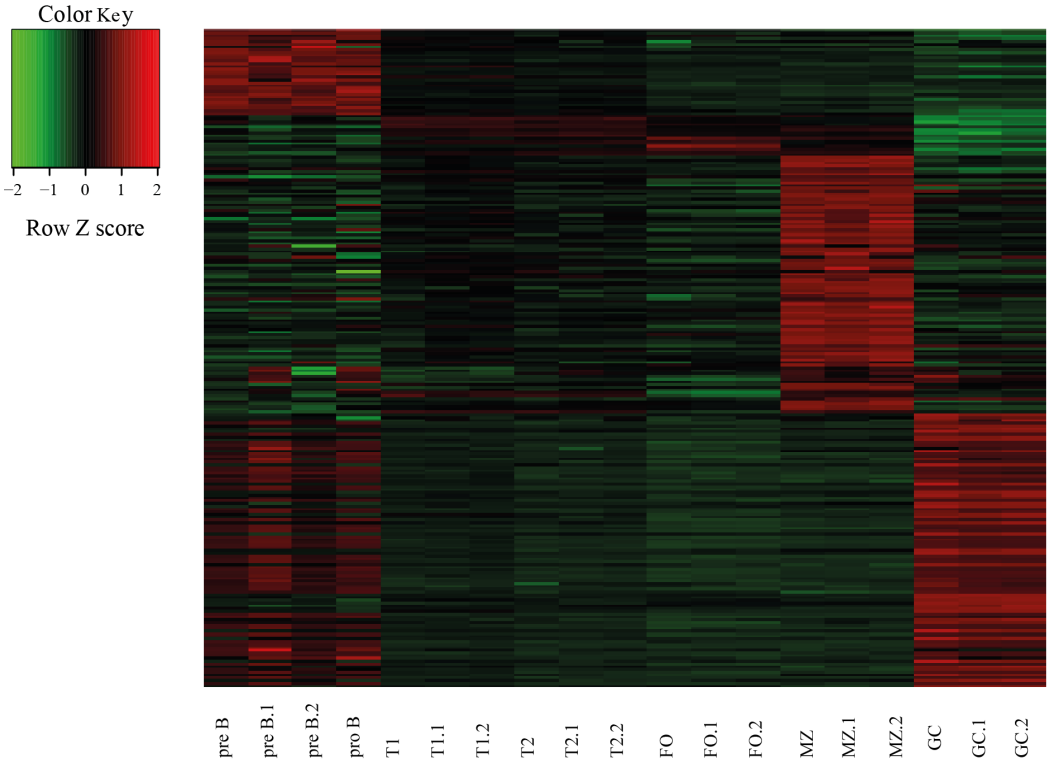

Figure 17: Expression of B cell stage-specific genes in WT B cell subsets

Heat map representation of stage-specific B cell signature in the indicated B cell subpopulations (pre B/pro B: B cell progenitors; T1/ T2: transitional B cells; FO: Follicular B cells; MZ: Marginal zone B cells; GC: germinal center B cells) of C57BL/6J control mice.

7.1.5 Acute Ezh2 inactivation in λ-MYC lymphomas unveils two classes of tumors

The substantial molecular heterogeneity featured by λ-MYC; $Ezh2^{fl/fl}$ lymphomas represented an opportunity to establish a putative function of Ezh2 to the epigenetic dysregulation that may contribute to the observed variability in tumor phenotype.

To study the role of Ezh2 function in MYC-driven lymphomas, we established primary lymphoma cell lines from the 6 independent λ-MYC; $Ezh2^{fl/fl}$ animals, which were subsequently subjected to *in vitro* TAT-Cre transduction. This procedure is based on the transient (45 minutes) incubation *in vitro* of target cell suspensions with cell permeable recombinant TAT-Cre protein (Peitz et al., 2002). This methodology allows efficient

delivery of the Cre proteins into target cells, avoiding toxic effects associated with long-term Cre expression (Peitz et al., 2002).

Following TAT-Cre transduction, lymphoma B cells were plated at limiting dilution in order to isolate individual subclones (Figure 18). Using this procedure we isolated an average of 25 clones for each transduced tumor. To assess the Ezh2 status in individual subclones, we subjected them to genomic PCR genotyping using a strategy that enables the selective amplification of the WT, un-recombined, *Ezh2* allele.

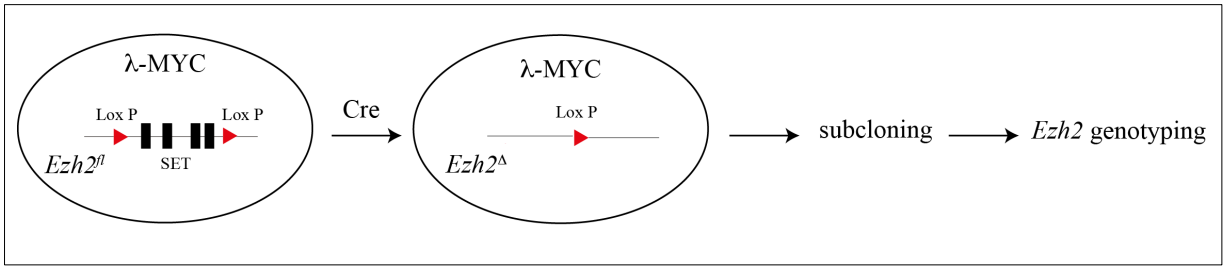

Figure 18: Conditional inactivation of *Ezh2* gene in primary lymphomas and identification of Ezh2 defective clones

Lymphomas developing in λ-MYC; $Ezh2^{fl/fl}$ compound mutant mice were isolated *ex vivo* and subjected to TAT-Cre transduction (Cre). Transduced cells were cultured at limiting dilution to isolate individual clones, which were ultimately subjected to *Ezh2* genotyping by PCR.

Genotyping of 12-40 clones obtained from each λ-MYC; $Ezh2^{fl/fl}$ lymphoma revealed a surprising result. For three tumors (classified as type-1), the frequency of subclones displaying bi-allelic loss of the SET coding exons was substantially under-represented when confronted with the number of Ezh2 proficient clones ($Ezh2^{fl/fl}$ or $Ezh2^{fl/\Delta}$) (Figure 19). From the remaining three lymphomas (classified as type-2), TAT-Cre transduction gave rise to a majority of Ezh2 mutant subclones characterized by bi-allelic *Ezh2* inactivation ($Ezh2^{\Delta/\Delta}$) (Figure 19). The substantial difference in the recovery rate of Ezh2 mutant clones between type-1 and type-2 λ–MYC lymphomas was not dependent on different TAT-Cre transduction efficiency. Indeed, quantification of the $Ezh2^{fl}$ allele soon after (48 hours)

transduction revealed comparable rates (50-80 %) of Cre-mediated recombination between the lymphomas of the two types (Figure 20). These results suggest the existence of two classes of MYC-driven lymphomas that differ in the capacity to overcome anoikis and, hence, outgrow starting from a single tumor cell. Specifically, whereas type-1 λ-MYC lymphomas appear strictly dependent on Ezh2 methyltransferase activity for single cell tumor outgrowth, type-2 tumors have selected alternative molecular pathway(s) that enable single lymphoma cells to grow undisturbed, despite inactivation of Ezh2.

A hint indicating the rapid counter-selection of Ezh2 mutant cells in type-1 lymphomas came from the quantification of *Ezh2* functional alleles in the pool of lymphoma cells transduced 6 days earlier with TAT-Cre. Indeed, genomic qPCR data indicated that while at 48 hours the average *Ezh2* gene copy number in the pool of tumor B cells was substantially reduced (indicative of Cre-mediated recombination), it reached levels close to control tumors at 6 days after transduction (Figure 20). This result supports a scenario whereby Ezh2 proficient tumor cells escaping Cre-mediated inactivation rapidly take over their Polycomb mutant counterparts during *in vitro* expansion. Instead, in type-2 lymphomas we failed to observe major differences in the average *Ezh2* gene copy number assessed in tumor cells at 2- and 6-days after TAT-Cre transduction, respectively (Figure 20). This result suggests that Ezh2 mutant lymphoma B cells can effectively expand in the presence of their Ezh2 proficient counterparts, pointing to a dispensable role for the Polycomb protein for *in vitro* tumor growth.

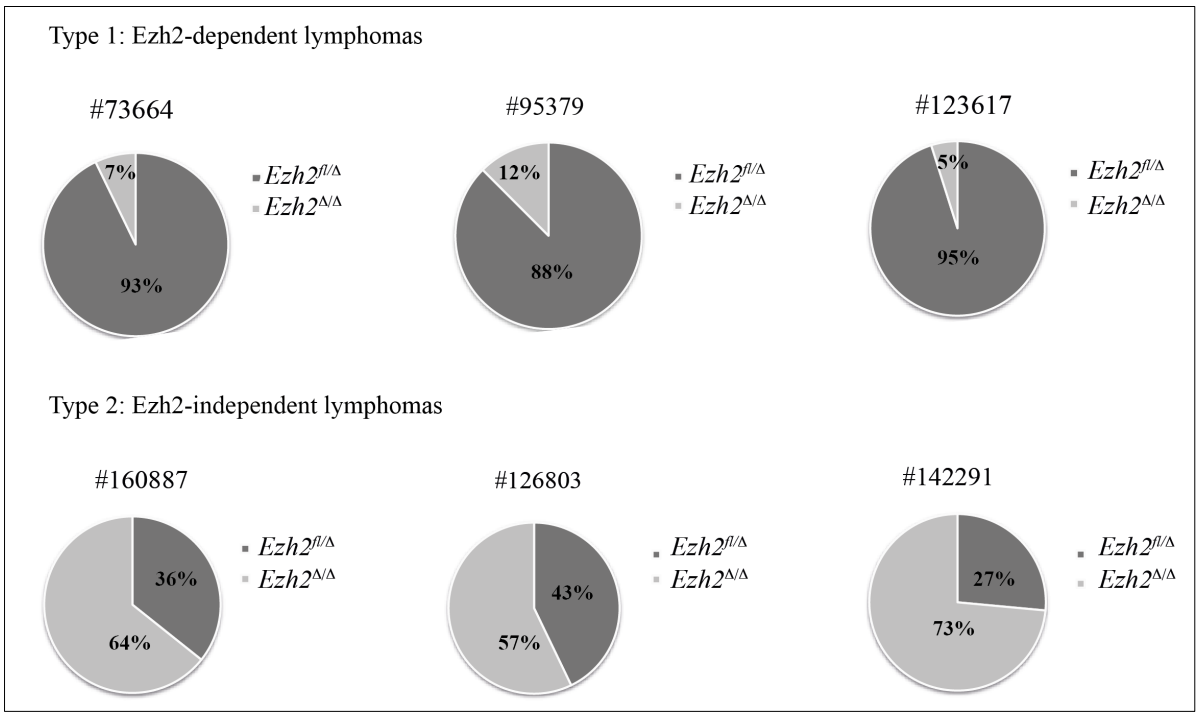

Figure 19: Effects of Ezh2 inactivation on cloning efficiency of lymphoma cells defines two types of λ-MYC; Ezh2$^{fl/fl}$ lymphomas

Pie chart representation of the distribution of the indicated *Ezh2* genotypes among tumor clones established after TAT-Cre transduction of 6 independent primary λ-MYC; Ezh2$^{fl/fl}$ lymphomas. Numbers indicated frequency of clones with the relative *Ezh2* genotype.

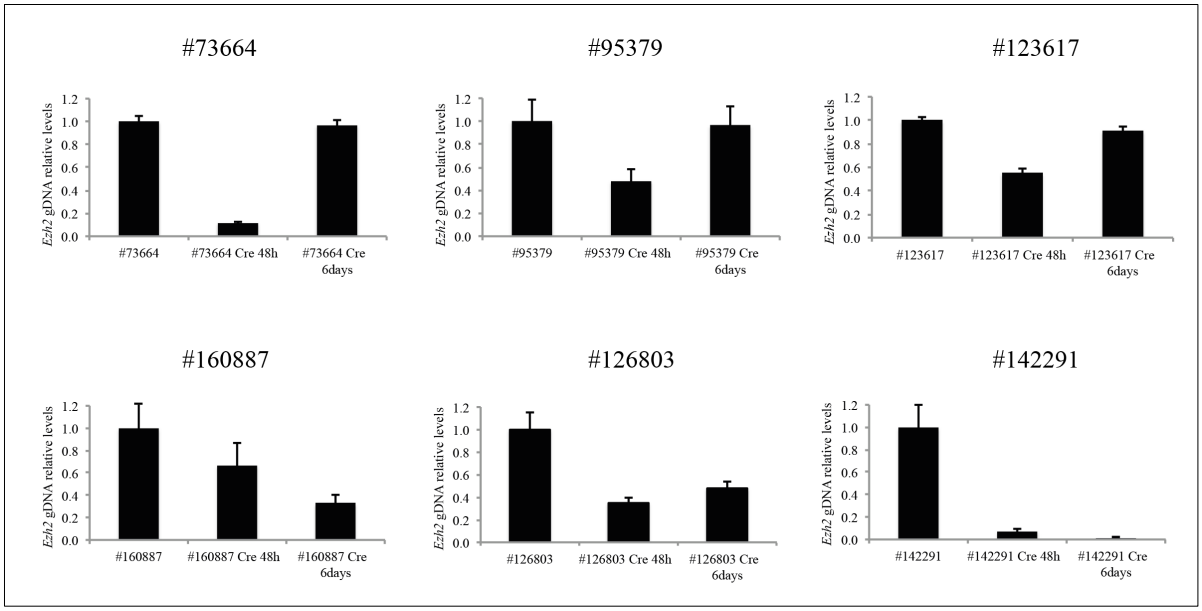

Figure 20: Effect of acute Ezh2 inactivation on short-term *in vitro* culture of λ-MYC; Ezh2$^{fl/fl}$ lymphomas

Representative qPCR quantification of WT *Ezh2* gene copy number in malignant B cells of the 6 independent λ-MYC; Ezh2$^{fl/fl}$ lymphomas at the indicated time points (48 hours and 6 days) after TAT-Cre transduction. *Ezh2* gene copy in tumor B cells was assessed after normalization for genomic input through the measurement of *Gapdh* copy number. Data are represented as *Ezh2* gene copy number relative to that of λ-MYC; Ezh2$^{fl/fl}$ lymphomas prior to TAT-Cre transduction (first column of each histogram plot). Columns indicate mean values of triplicates ± standard deviation (SD).

Despite the rapid counter-selection of Ezh2 mutant cells after TAT-Cre transduction of type-1 λ-MYC lymphomas, we succeeded to isolate a restricted number of subclones carrying two inactive copies of the *Ezh2* gene (Figure 19). This result indicates that a small subset of lymphoma cells succeeded to activate compensatory mechanisms to circumvent the loss of Ezh2 methyltransferase activity. To investigate whether the mechanism accounting for the resistance to Ezh2 inactivation resulted in restoration of H3K27me3, we measured global H3K27me3 levels in representative Ezh2$^{\Delta/\Delta}$ subclones derived from type-1 λ-MYC lymphomas. Quantification of western blotting data revealed that type-1 lymphomas, acquiring resistance to Ezh2 inactivation, lost over 90 % of the initial H3K27me3 levels. Hence, compensation for Ezh2 inactivation in type-1 lymphomas does not require recovery

of global H3K27 trimethylation. Quantification of H3K27me3 levels was extended to a subclone of type-2 lymphoma. Global loss (>90 %) of H3K27me3 levels was observed in Ezh2 mutant cells, confirming the results obtained in Ezh2 defective λ-MYC type-1 lymphomas (Figure 21). All together these results indicate that global loss of H3K27 trimethylation is compatible with the growth of MYC-transformed B cells.

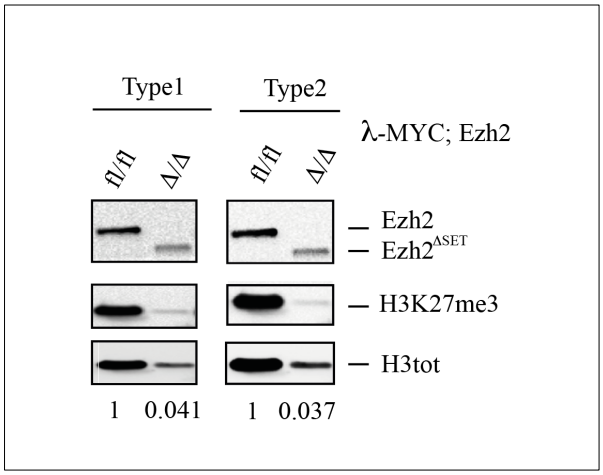

Figure 21: H3K27me3 levels in Ezh2 defective B cell lymphomas

Immunoblot analysis of Ezh2 and H3K27me3 levels in representative Ezh2 proficient (*Ezh2*$^{fl/fl}$) and catalytic-dead (*Ezh2*$^{\Delta/\Delta}$*)* tumor clones established after TAT-Cre transduction of Ezh2-dependent (type-1; #123617) and -independent (type-2; #126803) λ-MYC lymphomas. Histone H3 levels were assed to control protein input. Upon Cre-mediated deletion of SET coding exons, lymphoma cells express a truncated form of Ezh2 (Ezh2$^{\Delta SET}$). Numbers below plots indicate normalized H3K27me3 levels in the indicated tumor samples.

7.1.6 Comparison of the *in vitro* growth properties of type-1 and -2 λ-MYC lymphomas

The different requirement for Ezh2 methyltransferase activity featured by type-1 and type-2 λ-MYC lymphomas prompted us to test whether such differences could depend on the growth properties of tumor cells belonging to the two categories of tumors. To test this hypothesis, we compared the *in vitro* growth behavior of representative cases of type-1 and type-2 lymphomas. Tumor cells were counted over a 14 days time interval, diluting the cells

every second day in fresh culture medium. Growth curve analyses revealed a very similar *in vitro* growth behavior between type-1 and type-2 lymphomas (Figure 22). These results were confirmed by cell cycle distribution analysis of lymphoma cells belonging to the two categories of λ-MYC tumors (Figure 23). All together these results indicate that *in vitro* growth analyses based on bulk cultures of type-1 and type-2 lymphomas do not allow to distinguish MYC-driven lymphomas that differ in the requirement for Ezh2 methyltransferase activity.

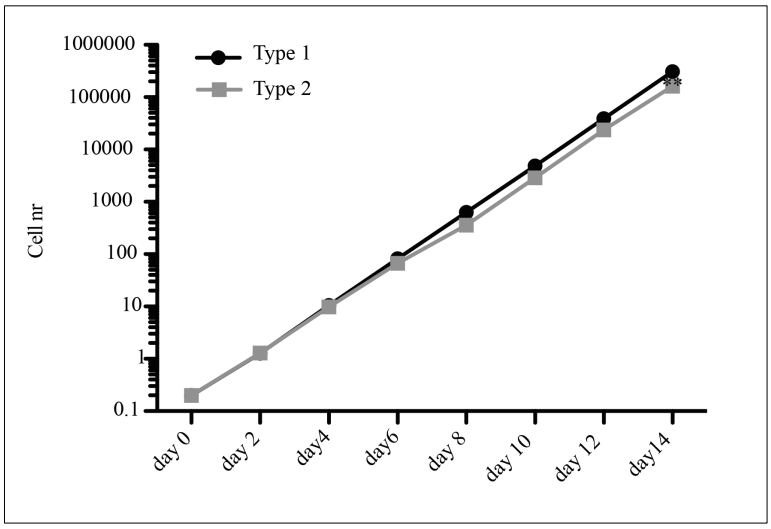

Figure 22: *In vitro* growth curves of Ezh2-dependent or independent lymphomas

Growth curve analysis of representative Ezh2-dependent (type-1, black line; #73664) and -independent (type-2, grey line; #160887) lymphomas cultured *in vitro* for 14 days. Tumor cells were counted every second day. Each time point represents the average count of 3 technical replicates ± Standard error (SE).

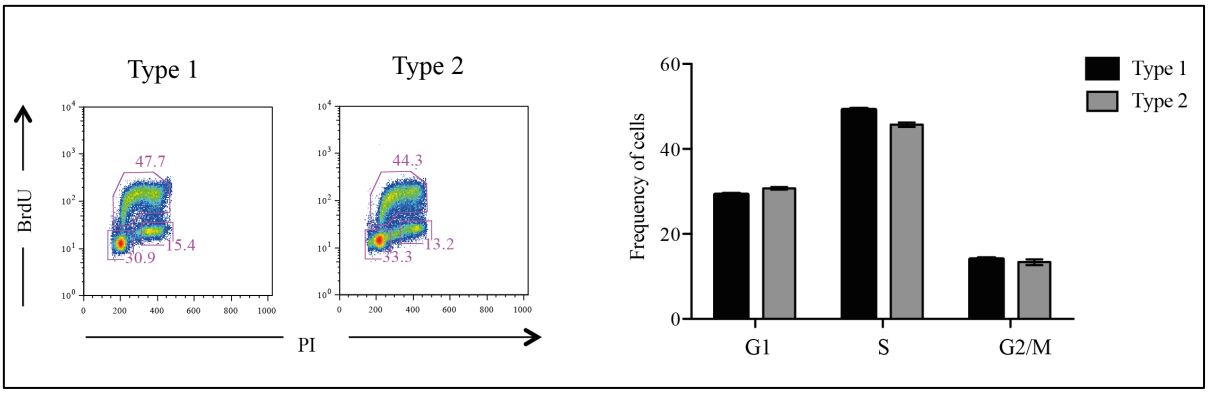

Figure 23: Cell cycle distribution analysis of Ezh2-dependent and -independent λ-MYC lymphomas

Representative flow cytometric analysis at day 6 of the cell cycle distribution of Ezh2-dependent (type-1; #73664) or -independent (type-2; #160887) tumors. Numbers indicate frequency of cells in boxed gates. Bar graph summarizes cell cycle distribution analyses obtained from 3 technical replicates (±SE) of representative Ezh2-dependent (type-1, black bar; #73664) and -independent lymphomas (type-2, grey bar; #160887).

7.1.7 Identification of a transcriptional signature clustering type-1 from type-2 lymphomas

We hypothesized that the different requirement of type-1 and type-2 lymphomas for Ezh2 could reflect distinct transcriptional networks active in the two categories of tumors. For this purpose, we searched for genes that were differentially expressed between type-1 (n= 3) and type-2 (n= 3) lymphomas. Comparison of RNA sequencing data allowed the identification of 351 differentially expressed genes (DEGs). Of these, 163 were down-regulated and 188 were up-regulated in type-2 lymphomas as compared to type-1 tumors (Figure 24).

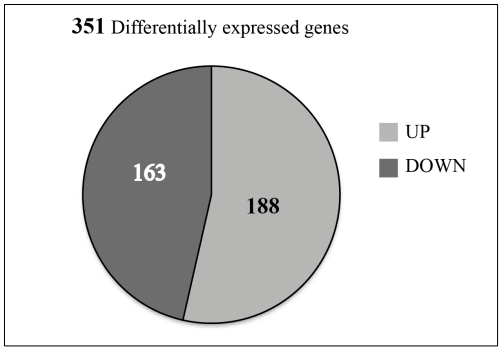

Figure 24: Differentially expressed genes in type-1 versus type-2 λ-MYC lymphomas
Pie chart representation of genes (nr.) that are respectively up- and down-regulated (FDR q value ≤ 0.05) in a consistent fashion (3 out of 3 tumors) in Ezh2-independent (type-2: #126803, #160887, #142291) lymhomas in comparison to Ezh2-dependent (type-1: #73664, #95379, #123617) λ-MYC lymphomas.

We performed a further filtering of the list of DEGs to ultimately select a subset of them (n= 166) with the best consistency when comparing three lymphomas of the first type to the same number of the second type (Figure 25). Among the core signature of 166 genes, 119 were up-regulated and 47 were down-regulated in type-2 lymphomas.

To assess whether DEGs belonged to specific functional categories, we performed gene ontology analysis on the core signature of 166 genes differing between type-1 and type-2 lymphomas (Figure 26). Interestingly, type-2 lymphomas expressed higher levels of cell cycle genes, as Cyclin-D2 (*Ccnd2*) and genes encoding for critical components of the DNA replication machinery, including Minichromosome maintenance complex component 2 and 4 (*Mcm2*, *Mcm4*) and DNA Primase 2 (*Prim2*). Furthermore, type 2 tumors significantly expressed higher levels of the pro-survival factor B cell lymphoma 2 (*Bcl2*) (Figure 27).

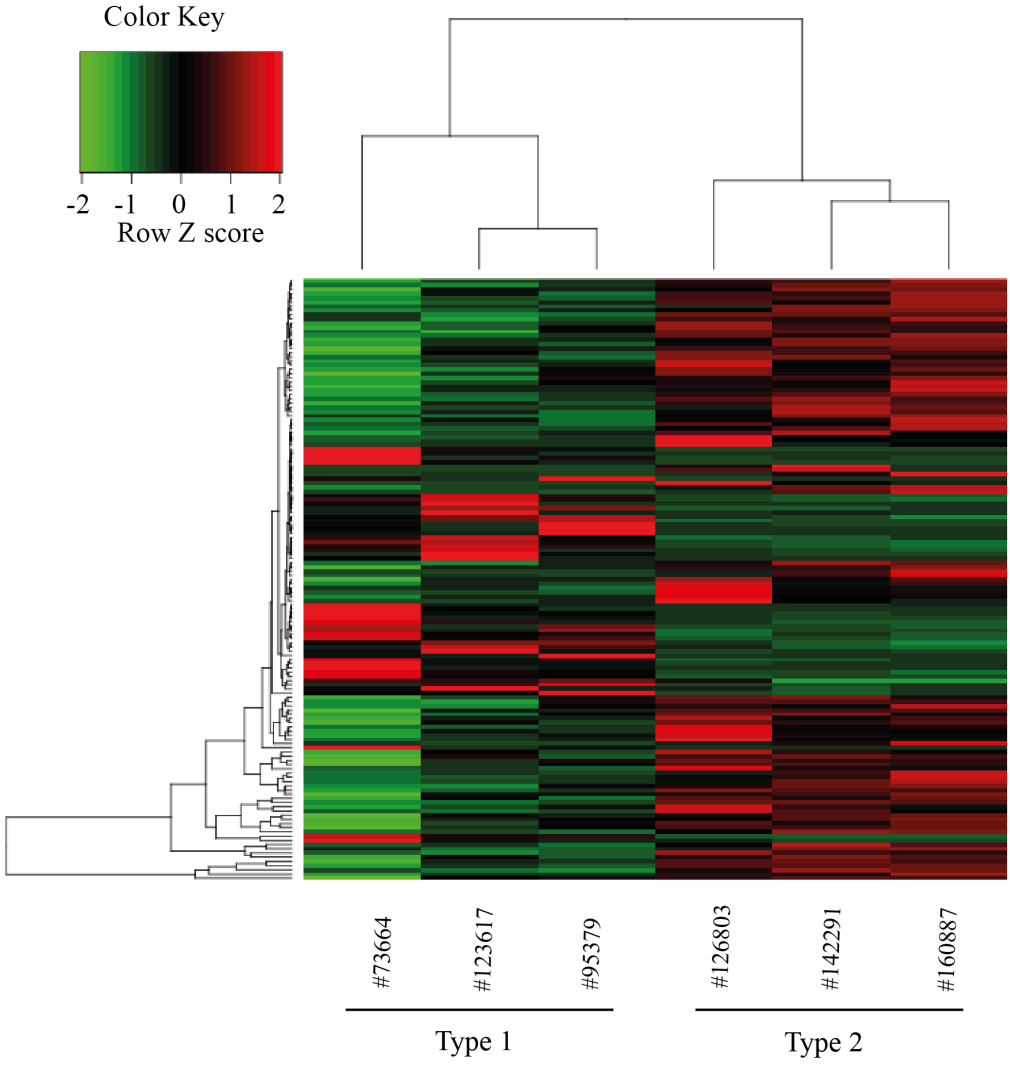

Figure 25: Expression pattern in type-1 and type-2 λ-MYC; Ezh2$^{fl/fl}$ lymphomas

Heat map representation of genes (n= 166) differentially expressed between Ezh2-dependent (type-1: #73664, #123617, #95379) and -independent (type-2: #142291, #126803, #160887) λ-MYC; Ezh2$^{fl/fl}$ lymphomas, selected according to fold change ≥2 and FDR qvalue< 0.05.

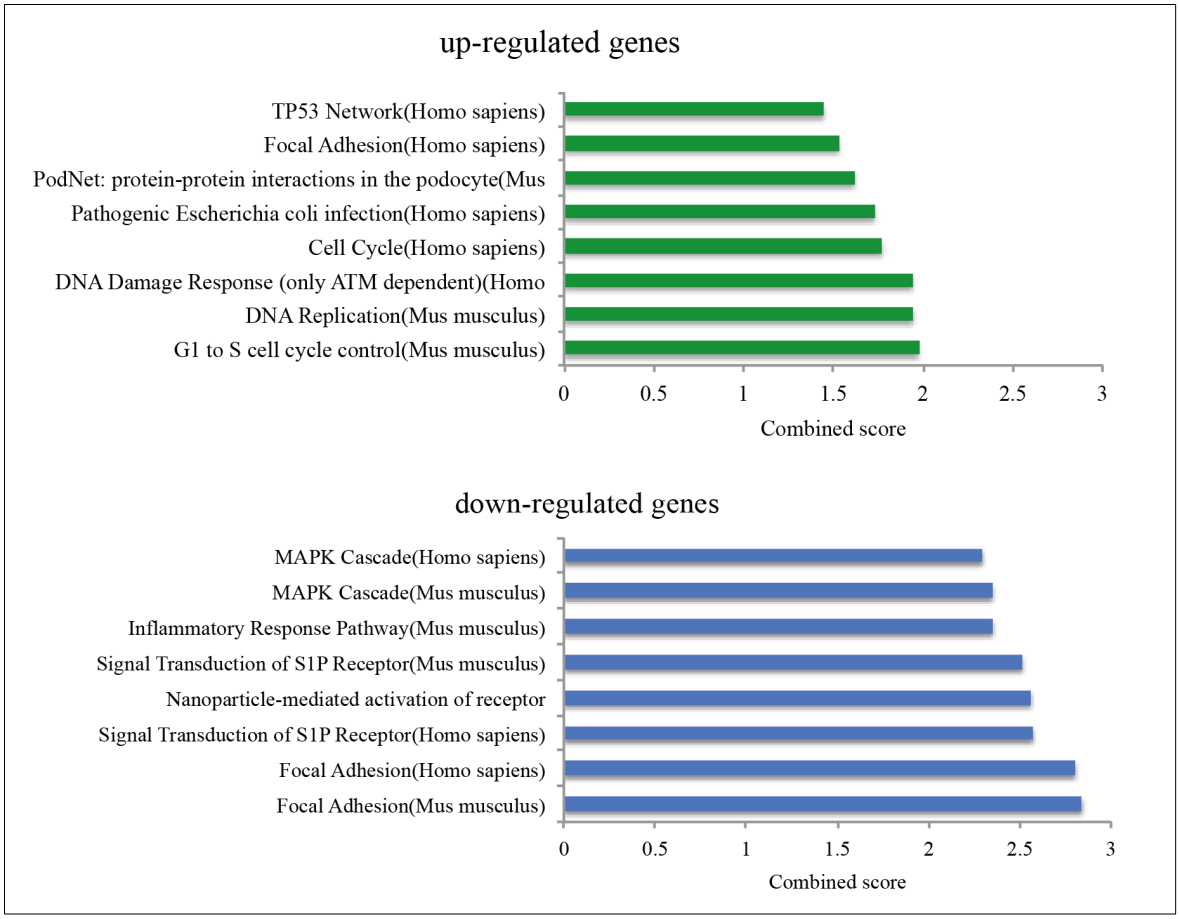

Figure 26: Functional categories of genes differentially expressed between type-1 and type-2 λ-MYC lymphomas

Wiki-pathway of top-8-enriched categories of genes up- (green bars) and down-regulated (blue bars) in Ezh2-independent lymphomas (n= 3) compared to their -dependent counterparts (n= 3), respectively. Analysis was performed using EnrichR software tool

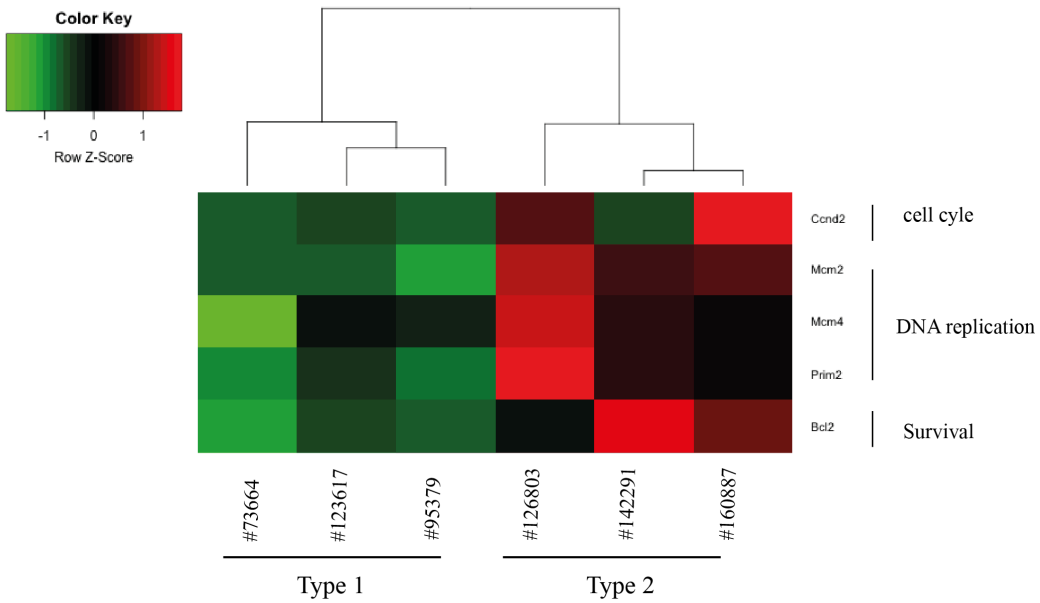

Figure 27: Minisignature of differentially expressed genes in type-1 and type-2 λ-MYC lymphomas

Heat map representation of expression levels of selected genes differentially expressed between type-1 and type-2 λ-MYC lymphomas (Fold change ≥ 2; FDR q value ≤0.05).

7.1.8 Can *Cdkn2a* and/or *Tp53* status discriminate type-1 from type-2 lymphomas?

Inactivation of tumor suppressor Cdkn2a represents a recurrent genetic lesion cooperating with deregulated MYC expression, in promoting B cell lymphomas (Schmitt et al., 1999). The *Cdkn2a* locus encodes for the cyclin-dependent kinase inhibitor $p16^{INK4a}$ and for $p19^{ARF}$, which triggers p53-dependent apoptosis by preventing its interaction with Murine double mutant 2 (Mdm2). Cdkn2a inactivation observed in tumor cells facilitates at the same time cell cycle progression and protection from p53-dependent apoptosis. Given the critical role exerted by the Polycomb axis in the negative regulation of the *Cdkn2a* locus (Bracken et al., 2007), we determined the functional status of Cdkn2a in type-1 and type-2 λ-MYC lymphomas, respectively. Genomic PCR using oligonucleotides annealing to the *Cdkn2a* locus revealed consistent retention of the locus in all tested λ-MYC type-1 lymphomas (n=

3). Instead, 1 of 3 type-2 lymphomas (#160887) showed bi-allelic loss of the *Cdkn2a* locus (Figure 28). The presence of genomic DNA in all samples was assessed by the amplification of *Gapdh* gene (data not shown). Moreover, transcriptome data identified an additional type-2 λ-MYC tumor (#142291), which displayed transcriptional silencing of the *Cdkn2a* locus (Figure 29). Hence despite the limited number of tumors so far analyzed, we observed a clear distinction between type-1 lymphomas that retained the tumor suppressor and Polycomb target locus *Cdkn2a* and type-2 lymphomas, which inactivated/silenced the tumor suppressor in 2 out of 3 cases.

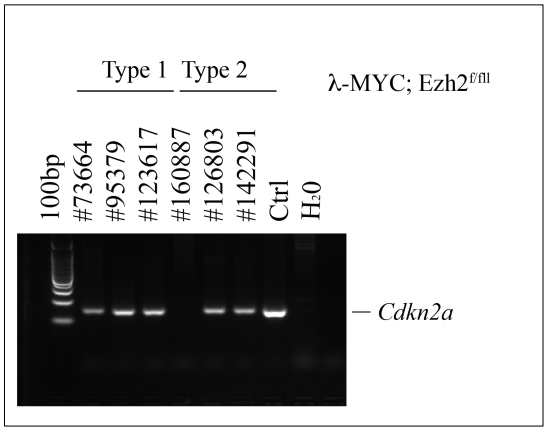

Figure 28: *Cdkn2a* gene status in λ-MYC; Ezh2$^{fl/fl}$ B cell lymphomas

Genomic PCR genotyping of the *Cdkn2a* locus in type-1 (n= 3) and type-2 (n= 3) λ-MYC; Ezh2$^{fl/fl}$ B cell lymphomas. The 100 bp ladder was used as reference to determine the size of PCR products.

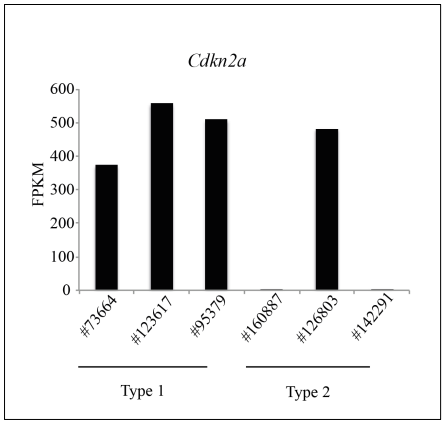

Figure 29: *Cdkn2a* mRNA levels in λ-MYC; Ezh2$^{fl/fl}$ B cell lymphomas

Quantification of *Cdkn2a* transcripts in the indicated lymphomas classified based on Ezh2 dependence (type-1: Ezh2-dependent and type-2: Ezh2 independent), as assessed by RNA-sequencing. Transcript levels are represented as fragments per kilobase of transcript per million mapped reads (FPKM) values.

Together with *Cdkn2a*, *Tp53* is the other most common tumor suppressor gene lost in MYC-driven lymphomas (Evan et al., 1992; Meyer et al., 2006; Schmitz et al., 2012). Therefore, we tested the functional integrity of the *Tp53* locus by treating λ-MYC lymphomas with the Mdm2 inhibitor nutlin (Tovar et al., 2006). Specifically, lymphoma cells were exposed to increasing doses of nutlin *in vitro* and cell viability assessed by PI staining. Three out of three type-1 lymphomas displayed nutlin resistance, indicating the acquisition of inactivating *Tp53* mutations. Instead, two out of three type-2 lymphomas were sensitive to nutlin treatment (Figure 30). In accordance with the established mutual exclusivity between Tp53 and Cdkn2a inactivation in tumor cells, type-2 lymphomas lacking functional Cdkn2a (two out of three cases) retained a functional Tp53 locus. These results will be further validated performing a genomic PCR analysis to discriminate the identity of p53 mutations in different lymphomas.

All together these results identify a possibly link between the persistence of a functional Cdkn2a locus in lymphoma cells and their dependence on Ezh2 to give rise to a tumor

starting from a single cell. Instead, tumors that have lost *Cdkn2a* during malignant transformation display limited dependence on Ezh2, when grown at low density.

Combining the data on the Cdkn2a and Tp53 locus, it appears that all tested λ-MYC lymphomas display inactivation of the Tp53-driven apoptosis, regardless of their dependence on Ezh2 catalytic activity.

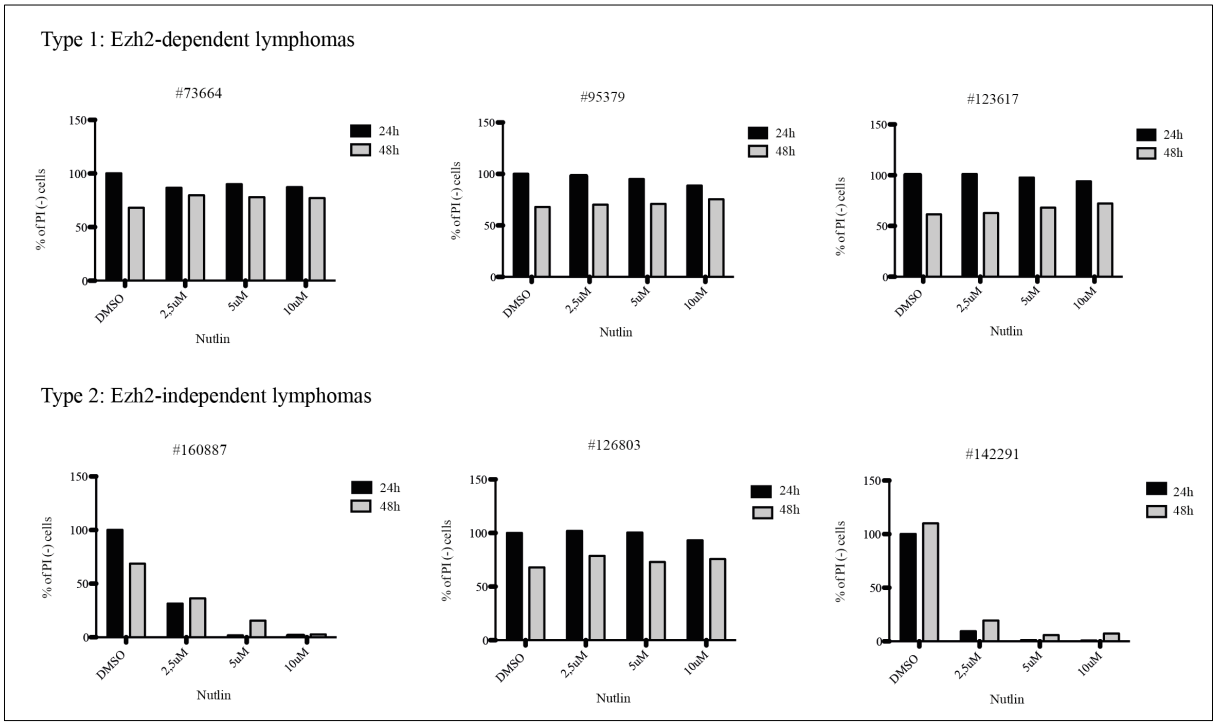

Figure 30: Differential sensitivity of λ-MYC; Ezh2$^{fl/fl}$ B cell lymphomas to the Mdm2 inhibitor nutlin

Flow cytometric assessment of cell viability revealed by PI staining in type-1 (#73664, #123617, #95379) and type-2 (#160887, #126803 and #142291) λ-MYC; Ezh2$^{fl/fl}$ lymphomas, at 24 hours (24h) (black) and 48 hours (48h) (grey bar), after treatment with increasing doses (2.5, 5 and 10 μM) of the Mdm2 inhibitor nutlin, respectively. Vehicle-treated (DMSO) tumor cells were used as reference.

7.2 Characterization of Ezh2 mutant lymphomas

7.2.1 Immunophenotypic characterization of Ezh2 mutant lymphomas

The establishment of Ezh2 mutant clones from both type-1 and type-2 lymphomas underscores the property of MYC lymphoma cells to overcome the inactivation of a main epigenetic determinant regulating cell identity, proliferation, survival and differentiation.

In the attempt to establish whether Ezh2 mutant cells underwent major epigenetic reprogramming, we performed a comprehensive flow cytometric analysis to unveil possible changes in their surface phenotype. For this analysis, we performed a side-by-side comparison between representative Ezh2 proficient and defective subclones.

Ezh2 mutant clones retained the pan B cell marker B220 and expressed levels of the other B cell markers to an extent similar to that of Ezh2 proficient tumor cells. An exception is represented by the chemokine receptor (Cxcr) 4, which was expressed at substantially higher levels in most Ezh2 mutant subclones when compared to their proficient counterparts (Figure 31). All together these results indicate that Ezh2 defective MYC-driven lymphomas retain a remarkably stable immunophenotype, despite suffering from a massive loss in H3K27me3 levels.

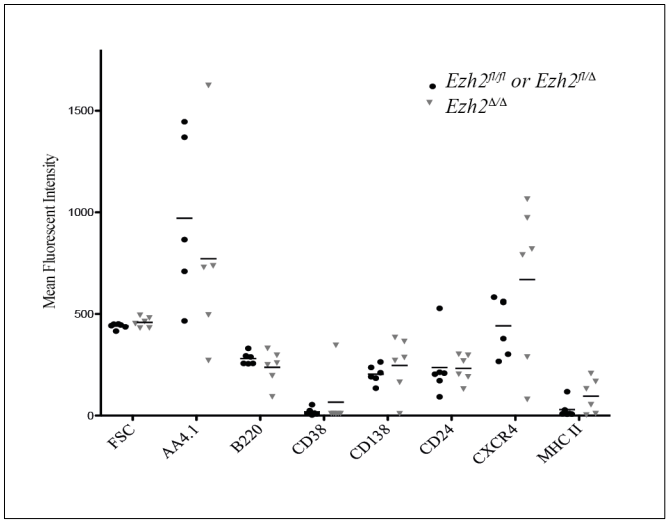

Figure 31: Comparison of the immunophenotype of Ezh2 proficient and defective λ-MYC lymphoma clones

Scatter plot chart showing expression levels (mean fluorescence intensity) of the indicated surface markers in λ-MYC; Ezh2 proficient (*Ezh2*$^{fl/fl}$ or *Ezh2*$^{fl/\Delta}$) (black filled dot, n= 5) and mutant (*Ezh2*$^{\Delta/\Delta}$) (grey filled dot, n= 6) clones established from a type-1 λ-MYC lymphoma (#73664). Each dot represents one independent measurement.

7.2.2 Effects of Ezh2 inactivation on λ-MYC lymphomas growth *in vitro*

To assess the effects of functional Ezh2 inhibition on the proliferative potential of λ-MYC lymphomas, we performed *in vitro* growth curve analysis comparing Ezh2 proficient subclones to their mutant counterparts, both established from the same primary lymphoma. For these studies, we chose to focus on subclones established from type-1 lymphomas, as they could help revealing the mechanisms through which MYC tumors overcome the loss of Ezh2. Monitoring the *in vitro* growth property of independent Ezh2 mutant subclones revealed a comparable behavior to that of Ezh2 proficient tumors (Figure 32). In accordance with this result, cell cycle distribution analyses failed to detect obvious differences between Ezh2 proficient and defective tumors (Figure 33). Together, these findings suggest that the rare Ezh2 mutant subclones, generated from type-1 lymphomas, may select compensatory mechanisms that ensure normal growth of tumor cells *in vitro*.

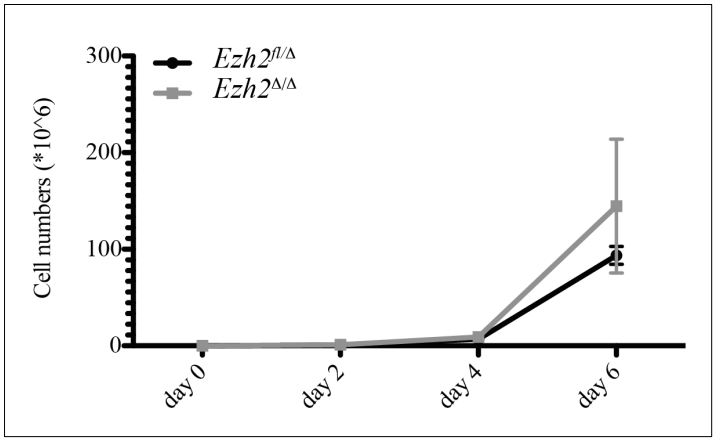

Figure 32: Ezh2 inactivation is compatible with lymphoma growth *in vitro*

Growth curve of representative Ezh2 proficient (*Ezh2*$^{fl/\Delta}$, black line, n= 3) and mutant (*Ezh2*$^{\Delta/\Delta}$, grey line, n= 3*)* tumor clones established *in vitro,* from a representative type-1 (#73664) λ-MYC primary tumor. Tumor cells were counted every second day. Cells were cultured for the indicated time points. Each symbol represents the average value of 3 measurements (±SE).

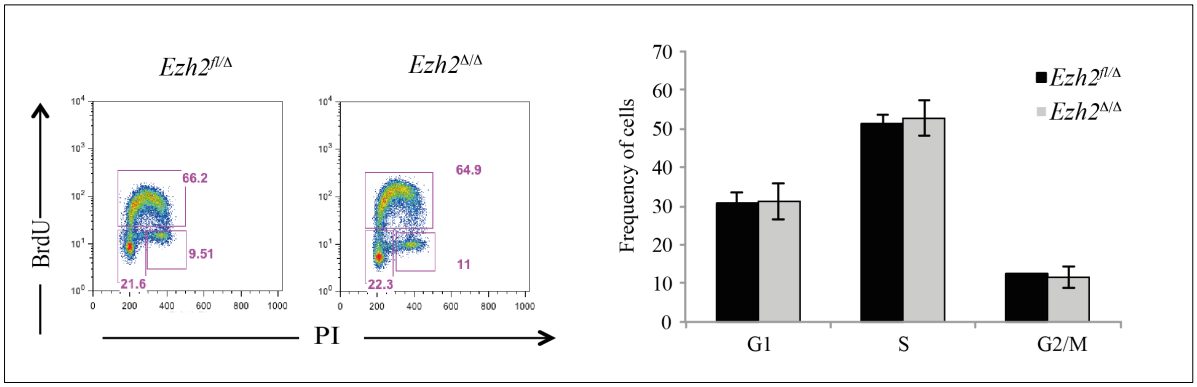

Figure 33: Ezh2 inactivation does not affect cell cycle progression in λ-MYC lymphomas

Flow cytometric analysis cell cycle distribution of representative Ezh2 proficient (*Ezh2*$^{fl/\Delta}$) and mutant (*Ezh2*$^{\Delta/\Delta}$) clones. Numbers within dot plots indicate frequency of boxed cells. Bar graph shows a summary of the flow cytometric data obtained from independent (n=3 per genotype) Ezh2 proficient (*Ezh2*$^{fl/\Delta}$, black bar) and mutant (*Ezh2*$^{\Delta/\Delta}$, grey bar*)* clones (±SE), established from a representative type-1 (#73664) λ-MYC lymphoma.

7.2.3 Ezh2 mutant lymphomas can expand *in vivo*

To verify whether inactivation of Ezh2 influenced the ability of λ-MYC lymphomas to grown *in vivo*, we performed transplantation studies. Specifically, representative Ezh2 proficient and mutant subclones, established from both type-1 and type-2 lymphomas, were injected intravenously into immunoproficient syngenic animals. Recipient animals were monitored over time for the development of secondary tumors. Tumor cells, efficiently engrafted in recipient animals, leading to the rapid worsening of the general health status of the animals. The expansion of tumor cells *in vivo* was not affected by Ezh2 status (Figure 34). Importantly, mice receiving Ezh2 mutant tumors derived from type-2 lymphomas became sick substantially faster than those transplanted with type-1 lymphomas (15 vs. 26 days post-transplantation; Figure 34).

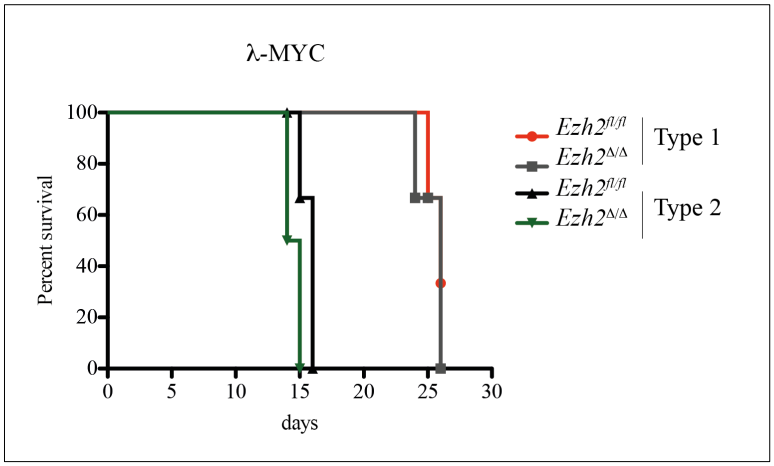

Figure 34: Ezh2 mutant lymphomas expand *in vivo* upon transplantation into immunoproficient syngenic recipients

Kaplan-Meier plots representing survival of animals (n= 3) receiving Ezh2 proficient (*Ezh2*$^{fl/fl}$, red line) and mutant (*Ezh2*$^{\Delta/\Delta}$, grey line) clones isolated from type-1 (#73664) and Ezh2 proficient (*Ezh2*$^{fl/fl}$, black line) and mutant (*Ezh2*$^{\Delta/\Delta}$, green line) clones from type-2 (#160887) λ-MYC lymphomas, respectively.

To confirm the identity of the injected tumors, we quantified *Ezh2* gene copy number on tumor cells retrieved from diseased animals. The analysis confirmed that mice injected with Ezh2 mutant subclones suffered from aggressive lymphomas, entirely consisting of Polycomb mutant cells (Figure 35). All together these results reveal that Ezh2 mutant lymphomas derived from both type-1 and type-2 lymphomas give rise to aggressive secondary tumors when injected into immunoproficient animals. Moreover, the faster tumor progression observed for type-2 lymphomas (regardless of Ezh2 genotype) provides the first functional indication of the existence of two different types of λ-MYC lymphomas.

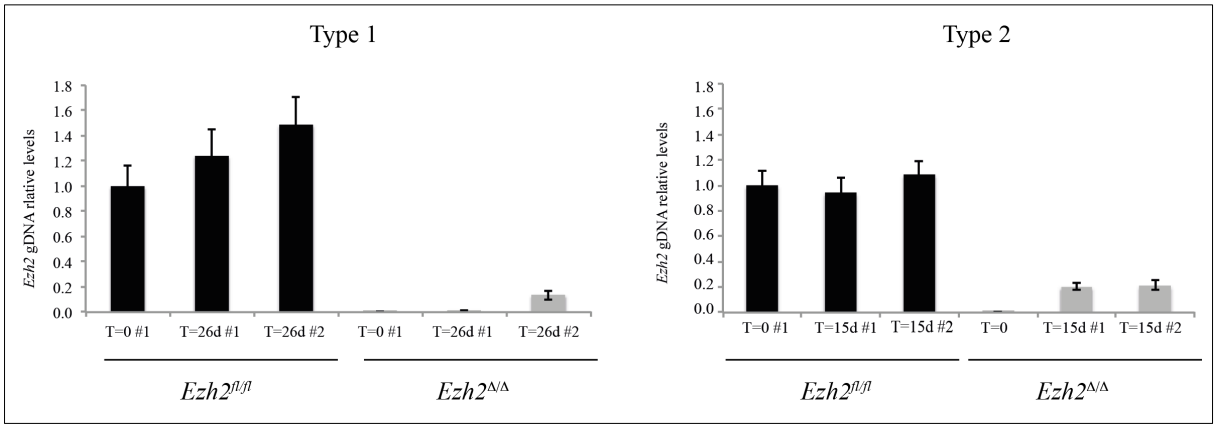

Figure 35: Assessment of *Ezh2* gene status in λ-MYC lymphomas retrieved after transplantation

qPCR quantification of *Ezh2* gene copy number in lymphoma cells prior to transplantation (T= 0) or retrieved from recipient animals 15-26 days (15d/26d) after transfer. Lymphoma clones with the indicated genotype and established from both representative type-1 (#73664) and type-2 (#160887) λ-MYC lymphomas were analyzed. Hash mark (#) refers to each recipient mouse transplanted with Ezh2 proficient or deficient clones. *Ezh2* gene copy number in tumor samples was determined after normalizing samples for DNA input assessed through the quantification of an unrelated gene (*Gapdh)*. Data are represented relative to *Ezh2* gene copy number in λ-MYC; $Ezh2^{fl/fl}$ primary lymphoma cells prior to transplantation.

7.2.4 Ezh2 mutant lymphomas retain residual H3K27me3 and express the Ezh1 paralog

The ability of Ezh2 defective clones to grow in a comparable fashion to their proficient counterparts both *in vitro* and *in vivo* indicated the existence of possible compensatory mechanisms sustaining the malignant phenotype of Polycomb mutant tumor B cells. Western blotting assessment of H3K27me3 levels in Ezh2 mutant subclones, derived from both type-1 and type-2 lymphomas, indicated that residual amounts (between 5 and 10 %) of H3K27me3 were consistently detected in Polycomb mutant lymphoma cells (Figure 21). This result raised the hypothesis that a different methyltransferase could at least partially substitute for Ezh2 inactivation in lymphoma B cells. In search for the latter enzyme, we focused our attention on the Ezh2 paralog, Ezh1. Ezh1 displays a substantially weaker H3K27 methytransferase activity than Ezh2 (Margueron et al., 2008; Shen et al., 2008), which has been shown to replace that of Ezh2 in various *in vivo* settings (Ezhkova et al., 2011; Fragola et al., 2013; Hidalgo et al., 2012). We quantified by qRT-PCR the transcript levels of Ezh1 in both Ezh2 proficient and defective lymphomas. *Ezh1* transcript could be successfully detected in λ-MYC lymphomas (Figure 36), compared to protein levels that were not analyzed due to the lack of an optimal antibody. Moreover, the loss of Ezh2 was associated to a modest, yet consistent, increase in Ezh1 transcript levels, pointing to a possible compensatory response of the lymphoma B cells (Figure 36). These data indicate that, upon inactivation of the main catalytic subunit of PRC2, MYC-driven B cell lymphomas retain residual H3K27me3 levels, possibly contributed by the Ezh2 paralog, Ezh1.

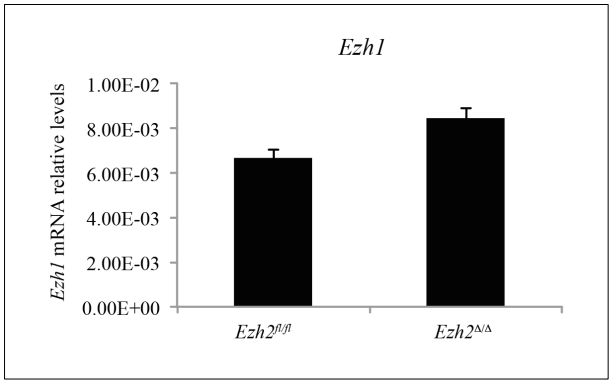

Figure 36: λ-MYC lymphomas express the *Ezh1* gene irrespective of Ezh2 status

Quantification by qRT-PCR of *Ezh1* transcripts in representative Ezh2 proficient (n= 3, $Ezh2^{fl/fl}$) and defective (n= 3, $Ezh2^{\Delta/\Delta}$) clones, established from a type-1 (#73664) λ-MYC lymphoma. *Ezh1* mRNA levels were normalized to those of the housekeeping *Rplp-0* gene.

7.2.5 Ezh2 mutant type-1 lymphomas are sensitive to combined Ezh1/2 inactivation

To assess whether Ezh1 could compensate for the loss of Ezh2 in type-1 λ-MYC lymphomas, we took advantage of the recently described Ezh1/2 double inhibitor, UNC1999 (Konze et al., 2013). First, we measured the short-term *in vitro* effects of UNC1999 on the viability of 3 Ezh2 proficient type-1 λ-MYC lymphomas. We observed a dose-dependent reduction in tumor cell number for all three lymphomas, yet to a different extent (Figure 37).

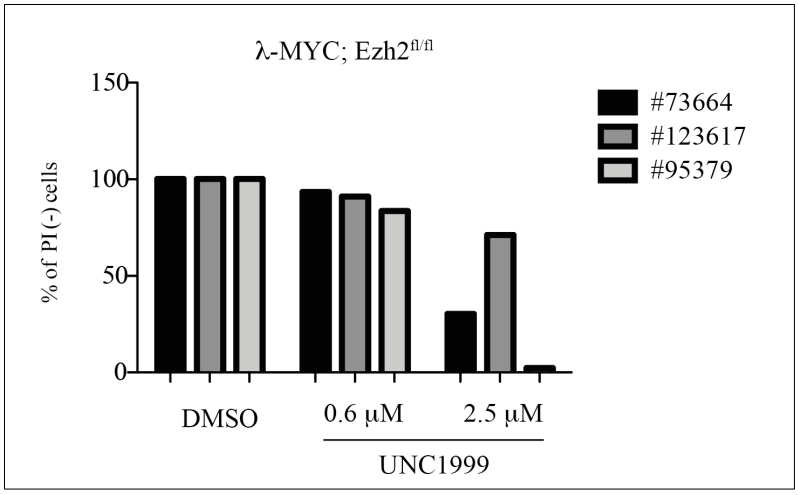

Figure 37: Response of λ-MYC; Ezh2$^{fl/fl}$ to the Ezh1/2 inhibitor UNC1999

Histograms showing proportion of viable (PI$^-$) lymphoma cells belonging to type-1 (n=3) λ-MYC; Ezh2$^{fl/fl}$ tumors 48 hours after exposure to either vehicle (DMSO) or to indicated doses of UNC1999.

Next, we tested whether UNC1999 could still interfere with *in vitro* growth of tumor subclones that had undergone Ezh2 inactivation. In the latter tumors, we hypothesized that Ezh1 replaced Ezh2 function to sustain tumor expansion. Growth curve analysis performed over a period of 10 days of treatment with UNC1999 revealed a significant *in vitro* growth retardation of Ezh2 mutant subclones that received the UNC1999 treatment (Figure 38). This result supports the model whereby acute loss of Ezh2 function in type-1 lymphomas selects in rare cells a compensatory mechanism centered on the methyltransferase activity of Ezh1.

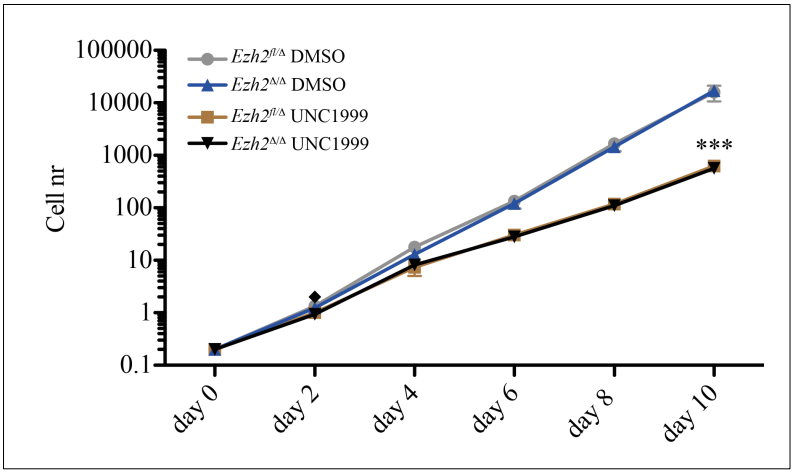

Figure 38: Ezh1/2 dual inhibition affects type-1 lymphomas growth *in vitro*

In vitro growth curves of representative Ezh2 proficient (*Ezh2*$^{fl/\Delta}$, grey line) and deficient (*Ezh2*$^{\Delta/\Delta}$, blue line) lymphoma subclones exposed either to vehicle (DMSO) or UNC1999 (2.5 μM) for 10 days. Clones were established from a representative type-1 (#73664) λ-MYC lymphoma. Tumor cells were counted every second day and each symbol represents the average cell count of 3 replicates (±SE). Statistical significance was calculating using Student's t test (***$p<0.001$).

To further validate this hypothesis, we measured H3K27me3 levels in Ezh2 proficient and mutant clones before and after UNC1999 treatment. The comparison by intracellular FACS analysis of H3K27me3 levels between Ezh2 proficient and deficient tumor subclones revealed a major loss of the histone mark in the latter lymphoma cells, in accordance with our own previous observations (Figure 21). Importantly, the treatment of a representative type-1 λ-MYC lymphoma with UNC1999 caused a reduction of H3K27me3 levels that appeared stronger than the one observed in tumor cells loosing Ezh2 (Figure 39). The data were to a large extent confirmed by western blotting quantification of residual H3K27me3 levels in Ezh2 proficient and defective subclones exposed for 2-6 days to UNC1999 (Figure 40).

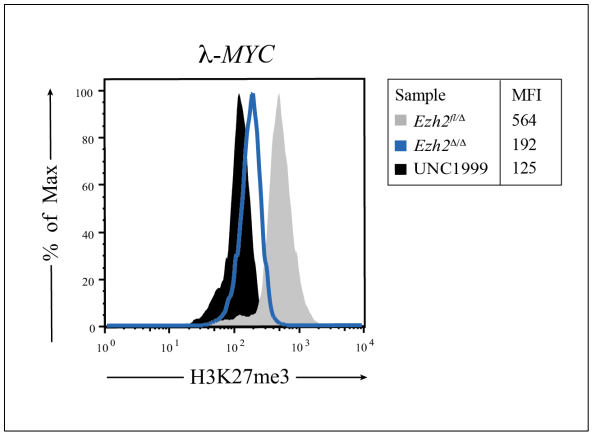

Figure 39: UNC1999 induces global loss of H3K27me3 in λ-MYC lymphomas

Intracellular flow cytometric determinantion of H3K27me3 levels in Ezh2 proficient λ-MYC lymphomas treated for 6 days with 2.5 μM of UNC1999 (black filled line) or DMSO (grey filled line), respectively. Ezh2 mutant cells (*Ezh2*$^{\Delta/\Delta}$) (blue line) were included as negative control. Clones were established from type-1 (#73664) λ-MYC lymphomas.

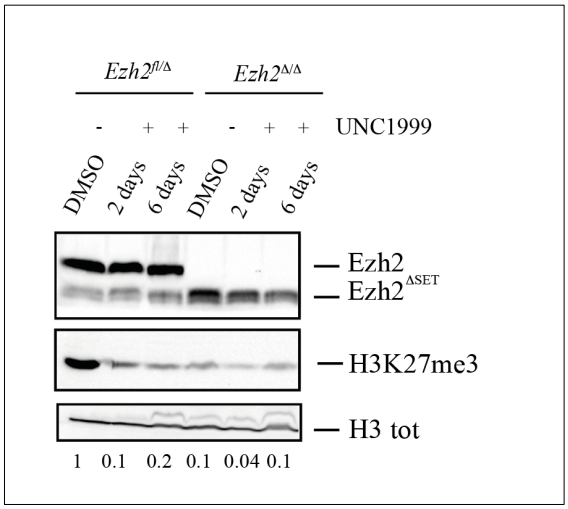

Figure 40: Quantification of H3K27me3 levels in UNC1999-treated lymphomas by immunoblotting analysis

Quantification by western blotting of global H3K27me3 levels in Ezh2 proficient (*Ezh2*$^{fl/\Delta}$) and mutant (*Ezh2*$^{\Delta/\Delta}$) lymphoma clones prior to, or at the indicated days of UNC1999 treatment (2.5 μM). Numbers indicate H3K27me3 levels after normalization for total H3 protein, used as input, and relative to vehicle-treated Ezh2 proficient cells. The lack of full-length Ezh2 protein confirms the identity of Ezh2 mutant cells.

Next, we assessed whether UNC1999 treatment could directly influence the expression of Ezh1. Quantification by qRT-PCR of *Ezh1* transcript in Ezh2 proficient and mutant subclones failed to detect significant changes of Ezh1 expression in response to UNC1999 treatment (Figure 41).

To establish the mechanisms through which combined Ezh1/2 inhibition interfered with the growth of both Ezh2 proficient and mutant type-1 lymphomas, we performed cell cycle distribution analysis. UNC1999 treatment did not cause major defects in cell cycle progression (Figure 42). Instead, we observed a significant increase in the fraction of sub-G1 apoptotic cells following combined Ezh1/2 inhibition (Figure 42). This result was true for both Ezh2 proficient and defective lymphoma B cells (Figure 42). Hence, in λ-MYC type-1 lymphomas PRC2 inhibition triggers a potent cytotoxic response. Moreover, our data suggest that inactivation of "canonical" PRC2 function, through the loss of Ezh2 methyltransferase activity, can be compensated by an alternative PRC2 complex consisting of Ezh1 as catalytic subunit.

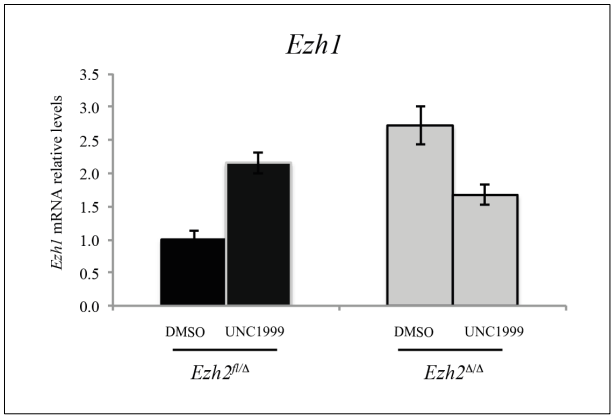

Figure 41: Expression of *Ezh1* in B cell lymphomas in response to UNC1999 treatment

qRT-PCR quantification of *Ezh1* transcripts in representative Ezh2 proficient ($Ezh2^{fl/\Delta}$, black filled bar, n= 2) and defective ($Ezh2^{\Delta/\Delta}$; grey filled bar, n= 2*)* lymphoma clones established from a representative type-1 tumor (#73664), cultured in vehicle-containing medium or in the presence of UNC1999 (2.5 μM). *Ezh1* levels were normalized to the housekeeping *Rplp-0* gene and represented as relative to those in Ezh2 proficient, vehicle-treated lymphoma cells.

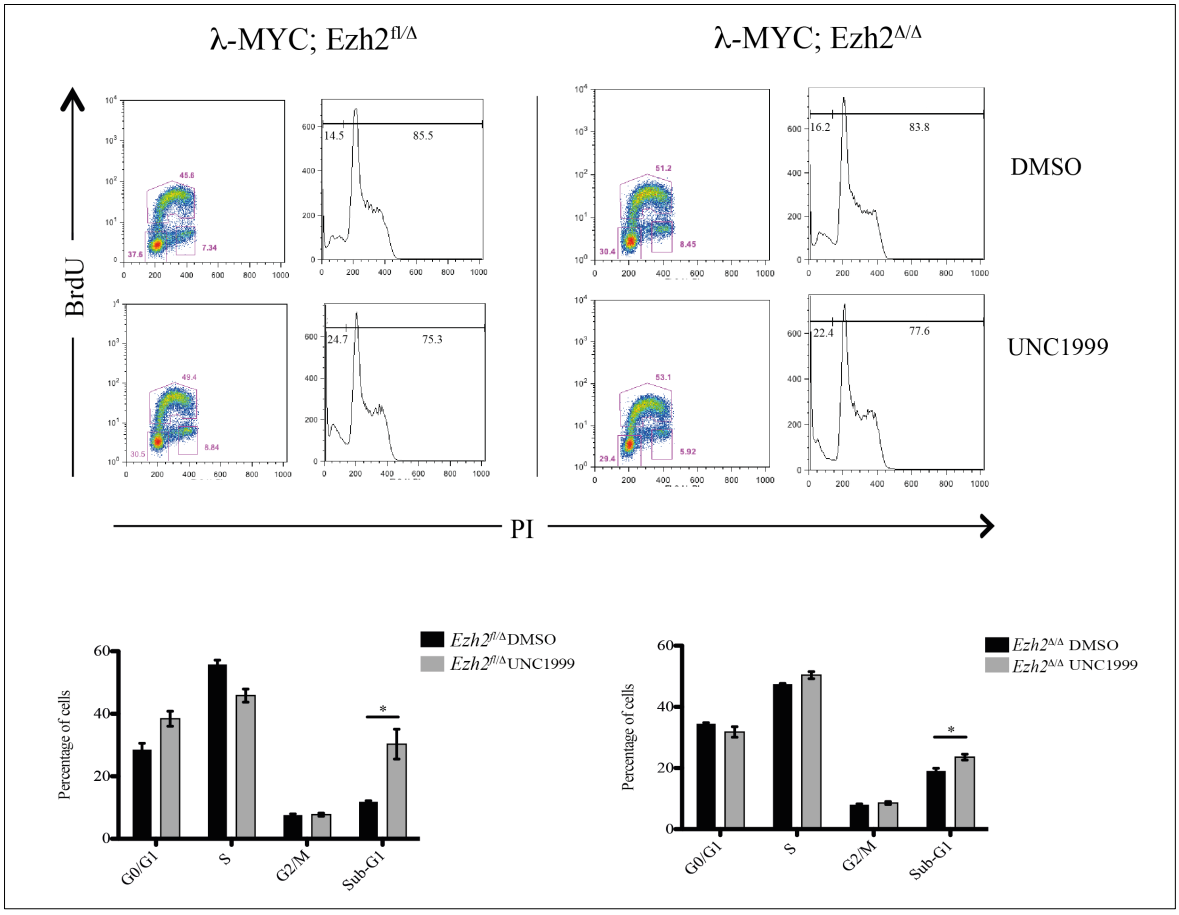

Figure 42: Ezh1/2 inhibition increases the death rate of λ-MYC lymphomas *in vitro*

Cell cycle distribution analysis of Ezh2 proficient (*Ezh2*$^{fl/\Delta}$) and mutant (*Ezh2*$^{\Delta/\Delta}$) clones established from a representative type-1 (#73664) lymphoma, after 6 days of treatment with UNC1999 (2.5 μM; grey bar). Vehicle-treated (DMSO; black bar) cells were used as comparison. Numbers within dot plots indicate frequency of boxed cells. Summary of cell cycle distribution data is shown below. UNC1999 leads to a significant (* p< 0,05, 2-Way-Anova statistical test) increase in the fraction of sub-G1 dead cells.

7.2.6 Is repression/silencing of Polycomb targets p21 and p16^{INK4a} associated with the acquisition of an Ezh2-independent phenotype in MYC lymphoma cells?

In an attempt to understand the mechanisms allowing the establishment of the rare Ezh2 mutant subclones derived from type-1 lymphomas, we hypothesized that tumor cells selected Ezh1 expression to ensure stable repression of tumor suppressors and Polycomb targets Cdkn1a/p21^{waf1} and p16^{INK4a}. To this end, we measured the effect of UNC1999 treatment on *p21* and *p16* expression in both Ezh2 proficient and defective subclones,

established from type-1 lymphomas. Transcript levels of both *p21* and *p16* were substantially elevated in Ezh2 mutant subclones, whereas their expression was repressed in Ezh2 proficient tumors (Figure 43). Moreover, treatment of lymphomas with UNC1999 led to a paradoxical reduction in *p16* and *p21* transcript levels in Ezh2 mutant tumor cells (Figure 43). These results exclude that the compensatory effect provided by Ezh1 in Ezh2 mutant subclones is exerted via repression of tumor suppressors $p16^{Ink4a}$ and $p21^{waf1}$.

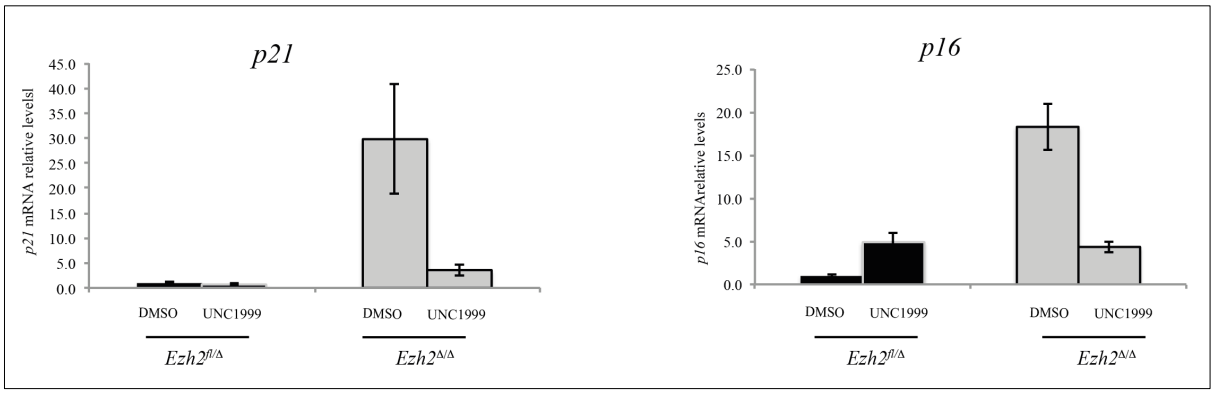

Figure 43: Expression of *CDK* inhibitors in λ-MYC lymphomas treated with UNC1999
Quantification by qRT-PCR of *Cdkn1a*/$p21^{waf1}$ and $p16^{INK4A}$ transcripts in representative Ezh2 proficient ($Ezh2^{fl/\Delta}$; black bar, n= 2) and deficient ($Ezh2^{\Delta/\Delta}$; grey bar, n= 2*)* clones, established from a type-1 (#73664) λ-MYC lymphoma, upon treatment with UNC1999 (2.5 μM). Lymphoma B cells treated with vehicle (DMSO) were used as control. Gene transcript levels were normalized to the housekeeping *Rplp-0* gene and represented as relative to those of vehicle-treated Ezh2 proficient lymphoma cells.

To further investigate a possible contribution of Cdkn2a silencing to the acquired resistance of type-1 lymphomas to Ezh2 inhibition, we subjected Ezh2 proficient and mutant subclones, established from a Cdkn2a proficient type-1 lymphoma, to *Cdkn2a* genotyping. Interestingly, whereas all Ezh2 proficient subclones retained the *Cdkn2a* locus, 1 out of 3 Ezh2 mutant clones underwent bi-allelic loss of the *Cdkn2a* locus (Figure 44). Moreover, growth curve analysis revealed that the Ezh2 mutant subclone acquiring loss of the *Cdkn2a* locus displayed a substantially higher proliferative potential when compared to its Cdkn2a

proficient counterparts and to Ezh2 proficient lymphoma cells (Figure 45). Hence, loss of *Cdkn2a* may represent one mechanism through which lymphoma cells circumvent acute inactivation of Ezh2, to ensure continuous tumor growth.

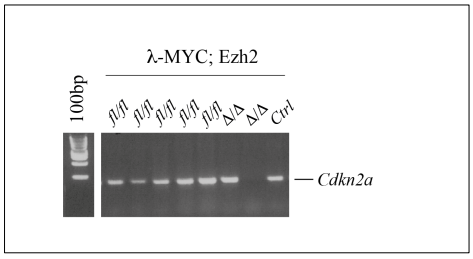

Figure 44: Status of the *Cdkn2a* locus in Ezh2 proficient and mutant lymphoma clones

Genomic PCR analysis to assess the status of the *Cdkn2a* locus in representative Ezh2 proficient ($Ezh2^{fl/fl}$) and mutant ($Ezh2^{\Delta/\Delta}$) clones established from type-1 (#73664) primary λ-MYC lymphomas that were used as control (Ctrl). Note that one of the two Ezh2 mutant clones has lost the *Cdkn2a* locus during clonal outgrowth starting from a single tumor cell.

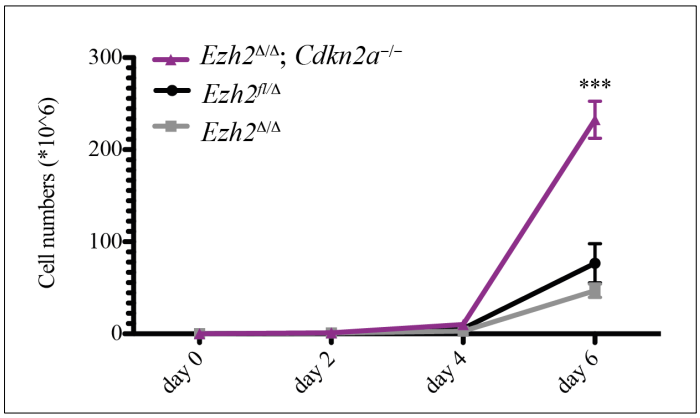

Figure 45: Loss of Cdkn2a contributes to increase proliferation of Ezh2 mutant lymphomas

Comparison of *in vitro* growth curves of Ezh2 mutant ($Ezh2^{\Delta/\Delta}$ grey line*)* lymphoma clones differing in the status of the *Cdkn2a* locus ($Ezh2^{\Delta/\Delta}$ vs. $Ezh2^{\Delta/\Delta}$*; Cdkn2a*$^{-/-}$), established from type-1 λ-MYC lymphoma (#73664). A representative Ezh2 proficient lymphoma clone was included in the analysis. Cells were counted at the indicated time points. Each symbol represents the average count of 3 replicates (±SE). Statistical significance was calculating using Student's t test (***$p<0.001$).

7.2.7 λ-MYC type-2 lymphomas are resistant to combined Ezh1/2 inhibition

The high recovery rate of Ezh2 mutant subclones after TAT-Cre transduction of type-2 lymphomas suggested a dispensable role for the Polycomb protein in clonal growth starting from single cells. The resistance of type-2 lymphomas to Ezh2 loss could depend on efficient compensation provided by Ezh1. To test this hypothesis, we exposed type-2 lymphomas to increasing doses of UNC1999. Short-term *in vitro* cultures revealed a surprising resistance of type-2 lymphomas to combined Ezh1/2 inhibition (Figure 46). To determine the effect of UNC1999 on the methyltransferase activities of Ezh1 and Ezh2 in type-2 λ-MYC lymphoma cells, we quantified H3K27me3 levels by immunoblotting analysis. Global H3K27me3 levels decreased in a dose-dependent manner in tumor B cells of three independent lymphomas, reaching levels that ranged between 5- and 10 % of those present in untreated cells (Figure 47). These results indicate that type-2 λ-MYC lymphomas evolved selecting molecular networks that render tumor cells largely resistant to acute PRC2 inactivation.

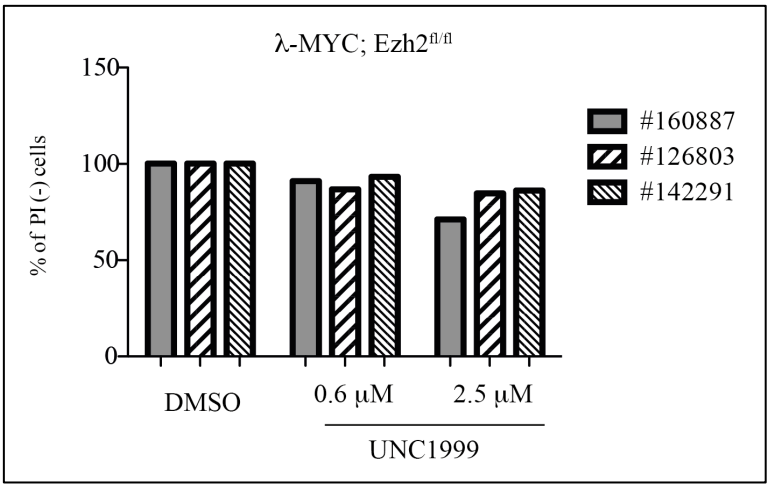

Figure 46: Type-2 λ-MYC lymphomas are resistant to pharmacological Ezh1/2 inhibition

Histograms representation of the percentage of viable (PI^-) lymphoma cells belonging to type-2 λ-MYC tumors (n= 3) after 48 hours treatment with the indicated doses of UNC1999. Vehicle-treated (DMSO) cells were used as control.

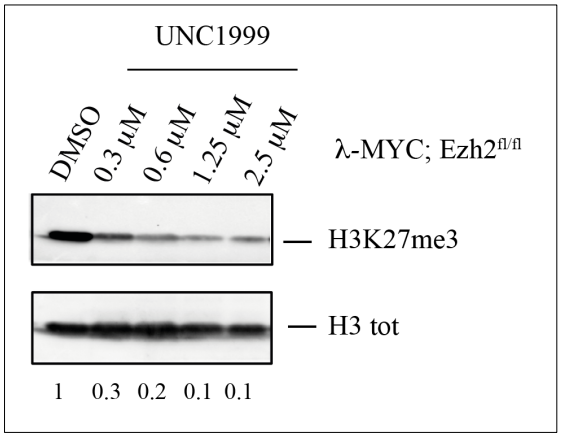

Figure 47: Reduction in global H3K27me3 levels in UNC1999-treated type-2 λ-MYC lymphomas

Immunoblotting determination of H3K27me3 levels in a representative type-2 λ-MYC; $Ezh2^{fl/fl}$ primary tumor (#160887), treated for 48 hours with the indicated doses of UNC1999. Numbers indicate H3K27me3 levels after normalization for protein input (assessed through histone H3 measurement) and are represented as relative to vehicle-treated (DMSO) lymphoma cells.

7.2.8 Ezh2 is required for optimal lymphoma fitness

The isolation of Ezh2 mutant subclones from both type-1 and type-2 lymphomas, combined with the ability of Polycomb mutant tumor B cells to grow both *in vitro* and *in vivo,* indicates that MYC-transformed B cells can circumvent the loss of the main catalytic subunit of the PRC2. We wondered whether the putative compensatory mechanisms set in place by Ezh2 mutant lymphoma B cells allowed the latter cells to compete *in vivo* with Ezh2 proficient tumors. To this end we performed two types of experiments. First, type-1 and type-2 lymphomas were TAT-Cre transduced to generate Ezh2 mutant tumor cells (Figure 48). The latter cells were then transplantated as a mixture into immunoproficient hosts. Quantification by genomic qPCR of *Ezh2* gene copy number in tumor cells retrieved from the bone marrow of diseased animals revealed a normal set of *Ezh2* alleles (Figure 48). This result was confirmed assessing H3K27me3 levels in the mixture of transduced cells prior to injection and after their retrieval from the bone marrow of diseased animals, respectively (Figure 49). Whereas tumor B cells displaying low H3K27me3 levels (likely representing Ezh2 mutant cells) were clearly detected at 48 hours after TAT-Cre transduction, they become undetectable in the bulk of the tumor retrieved from the bone marrow of transplanted mice (Figure 49).

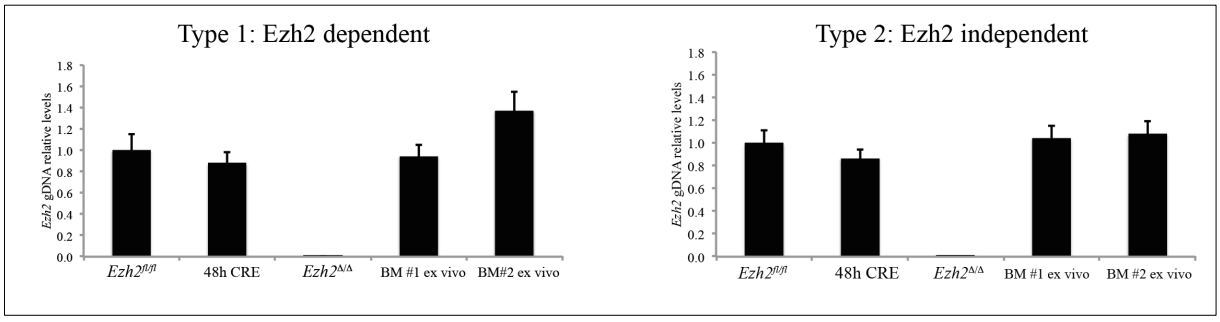

Figure 48: *In vivo* effects of acute inactivation of Ezh2 on primary λ-MYC lymphomas
Genomic qPCR quantification of *Ezh2* gene copy number in representative type-1 (#73664) and type-2 (#160887) λ-MYC lymphomas prior to ($Ezh2^{fl/fl}$) and 48 hours after TAT-Cre transduction (48h Cre). The mixture of transduced cells was transplanted into mice and *Ezh2*

gene copy number assessed in the pool of tumor B cells retrieved from the bone marrow (BM) of two recipients (#1 and #2). Data on *Ezh2* gene copy number were normalized for DNA input and represented as relative to those in Ezh2 proficient lymphoma cells (*Ezh2*$^{fl/fl}$).

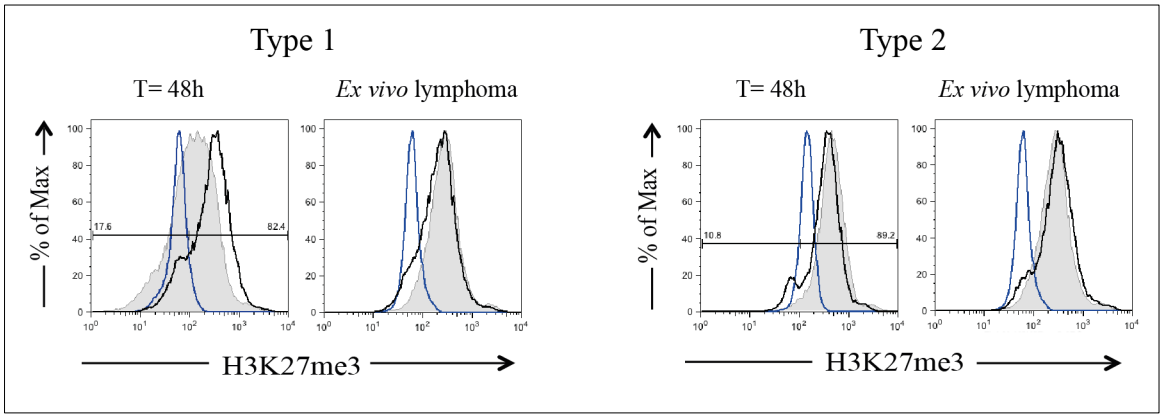

Figure 49: Lymphomas acutely loosing Ezh2 activity are counter-selected *in vivo*
Quantification of H3K27me3 levels by intracellular FACS analysis in type-1 (#73664) and type-2 (#160887) λ-MYC lymphomas prior to (grey filled line) and 48 hours (48h) after TAT-Cre transduction (black thin line). H3K27me3 levels are also shown in lymphomas retrieved from the bone marrow of mice transplanted with the mixture of TAT-Cre transduced cells (*ex vivo* lymphoma). An Ezh2 mutant lymphoma clone was included in the analysis as negative control for H3K27me3 (blu thin line).

A second approach to study the competitive potential of Ezh2 mutant lymphoma cells is based on the transplantation of 1:1 mixtures of Ezh2 proficient and mutant lymphoma subclones. This strategy avoids imbalances in the proportion of Ezh2 proficient and defective tumor cells at the onset of the competition assay. Quantification of *Ezh2* gene copy number in tumor cells retrieved from the bone marrow of diseased transplanted animals indicated the existence of two functional copies of *Ezh2* in most lymphoma B cells (Figure 50). To validate the *Ezh2* genotyping result, we compared H3K27me3 levels in 1:1 mixtures of Ezh2 proficient (*Ezh2*$^{fl/\Delta}$) and mutant (*Ezh2*$^{\Delta/\Delta}$) lymphoma cells prior to, and after, transplantation into recipient animals. Western blotting analysis confirmed the counter-selection of Ezh2 mutant lymphoma cells in the bone marrow of diseased animals at the

expense of Ezh2 proficient tumor cells expressing normal levels of H3K27me3 (Figure 51). Similar results were obtained measuring H3K27me3 at the single cell level by intracellular FACS analysis of tumor-enriched bone marrow cells (Figure 52).

All together these results reveal that acute loss of Ezh2 impairs *in vivo* fitness of malignant B cells of both type-1 and type-2 lymphomas. Moreover, whereas Ezh2 mutant subclones can be successfully established from both type-1 and type-2 lymphomas, their capacity to grow *in vivo* is severely compromised by the presence of Ezh2 proficient tumors. Hence, compensatory mechanisms, set in place in tumor B cells in response to Ezh2 inactivation, can only partially bypass functional inactivation of the Polycomb protein, even in type-2 lymphomas.

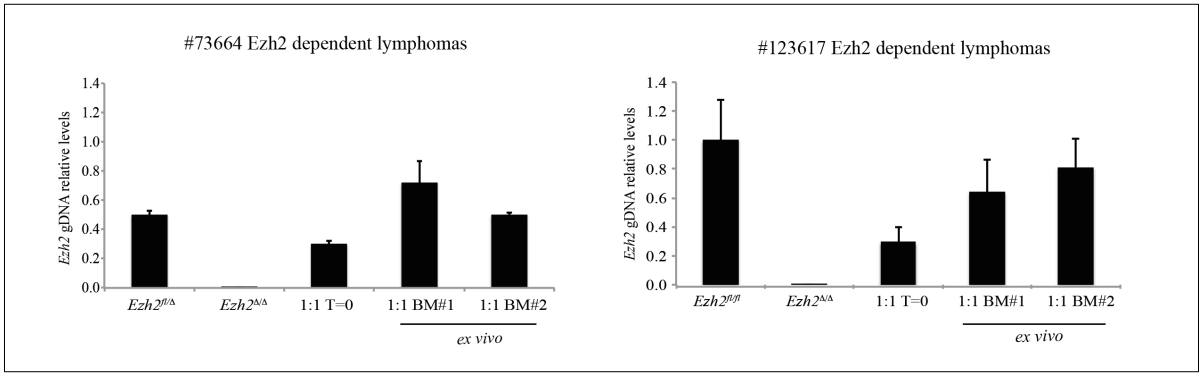

Figure 50: Ezh2 inactivation impairs the capacity of λ-MYC lymphoma cells to compete *in vivo* with Ezh2 proficient lymphomas

Genomic qPCR quantification of *Ezh2* gene copy number in pools of lymphoma cells retrieved from the bone marrow (BM) of two animals transplanted with 1:1 mixtures of Ezh2 proficient (*Ezh2*$^{fl/fl}$ or *Ezh2*$^{fl/\Delta}$) and defective (*Ezh2*$^{\Delta/\Delta}$) lymphoma cells. Ezh2 proficient and mutant clones alone or within a 1:1 mixture prior to transplantation (1:1 T=0) were used as controls. *In vivo* competition assays were performed using representative clones established from type-1 λ-MYC lymphomas (#73664 and #123617). *Ezh2* gene copy number data were normalized for DNA input and represented as relative to those of Ezh2 proficient clones used for the competition assays.

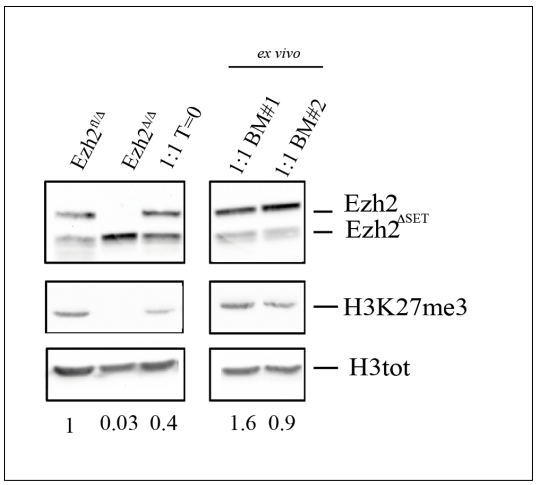

Figure 51: Ezh2 mutant lymphoma cells are counter-selected *in vivo* by Ezh2 proficient tumors

Immunoblot analysis to assess H3K27me3 and Ezh2 levels in pools of lymphoma B cells retrieved *ex vivo* from the bone marrow (BM) of two animals (#1 and #2) injected 26 days earlier with 1:1 mixtures of Ezh2 proficient and deficient lymphomas. Levels of H3K27me3 and Ezh2 in the starting Ezh2 proficient ($Ezh2^{fl/\Delta}$) and mutant ($Ezh2^{\Delta/\Delta}$) lymphoma cells are also indicated. Numbers indicate normalized H3K27me3 levels, represented as relative to those in Ezh2 proficient ($Ezh2^{fl/\Delta}$) lymphoma cells. Note that tumor cells retrieved from the BM of transplanted mice displayed a ratio between Ezh2 full length and its ΔSET mutant counterpart that is higher than the one measured in the 1:1 tumor mixture prior to transplantation (1:1 T=0).

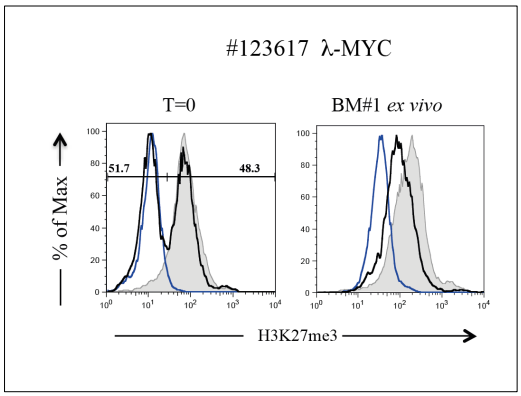

Figure 52: Flow cytometric determination of H3K27me3 levels in tumor B cells retrieved after transplantation of 1:1 Ezh2 proficient/defective tumor mixtures

Determination of H3K27me3 levels by intracellular FACS analysis, in representative Ezh2 proficient ($Ezh2^{fl/fl}$; gray filled line), and deficient ($Ezh2^{\Delta/\Delta}$) (blue line) lymphoma clones, 1:1 Ezh2 proficient/defective tumor mixtures (black line) prior (T=0) to transplantation and

in the pool of lymphoma cells isolated *ex vivo* from the bone marrow (BM) of a transplanted animal. Numbers indicate frequency of H3K27me3-positive and negative cells in 1:1 tumor mixtures prior to transplantation.

7.3 Analysis of the H3K27me3 epigenome in λ-MYC lymphomas

7.3.1 Genome wide distribution of H3K27me3 in λ-MYC lymphomas

To understand the contribution of H3K27me3 to the maintenance of the transformed B cell phenotype, we performed ChIP using an antibody against H3K27me3, coupled to ultra deep sequencing of the immunoprecipitated genomic material (ChIP-sequencing or ChIP-seq). This analysis was performed on two λ-MYC tumors representative of type-1 and type-2 lymphomas, respectively. Bioinformatic analysis of the sequencing data was performed using the MACS algorithm to identify genomic intervals overlapping transcriptional start sites (+/- 5 Kb) that were significantly ($p< 10^{-5}$) enriched for H3K27me3 deposition. The analysis identified 1814 H3K27me3 targets in type-1 lymphomas, whereas type-2 lymphoma displayed around 1000 target genes (Figure 53). The intersection of the lists of H3K27me3-marked genes identified in the two types of lymphomas revealed a good number of shared targets, with yet a substantial proportion of genes that were marked by H3K27me3 in a tumor-specific fashion (Figure 53). We confronted the list of H3K27me3 marked genes to databases containing a comprehensive list of ChIP-seq datasets, using the Enrichr open source software. The analysis revealed that genes marked by H3K27me3 in λ-MYC lymphomas were significantly enriched for components of both PRC1 (Rnf2) and PRC2 (Ezh2, Suz12, Jarid2) and were shared with H3K27me3 targets in mouse embryonic stem cells. A further support for the assignment of H3K27me3-marked genes in λ-MYC lymphomas to the group of *bona fide* Polycomb targets came from the observation, that such genes are commonly deregulated in Polycomb mutant (*Eed* and *Rnf2* knockout) ES cells

(Figure 54). Gene ontology analysis applied to H3K27me3 targets in λ-MYC lymphomas revealed enrichment for functional categories including Wnt signaling and ES cells pluripotency (Figure 55).

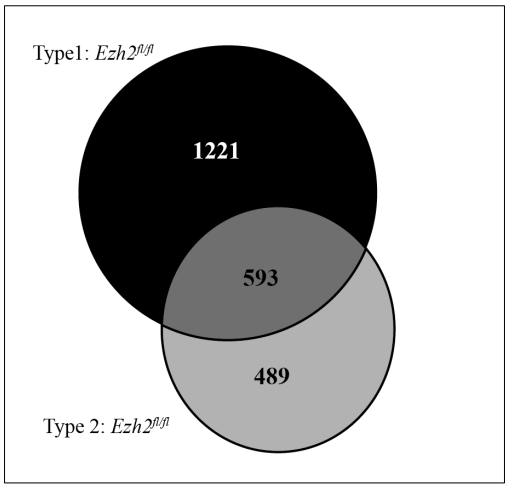

Figure 53: Ezh2 proficient clones established from type-1 and type-2 λ-MYC lymphomas share a consistent number of H3K27me3 target genes

Venn diagram representing H3K27me3-marked genes identified by MACS algorithm ($p< 10^{-5}$) in Ezh2 proficient (*Ezh2*$^{fl/fl}$) clones from representative type-1 (#73664: black) and type-2 (#126803: light grey) λ-MYC lymphomas, respectively.

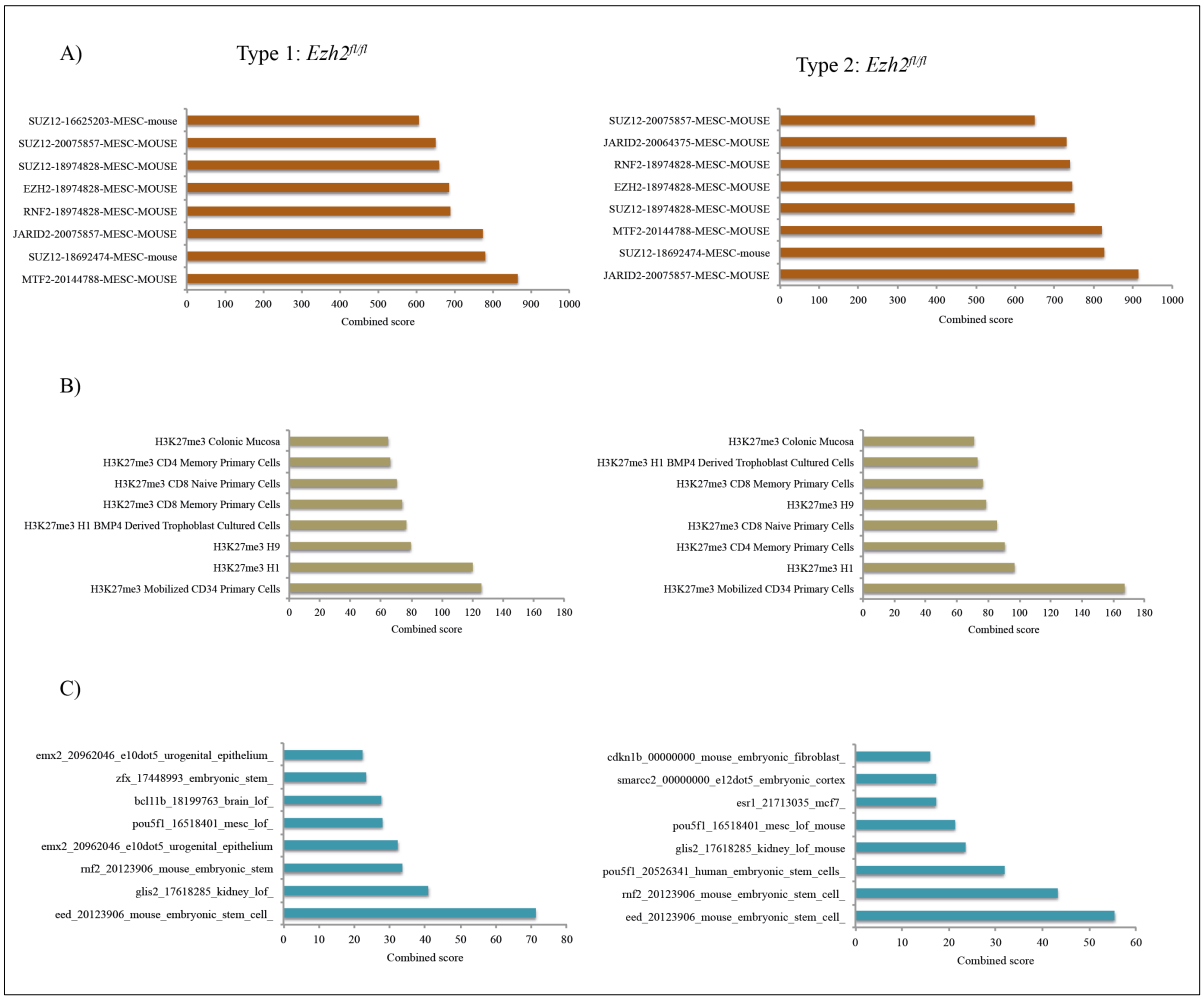

Figure 54: Features of H3K27me3 target genes in Ezh2 proficient lymphomas

List of genes marked by H3K27me3 in Ezh2 proficient (*Ezh2*$^{fl/fl}$) clones (#73664 for type-1 and #126803 for type-2) were confronted with previously published ChIP-seq dataset using EnrichR software tool. Bar-representation of the top-8 ChIP-seq datasets for chromatin bound proteins (A) and histone marks (B) revealed by ChIP enrichment analysis (ChEA and Epigenomics, EnrichR). Top-8 transcriptome datasets (deposited in GEO) enriched in genes marked by H3K27me3 in Ezh2 proficient (*Ezh2*$^{fl/fl}$) lymphomas, as reveled though EnichR (LHF-TF, EnichR) tool (C) established from type-1 (#73664) and type-2 (#126803) λ-MYC lymphomas.

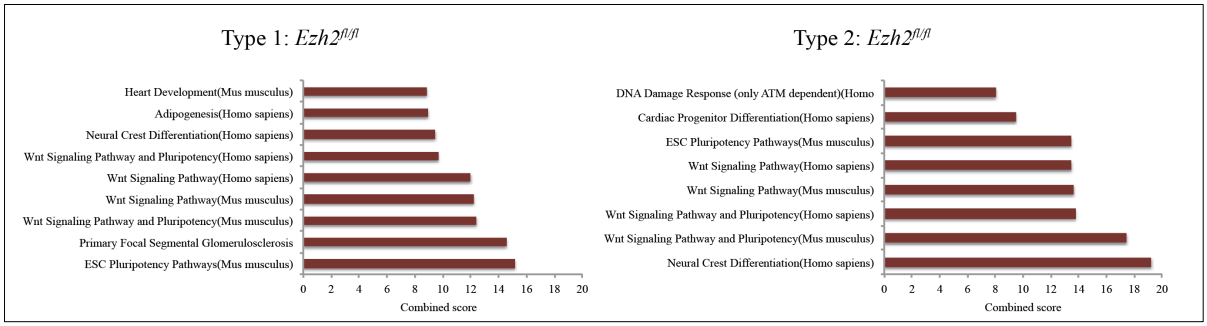

Figure 55: Functional categories of H3K27me3 target genes in Ezh2 proficient lymphomas

Wiki-pathway of top-8-enriched categories for H3K27me3 target genes identifies in Ezh2 proficient (*Ezh2*$^{fl/fl}$) type-1 (#73664) and type-2 (#126803) independent λ-MYC lymphomas. Analysis was performed using EnrichR software tool.

7.3.2 Effects of Ezh2 inactivation on the H3K27me3 epigenome of λ-MYC lymphomas

To assess the effects of Ezh2 inactivation on the H3K27me3 genome wide distribution, we extended ChIP-seq to Ezh2 mutant subclones isolated from type-1 and type-2 lymphomas, respectively. Bioinformatic analysis of H3K27me3 ChIP-seq data revealed a 95-to-98 % reduction in the number of H3K27me3 targets in lymphoma B cells of both types as a consequence of Ezh2 inactivation (Figure 56). In support of this result, distribution of H3K27me3 reads around the TSS of target genes in Polycomb proficient tumor cells was lost in the Ezh2 mutant lymphomas (Figure 57). This result indicates that sustained growth of λ-MYC lymphoma is compatible with a close-to-complete loss of H3K27 methylation genome wide.

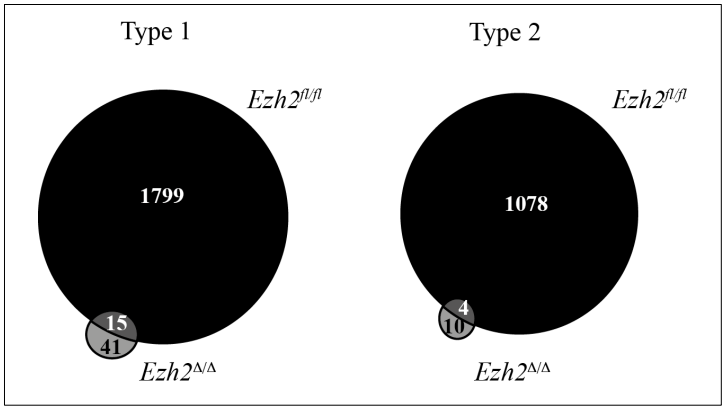

Figure 56: Significant loss of H3K27me3 target genes in Ezh2 mutant lymphomas

Venn diagram representing numbers of genes marked by H3K27me3 in Ezh2 proficient (*Ezh2*$^{fl/fl}$: black) and defective (*Ezh2*$^{\Delta/\Delta}$: light grey) subclones established from type-1 (#73664) and type-2 (#126803) independent λ-MYC lymphomas, respectively. H3K27me3 enriched targets were identified by MACS algorithm ($p<10^{-5}$).

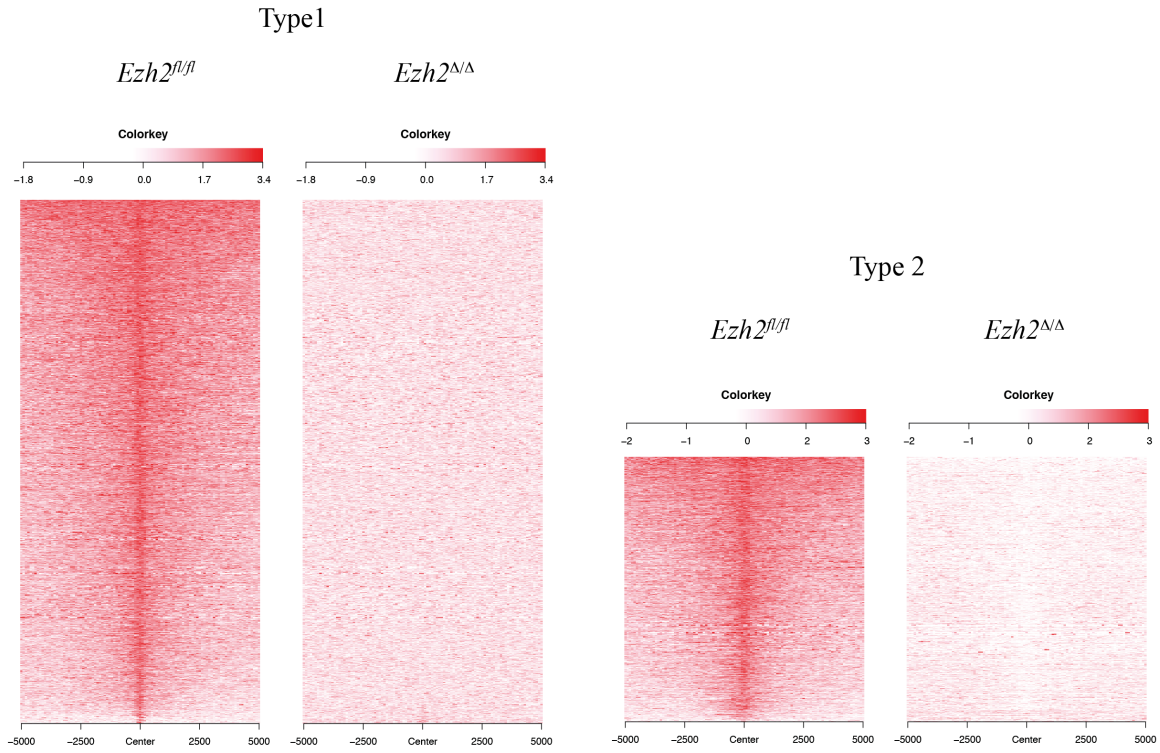

Figure 57: Distribution of H3K27me3 around the TSS of target genes in Ezh2 proficient and mutant lymphomas

Heat map representation of H3K27me3 distribution in a ±5 Kb genomic interval centered around the TSS of target genes identified by the MACS algorithm to be enriched for the histone mark in Ezh2 proficient (*Ezh2*$^{fl/fl}$) and mutant (*Ezh2*$^{\Delta/\Delta}$) subclones, established from

type-1 (#73664) and -2 (#126803) λ-MYC lymphomas. Reads were clustered according to the H3K27me3 levels.

7.3.3 Effect of the loss of H3K27 methylation on target gene expression in Ezh2 mutant lymphomas

To assess whether the loss of H3K27me3 around the TSS of target genes affected their expression, we performed RNA sequencing comparing Ezh2 proficient to mutant clones isolated from representative cases of type-1 and type-2 lymphomas. A pairwise comparison of Ezh2 proficient and mutant clones derived from the same primary tumor revealed a strong correlation (Pearson correlation coefficient R= 0.979) (Figure 58) in the expression levels of H3K27me3 targets for type-1 established subclones. Remarkably, instead, the degree of similarity in the expression of H3K27me3-marked genes between Ezh2 proficient and defective clones derived from type-2 lymphomas was substantially weaker, with most genes becoming up-regulated in Ezh2 mutant cells (R= 0.439) (Figure 58). This result suggests that establishment of Ezh2 mutant lymphomas from type-1 lymphomas requires the activation of compensatory (repressive) mechanisms in order to retain the correct regulation of H3K27me3 targets. Instead, Ezh2 mutant clones derived from type-2 lymphomas appear much less dependent on the correct regulation of H3K27me3 target genes in order to sustain tumor growth. This result is in accordance with our previous evidences indicating primary resistance of type-2 lymphomas to pharmacological PRC2 inactivation.

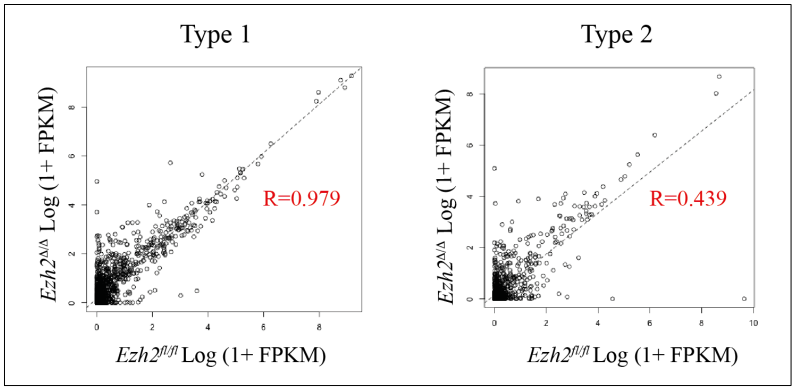

Figure 58: Expression of H3K27me3-marked genes in Ezh2 proficient and mutant subclones

Scatter plot representation of transcript levels of H3K27me3-marked genes between Ezh2 proficient and mutant subclones isolated from representative type-1 (#73664) and type-2 (#126803) λ-MYC lymphomas. Each dot represents transcript levels of one H3K27me3-marked genes in pairwise samples as assessed by RNA-sequencing. For both types of lymphomas, Pearson's coefficient (R) was calculated.

7.3.4 Where is H3K27me3 retained in Ezh2 mutant lymphomas?

The sensitivity of Ezh2 mutant subclones derived from type-1 lymphomas to the Ezh1/2 inhibitor UNC1999, coupled to the evidence that residual global H3K27me3 levels are detected in Polycomb mutant tumor cells, suggests the existence, in these cells, of a non-canonical PRC2 composed of Ezh1 that may be required to sustain tumor growth.

In order to have a more comprehensive outlook at targets that retained H3K27me3 in Ezh2 mutant subclones, we extended ChIP-seq data to a second Polycomb mutant subclone. Interestingly, in the latter tumor, the number of target genes that retained the H3K27me3 mark was substantially higher than in the first analyzed clone (432 vs. 56), pointing to remarkable epigenetic variability linked to the establishment/selection of Ezh2 mutant clones. Analysis of the distribution of residual H3K27me3 at target sites in Ezh2 mutant clones revealed an enrichment for the histone mark proximal to the TSS, in agreement with the mode of action of canonical PRC2 (Figure 59A). Surprisingly, the same set of genes was

devoid of H3K27me3 enrichment in Ezh2 proficient tumors (Figure 59A), suggesting the recruitment of a non-canonical Ezh1/PRC2 to novel genomic regions in Ezh2 mutant lymphoma B cells. The evidence that genes displaying H3K27me3 enrichment in Ezh2 mutant lymphomas were not recognized as *bona fide* Polycomb targets supports this hypothesis (Figure 59B). Indeed, we found that genes marked by H3K27me3 in Ezh2 mutant lymphomas were significantly enriched for targets of H3K4 methylation, which is associated to active gene transcription (Figure 59B). Finally, we tested whether genes marked by H3K27me3 in Ezh2 mutant lymphomas had undergone changes in gene expression when compared with Ezh2 proficient tumors. The pairwise comparison revealed a substantial modulation in gene expression due to *de novo* H3K27 trimethylation in Ezh2 mutant lymphomas (R= 0.56; Figure 60).

All together these results support a scenario whereby Ezh2 inactivation in type-1 λ-MYC lymphoma B cells unleashes the activity of a non-canonical PRC2 complex composed of Ezh1, which gets recruited to novel transcriptionally active genes, where it likely controls their expression.

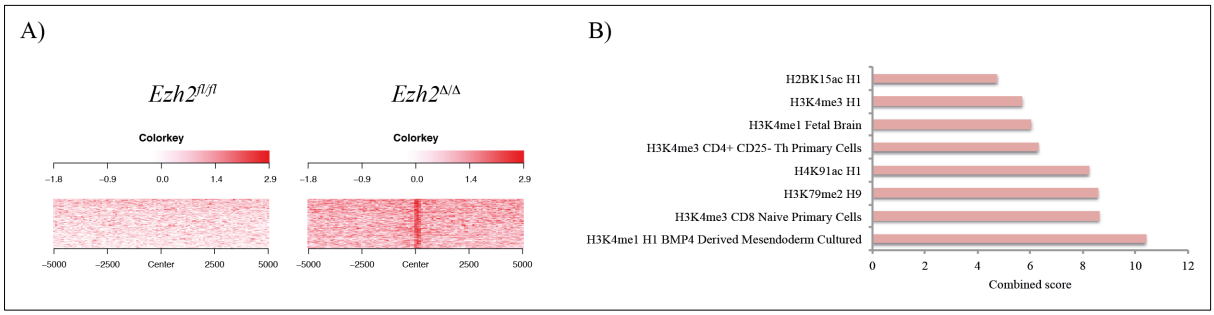

Figure 59: Distribution of residual H3K27me3 in Ezh2 mutant lymphomas

Heat map representation of H3K27me3 distribution in a ±5 Kb genomic interval centered around the TSS of genes identified by the MACS algorithm to be enriched for the histone mark in Ezh2 defective tumor B cells established from type-1 (#123617) λ-MYC lymphomas. Ezh2 proficient (*Ezh2*$^{fl/fl}$) and mutant (*Ezh2*$^{Δ/Δ}$) lymphoma subclones were compared. Reads were clustered according to the level of H3K27me3 (A). Bar representation of top-8 ChIP-seq datasets for histone marks enriched for H3K27me3 target

genes identified in Ezh2 mutant clone from type-1 (#123617) λ-MYC lymphomas, revealed by histones enrichment analysis (Epigenomics, EnrichR) (B).

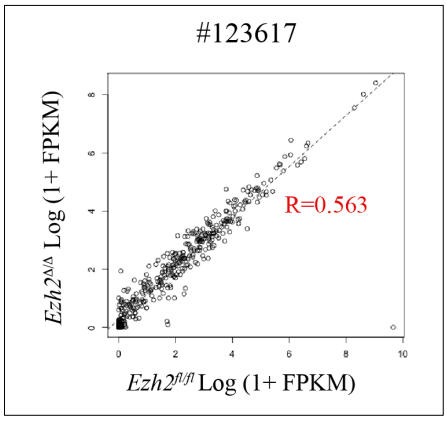

Figure 60: H3K27me3 modulates expression of target genes in Ezh2 mutant type-1 lymphomas

Scatter plot representation of transcript levels of genes marked by H3K27me3 in Ezh2 mutant lymphoma cells. Pairwise comparison between Ezh2 proficient and defective subclones from type-1 (#123617) λ-MYC lymphomas is represented. Each dot represents transcript levels of one of H3K27me3-marked genes, assessed by RNA-sequencing. Pearson's coefficient (R) is shown for each comparison.

7.4 Acquired resistance to PRC2 inactivation in MYC-driven lymphomas

7.4.1 Generation of λ-MYC lymphomas acquiring resistance to UNC1999 treatment

Small molecule inhibitors targeting Ezh2 are currently in several clinical trials for the treatment of both solid and blood cancers, including high-grade lymphomas. Our studies based on the λ-MYC lymphoma model unveiled strategies selected by tumor cells to circumvent the need for Ezh2. One possible compensatory mechanism is centered on the activity of Ezh1. Indeed, type-1 lymphomas that succeeded to bypass the requirement for Ezh2 remained sensitive to the Ezh1/2 double inhibitor, UNC1999. Based on our results, UNC1999 may represent a better option than Ezh2 inhibitors in anti-cancer treatments.

In this context, we asked whether tumors could also acquire secondary resistance to pharmacological inhibition of Ezh1/2. To address this, we subjected both type-1 and type-2 lymphomas to a prolonged *in vitro* treatment with low doses of UNC1999. Under these experimental conditions, lymphomas continued to grow *in vitro*, although at a lower pace when confronted to vehicle-treated tumors (Figure 61).

To monitor the action of UNC1999, we determined H3K27me3 levels by intracellular FACS analysis over time. We observed two distinct behaviors. Type-2 lymphomas displayed from the first days of treatment a substantial loss in H3K27me3 levels, which remained the same throughout the treatment period. Instead, type-1 lymphomas displayed an initial phase when most lymphoma cells suffered from a significant loss in H3K27me3 levels. Strikingly, starting from day 10 of treatment, we identified a distinct subset of tumor cells that had restored H3K27me3 activity. The fraction of H3K27me3^{+} tumor cells steadily grew over time, becoming the dominant population by day 20 of the treatment (Figure 62). H3K27me3 Western blotting analysis was employed to confirm the differential response of type-1 and -2 lymphoma cells to chronic UNC1999 treatment (Figure 63).

All together these results reveal that type-1 lymphomas under chronic treatment with a PRC2 inhibitor select a resistance mechanism that ensures restoration of H3K27me3 activity. In striking contrast, type-2 lymphomas lack any selection pressure to re-establish H3K27me3 in order to sustain tumor growth in the presence of UNC1999.

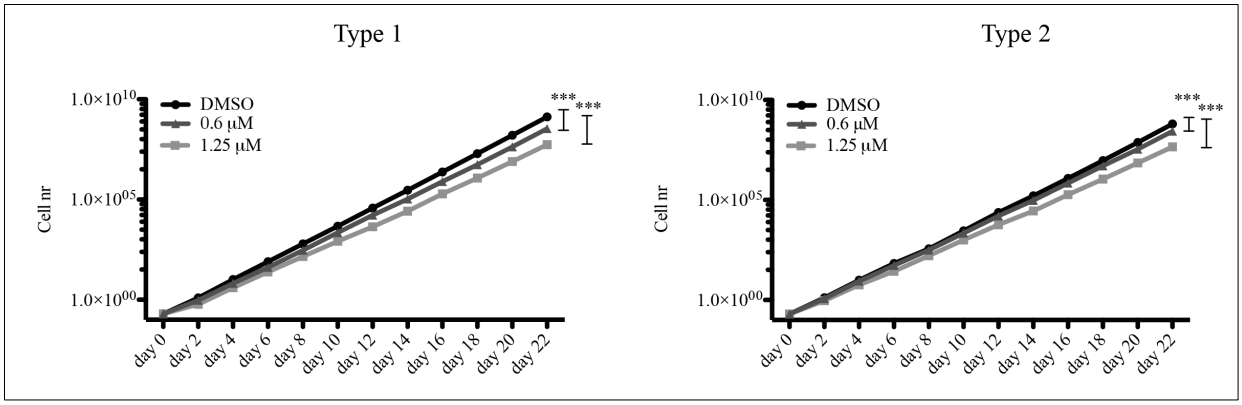

Figure 61: Growth curve of λ-MYC; Ezh2$^{fl/fl}$ lymphomas chronically exposed to low doses of UNC1999

In vitro growth curves of representative type-1 (#73664) and type-2 (#160887) λ-MYC; Ezh2$^{fl/fl}$ lymphomas treated for the indicated days with either vehicle (DMSO, black line) or low doses (0.6 μM and 1.25 μM) UNC1999. Each symbol represents the average of 3 measurements (±SE). Statistical significance was calculating using 2-Way-Anova statistical test (***$p<0.001$).

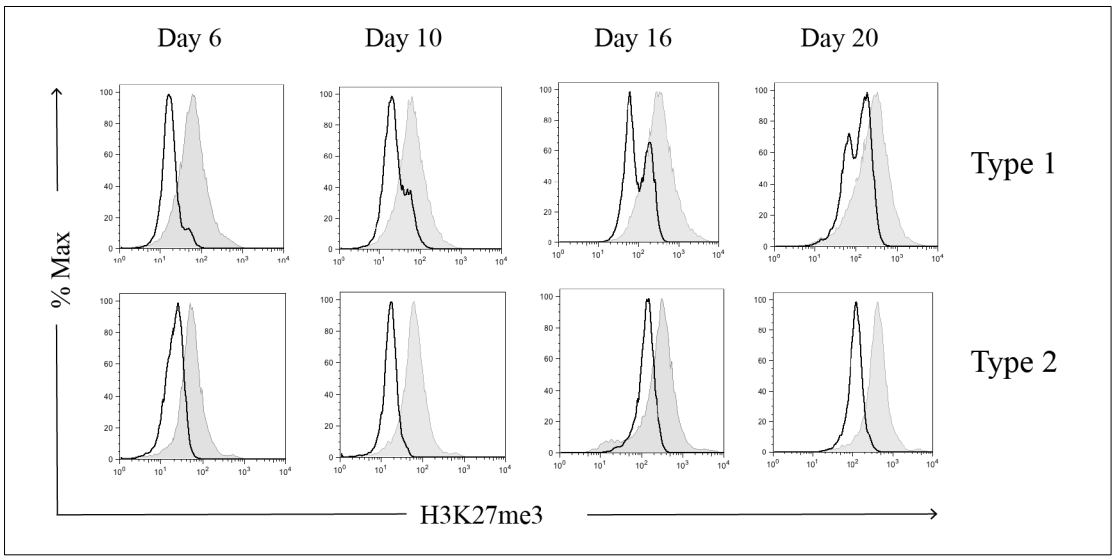

Figure 62: Type-1 λ-MYC; Ezh2$^{fl/fl}$ lymphomas restore H3K27 trimethylation after chronic exposure to low doses of UNC1999

Quantification of H3K27me3 levels by intracellular FACS analysis in representative type-1 (#73664) and type-2 (#160887) λ-MYC; Ezh2$^{fl/fl}$ lymphomas exposed for the indicated days to UNC1999 (1.25 μM) (black thin line). Vehicle-treated (DMSO) lymphoma cells were used as positive control (grey filled line).

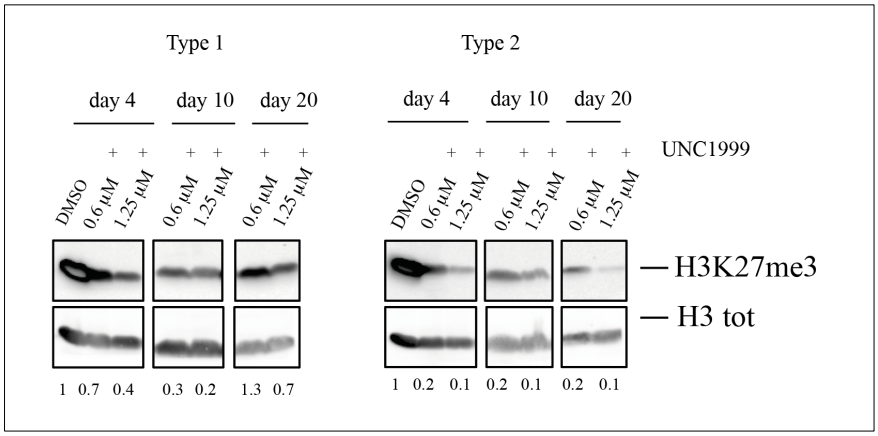

Figure 63: Western blot quantification of H3K27me3 levels in lymphomas chronically exposed to low doses of UNC1999

Immunoblotting determination of global H3K27me3 levels in representative type-1 (#73664) and type-2 (#160887) λ-MYC; Ezh2$^{fl/fl}$ lymphomas treated for the indicated days and doses with either UNC1999 or vehicle (DMSO). Histone H3 was used as loading control. Numbers indicate normalized H3K27me3 levels relative to those measured in vehicle-treated lymphoma cells.

7.4.2 Isolation of UNC19999 resistant λ-MYC subclones

To identify the genetic basis underlying acquired resistance of λ-MYC lymphomas to pharmacological inhibition of PRC2, we established through limiting dilution assays, a representative number of subclones from pools of UNC1999 chronically treated type-1 and type-2 lymphomas (Figure 64). Flow cytometric quantification of H3K27me3 in representative UNC1999-resistant subclones (expanded in the absence of the inhibitor), revealed levels of the histone mark fairly similar to Ezh2 proficient untreated lymphomas (Figure 65). These results indicate that UNC1999 resistant tumor cells retain a PRC2 complex with intact methyltransferase activity. Future experiments based on the sequencing of the coding sequences of Ezh1 and Ezh2 in individual UNC1999-resistant clones will determine whether lymphoma cells selected mutations in the Polycomb proteins that prevent the binding to the inhibitor.

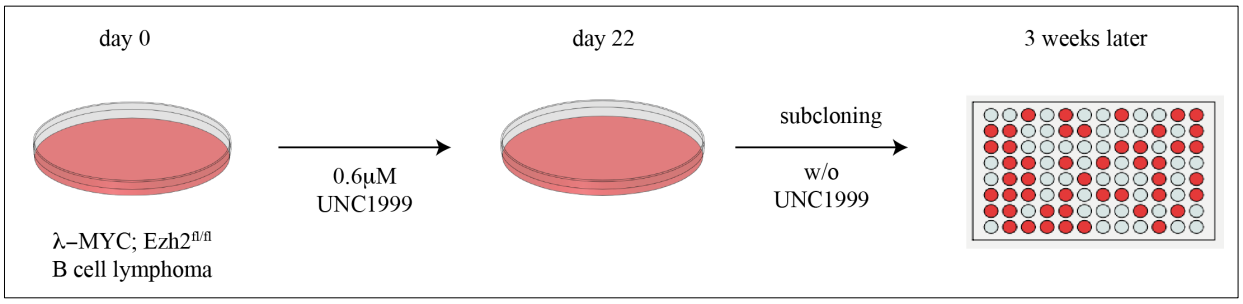

Figure 64: Isolation of λ-MYC; Ezh2$^{fl/fl}$ clonal variants acquiring resistance to UNC1999 treatment

Cartoon depicting the strategy to isolate λ-MYC; Ezh2$^{fl/fl}$ subclones acquiring resistance to Ezh1/2 inhibition. Briefly, representative type-1 (#73664) and type-2 (#160887) lymphomas were treated for 22 days with a low dose (0.6 μM) of UNC1999. Tumor cells were then cloned by limiting dilution in the absence of UNC1999. Clones were isolated 3 weeks later and further expanded.

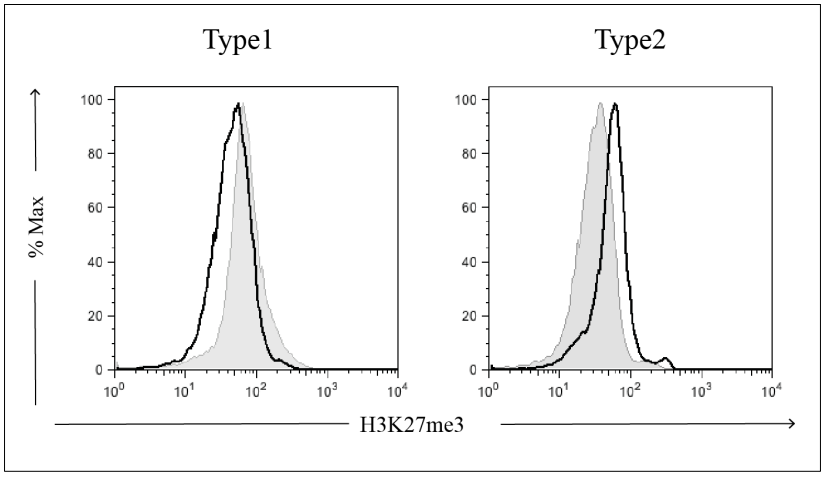

Figure 65: UNC1999 resistant clones display similar H3K27me3 levels to parental tumors

Quantification of H3K27me3 levels by intracellular FACS analysis in representative UNC1999-resistant subclones (black line), established from type-1 (#73664) and type-2 (#160887) λ-MYC; $Ezh2^{fl/fl}$ lymphomas. FACS measurements were made with lymphoma cells grown in the absence of UNC1999. H3K27me3 levels were compared to those present in the parental tumor (grey filled line).

8 Discussion

The PRC2 catalytic subunit Ezh2 is highly expressed in proliferating B cell compartments, namely progenitors and GC B cells (Caganova et al., 2013). Elevated Ezh2 levels are also detected in high-grade B cell lymphomas, including BL (Dukers et al., 2004; Sander et al., 2008; van Kemenade et al., 2001). These observations, coupled to genome mutation analysis indicating recurrent hyper-activation of EZH2 function in GC-derived DLBCL and FL, have identified the Polycomb protein as a novel marker gene of B cell lymphomas (Morin et al., 2011; Lohr et al., PNAS 2012). The contribution of Ezh2 to the malignant nature of B cell lymphomas may fall in line of its essential role in the control of cell proliferation, survival and differentiation (Margueron and Reinberg, 2011). In addition, the function played by PRC2 to sustain the pluripotency network in embryonic, adult and induced pluripotent stem cells may represent a further strategy hijacked by malignant cells to maintain their immortal nature (Laugesen and Helin, 2014).

High Ezh2 levels are contributed by the activation of the transcription factor E2F1 (Bracken et al., 2003). In proliferating cells, including B lymphocytes, Ezh2 plays a major role in the active regulation of cell cycle progression. In particular, Ezh2 acts within the PRC2 to regulate the G1-to-S transition through the active repression of genes encoding for the CDK inhibitors Cdkn2a, Cdkn1a/p21^{WAF}, Cdkn1b/p27^{Kip1} and Cdkn1c/p57^{Kip2} (Fan et al., 2011; Fasano et al., 2007; Guo et al., 2011; Itahana et al., 2003; Yang et al., 2009). The failure to repress such genes represents a major cause of the proliferative defects observed in primary cells of mutant animals lacking expression of Ezh2 or other core components of the PRC2 complex (Chen et al., 2009; Dhawan et al., 2009; Jacobs et al., 1999; Miyazaki et al., 2008). The contribution of Ezh2 and Polycomb proteins to cell cycle progression is not limited to the regulation of the G1-to-S transition. Indeed, recent lines of evidence have unveiled an active role for PRC1 and PRC2 in the control of DNA replication during S phase (Piunti et al., 2014).

Ezh2 also imposes a strict control over cell survival. This is achieved through the negative regulation of the tumor suppressor $p19^{ARF}$, encoded by the *Cdkn2a* locus (Sherr, 2012). Cells undergoing inactivation of Ezh2, as well as other Polycomb components of PRC2 and PRC1, commonly activate $p19^{ARF}$, which triggers p53-driven programmed cell death, in response to apoptotic stimuli (Kim and Sharpless, 2006; Sherr, 2012). In line with these observations, Polycomb mutant cells display increased sensitivity to genotoxic damage induced by oxidative stress, DNA damaging agents and/or endogenous mutagenic processes. For example, Ezh2 protects GC B cells from genotoxic stress, induced by AID during Ig SHM and isotype switching (Caganova et al., 2013). The ability of Polycomb proteins to protect cells from genotoxic damage may also be mediated by mechanisms other than $p19^{ARF}$ repression. In support of this, recent evidence has suggested that Polycomb proteins are directly involved in the early stages of the DNA damage response (Campbell et al., 2013; Ginjala et al., 2011; Ismail et al., 2010; Wu et al., 2011)

Ezh2, as well as other members of PRC1 and PRC2, exerts a fine temporal control over the expression of TFs that guide step-wise somatic cell differentiation, including B lymphopoiesis. Indeed, conditional gene inactivation studies have highlighted the essential role played by Ezh2 during early B cell differentiation and in mature B cells, recruited in the GC response (Beguelin et al., 2013; Caganova et al., 2013). In particular, *Ezh2* inactivation in GC B cells caused a premature induction of the tumor suppressor and master regulator of terminal B cell differentiation, Blimp1, thereby limiting the persistence of B cells within the GC (Beguelin et al., 2013; Caganova et al., 2013). Conversely, constitutive activity and/or expression of Ezh2 may cause an enforced repression of developmental regulators under its control, stalling differentiation, thereby facilitating malignant transformation (Lund et al., 2014). These results unveil the relevance of a strict control over Ezh2 expression/function to guarantee the normal transition of B cells, as well as other cellular lineages, through subsequent maturation stages. In embryonic, adult and induced pluripotent stem cells, Ezh2

sustains the activity of the pluripotency network through epigenetic silencing of cell fate determinants and by supporting stem cell self-renewal (Margueron and Reinberg, 2011). These properties render Ezh2 a likely determinant of the acquired self-renewal properties of malignant cells, in particular of those transformed by the c-MYC oncogene (Wee et al., 2014).

B cell lymphomas represent a heterogeneous group of diseases, predominantly originating from mature B cells recruited into the GC reaction (Basso and Dalla-Favera, 2015). The high Ezh2 expression levels detected in GC B cells, coupled to its critical role in protecting the cells from DNA damage-induced apoptosis, in restraining terminal differentiation and in facilitating cell proliferation, render the Polycomb protein a possible determinant of GC-derived B cell lymphomas (Beguelin et al., 2013; Caganova et al., 2013). In support of this, whole exome/genome sequencing data have identified a substantial proportion (over 20 %) of DLBCL and FL, displaying heterozygous EZH2 g.o.f. mutations (Lohr et al., 2012; Morin et al., 2011; Yap et al., 2011). Two further sets of data support the relevance of *Ezh2* as a GC B cell oncogene. First, transgenic mice expressing mutant forms of EZH2 identified in DLBCL and FL, display GC B cell hyperplasia, which precedes malignant transformation if expression of the mutant Polycomb protein is combined with a BCL2 transgene (Beguelin et al., 2013). Importantly, Ezh2 mutations are more frequently observed in patients with DLBCL displaying BCL2 translocations. Second, g.o.f. mutations of the *EZH2* gene are already observed in the early indolent stages of FL, pointing to a role of the Polycomb protein as a driver of malignant GC B cell transformation (Bodor et al., 2013; Pasqualucci et al., 2014).

Another highly aggressive B cell lymphoma arising from GC B cells is BL. In BL, balanced chromosomal translocations juxtaposing the MYC oncogene to Ig heavy or light chain regulatory regions lead to constitutive expression of the proto-oncogene. Acquisition of

additional genetic alterations in BL precursor cells represents a strict requirement for pre-tumoral cells to counteract the potent pro-apoptotic response, triggered by deregulated c-MYC. Analyses of MYC-driven B cell lymphoma mouse models, including the λ-MYC model, have revealed a substantial increase in Ezh2 expression at the transition between the pre-tumoral and tumoral stage (van Kemenade et al., 2001). High Ezh2 levels, observed in murine MYC-driven lymphomas, BL primary tumors and BL cell lines, may be selected by malignant B cells to sustain their high rate of cell proliferation, further preventing differentiation (Dukers et al., 2004; Sander et al., 2008; van Kemenade et al., 2001). Alternatively, high Ezh2 levels may correspond to the levels of expression of the Polycomb protein in GC B centroblasts, the BL precursor cells (Calado et al., 2012; Dominguez-Sola et al., 2012; Victora et al., 2012).

Regardless of the mechanism responsible for the high EZH2 expression in BL cells, it remains unknown whether the Polycomb protein contributes to their aggressiveness, as well as that of other malignant cancer types (Volkel et al., 2015). This question has remarkable clinical relevance, as small molecule inhibitors targeting the EZH2 protein in a highly selective manner have been recently developed. Moreover, tumors that may benefit from such drugs are currently being identified in phase-1 and -2 clinical trials (http://clinicaltrials.gov/ct2/show/NCT01897571)(http://clinicaltrials.gov/ct2/show/NCT02082977).

Studies based on the Eμ-MYC lymphoma model have assigned opposing roles to the Polycomb protein in B cell lymphomagenesis. Whereas in Lee et al., the inactivation of Ezh2 favored the development of B cell lymphomas (Lee et al., 2013), recent work based on transgenic B cell-specific g.o.f. EZH2 mutants revealed cooperation between deregulated EZH2 and c-MYC in B cell tumorigenesis (Berg et al., 2014). Remarkably, while progenitors B cells represented the main target of transformation in the study by Lee et al., tumors described in the study by Berg and colleagues originated from immature/transitional B cells (Berg et al., 2014). These results suggest that the cell context plays an important role

in defining the specific contribution of Ezh2 to tumorigenesis. Hence, whereas in mature B cells recruited into the GC Ezh2 activity promotes tumorigenesis, it acts as a tumor suppressor in progenitor B cells. A tumor suppressor role for Ezh2 has also been proposed in myeloid and T-cell malignancies, which showed recurrent inactivating mutations also in other PRC2 components as well (Nikoloski et al., 2010; Ntziachristos et al., 2012; Simon et al., 2012).

The studies based on the Eμ-MYC lymphoma model have started to uncover possible functions of Ezh2 during the onset of MYC-driven B cell lymphomas. However, the nature of the experiments (e.g. concomitant inactivation/activation of Ezh2 and c-MYC) renders them of limited help to define the importance of Ezh2 function in tumor maintenance and/or progression. Answering the latter question represented the main goal of this study. In particular, we were interested to establish whether high expression of Ezh2 (rather than its constitutive activation) is needed to sustain the malignant phenotype of aggressive B cell lymphomas. In order to achieve this goal, the tumor model had to fulfill the following criteria: 1) expression of Ezh2 increases in the transition from the pre-tumoral to the tumoral stage; 2) the tumor model should resemble a human lymphoma in terms of histological appearance, mode of dissemination and genetics and 3) the tumor model should allow time-controlled inactivation of Ezh2 catalytic function. We succeeded to establish such model, combining the λ-MYC transgene to a conditional knockout allele for *Ezh2* (Su et al., 2003). In λ-MYC; $Ezh2^{fl/fl}$ compound mice, IgM^{+} B cell lymphomas developed at high penetrance. Histologically, tumors resembled BL with typical "starry-sky" histological appearance. Tumors displayed a high mitotic index and could be easily transplanted into immunoproficient syngenic mice, pointing to an aggressive nature of the lymphomas. The establishment of primary cell lines from lymphomas isolated *ex vivo* from diseased animals was instrumental to conditionally inactivate Ezh2 in the malignant B cells. Transient delivery of Cre protein to tumor cells, using a transduction approach limiting the exposure to

the enzyme to malignant B cells, avoids the risk to observe toxic effects associated with prolonged Cre-mediated recombination (Peitz et al., 2002). TAT-Cre transduction allowed a good degree of recombination without interfering with the potential of tumor cells to grow *in vitro* and/or expand *in vivo* upon transplantation into immunoproficient syngenic animals.

To determine the effects of acute inactivation of the Ezh2 methyltransferase activity on the growth of highly aggressive MYC-driven B cell lymphomas, we chose to monitor the capacity of single tumor cells to overcome anoikis and give rise to a clonal population of tumor cells. This stringent test revealed the existence of two major types of MYC-transformed lymphomas. Specifically, whereas, type-1 lymphomas gave rise to a small fraction of Ezh2 mutant subclones following TAT-Cre transduction, type-2 lymphomas mostly generated Polycomb mutant subclones after treatment with the recombinant protein. This striking difference in the yield of Polycomb mutant clones starting from single cells was not caused by differences in the efficiency of TAT-Cre transduction, but rather reflected differences in the dependence of the two types of tumors on Ezh2 methyltransferase activity. This result has important implications for the biology of MYC-driven transformation. Indeed, our results suggest the existence of two major paths leading a MYC-overexpressing B cell to evolve into a malignant lymphoma. In type-1 lymphomas, epigenome rewiring in malignant B cells as a consequence of constitutive MYC expression strictly relies on continuous Ezh2 methyltransferase activity. Acute loss of such activity renders the majority of lymphoma B cells incapable to grow and/or survive as single cells. In contrast, type-2 lymphomas evolved selecting transcriptional/epigenetic networks and/or pathways, which were less dependent on Ezh2 activity, allowing a better adaptation to its loss when grown starting from single cells. The opposite response to Ezh2 inhibition observed for type-1 and type-2 lymphomas was not due to differences in the degree of H3K27me3 loss, as the residual levels of the mark in Polycomb mutant subclones established from the two types of

tumors was comparable. Remarkably, all tested Ezh2 mutant subclones displayed over 95 % loss of global H3K27me3 levels. This result indicates that MYC-lymphomas can support a close-to-complete genome wide loss of H3K27me3 without suffering from major limitations in both *in vitro* and *in vivo* growth.

In an effort to understand the molecular basis for the different requirement of type-1 and -2 lymphomas for Ezh2, we performed whole transcriptome analysis. This approach also harbors the potential to identify possible biomarker(s) that could be used in the clinics to select lymphoma patients that may benefit from anti-EZH2 therapies. The comparison of the transcriptional profiles of type-1 and -2 primary tumors revealed a core subset of around 160 genes that consistently discriminated the two types of MYC-driven lymphomas. Among the genes that were expressed at higher levels in type-2 lymphomas, we identified *Cyclin D2* and components of the DNA replication machinery (*Mcm2, Mcm4* and *Prim2*). Higher levels of these genes may facilitate proliferation of MYC-expressing tumor cells starting from single cells. We also found that type-2 lymphomas expressed higher levels of the anti-apoptotic protein *Bcl2*, which may represent a strategy for tumor cells to overcome anoikis, as previously described (Galante et al., 2009; Hausmann et al., 2011; Martin and Vuori, 2004).

The importance of Ezh2 in the negative regulation of the tumor suppressor *Cdkn2a* led us to hypothesize that type-1 and -2 MYC-driven lymphomas may differ in the functional status of *Cdkn2a* and thereby in the response to Ezh2 inhibition. According to this hypothesis, whereas type-1 lymphomas would retain a functional *Cdkn2a* gene, and therefore require Ezh2 to ensure its repression and guarantee cell cycle progression, type-2 tumors would lose *Cdkn2a* function to overcome negative regulation of G1-to-S transition. Upon Ezh2 inactivation, type-1 lymphomas will suffer from de-repressed *Cdkn2a* expression, whereas Cdkn2a defective type-2 lymphoma will continue to grow. In support of our model, we observed that two out of three type-2 primary MYC lymphomas lost the integrity and/or the

expression of *Cdkn2a* locus. Instead, all type-1 tumors retained *Cdkn2a* locus and were able to up-regulate its expression upon Ezh2 inactivation. Another line of evidence supporting the importance of Cdkn2a regulation in the response of tumors to Ezh2 inactivation comes from the genetic analysis of the *Cdkn2a* locus in Ezh2 mutant clones established from Cdkn2a proficient type-1 lymphomas. Indeed, in one instance, we found that the establishment of an Ezh2 mutant clone was associated with bi-allelic loss of the *Cdkn2a* locus. The confirmation that the loss of the tumor suppressor locus *Cdkn2a* confers tumor resistance to Ezh2 inhibition on a larger series of MYC-driven lymphomas (including BL cell lines), will provide a clear rationale to screen lymphoma patients for the loss/silencing of the *Cdkn2a* locus, before enrolling them in clinical trials and/or treatment regimens based on anti-Ezh2 inhibitors.

The inactivation of Ezh2 in type-1 lymphomas led to the infrequent isolation of Ezh2 mutant subclones. We predicted that rare cells in the latter primary tumors had succeeded to overcome the acute loss of Ezh2 through the activation of compensatory mechanisms. The observation that Ezh2 mutant subclones, derived from type-1 lymphomas, had residual H3K27me3 levels led us to hypothesize that an alternative, non-canonical PRC2 complex consisting of Ezh1 replaced, at least partially, Ezh2 function in Ezh2 mutant cells, thereby facilitating clonal outgrowth starting from a single cell. To support this hypothesis, *Ezh1* transcripts were measured in λ-MYC lymphomas and found to be slightly up-regulated in Ezh2 mutant clones, suggesting a possible compensatory effect. We took advantage of a recently described Ezh1/2 double inhibitor, UNC1999 (Konze et al., 2013), to verify whether Ezh2 mutant lymphomas were dependent on Ezh1 for continuous growth. Indeed, significant *in vitro* growth impairment was observed in cultures of UNC1999-treated Ezh2 mutant lymphoma cells when compared to vehicle-treated cells. The evidence that UNC1999 acted via inhibition of residual H3K27 methyltransferase activity (possibly provided by Ezh1) came from the observation that low H3K27me3 levels detected in Ezh2

mutant subclones were further reduced after treatment with the inhibitor. These results, combined with the observation that the vast majority of the genome remained devoid of H3K27me3 in Ezh2 mutant subclones, are compatible with a model whereby an alternative Ezh1/PRC2 gets preferentially recruited onto a small subset of Ezh2/PRC2 target genes to ensure their repression in order to sustain tumor growth. Ezh1 functional redundancy has been previously proposed to explain experimental observations in induced pluripotent stem cells, hair follicle stem cells, and hematopoietic progenitors undergoing acute Ezh2 inactivation (Ezhkova et al., 2011; Fragola et al., 2013; Hidalgo et al., 2012)

However, the intersection of transcriptome data with H3K27me3 genome wide distribution results from both Ezh2 proficient and mutant clones revealed a more complex scenario. The repertoire of H3K27me3 marked genes in Ezh2 proficient tumors was significantly enriched for *bona fide* Polycomb targets. The vast majority of the latter genes lost H3K27me3 in Ezh2 mutant subclones, in line with previous studies showing up-regulation of such genes in Polycomb mutant cells (Leeb et al., 2010). Together, these results suggested that Ezh2 negatively regulates genes marked by H3K27me3 in lymphoma cells. Surprisingly, however, expression of the genes marked by H3K27me3 in Ezh2 proficient tumors remained largely unaffected after inactivation of the methyltransferase in type-1 lymphomas. These results suggest that the few Ezh2 mutant subclones established from type-1 lymphomas had set in place H3K27me3-independent (compensatory) mechanisms to ensure normal expression of Ezh2 targets. Gene ontology classification of the latter genes identified functional categories related to stem cell pluripotency. In particular, genes marked by H3K27me3 and unaffected in type-1 lymphomas were enriched for modulators of the Wnt/β−catening signaling.

Instead, inactivation of Ezh2 altered the expression of the majority of target genes in type-2 lymphomas. The fairly weak correlation in the expression profile of H3K27me3 targets in Ezh2 mutant compared to Ezh2 proficient subclones, established from type-2 lymphomas,

reinforce the view that repression of H3K27me3 targets in this set of tumors is not strictly required to sustain the growth of lymphoma cells.

Another unexpected observation came from the combined analysis of transcriptome and H3K27me3 distribution data obtained from type-1 Ezh2 mutant lymphoma cells. Specifically, bioinformatics analysis revealed that genes marked by H3K27me3 in Ezh2 mutant tumor cells were not previously identified as Polycomb targets. Instead, they were classified as genes usually decorated by histone marks (H3K4me3 and H3K4me1) indicative of active transcription. In support of this, we failed to observe any enrichment for H3K27me3 at the promoter of these genes in Ezh2 proficient tumors. These results indicate that a non-canonical PRC2, likely composed of Ezh1, gets relocated onto new target genes in Ezh2 mutant lymphomas and contributes to their H3K27 trimethylation (Mousavi et al., 2012). Pairwise comparison of the expression of the latter genes between Ezh2 proficient and mutant lymphomas revealed a poor correlation between the two experimental samples, pointing to a modulation of gene expression in Ezh2 mutant cells as a result of *de novo* H3K27me3 deposition by an alternative PRC2 complex.

All together the data support a model whereby the acute inactivation of Ezh2 is compensated by transcriptional and/or epigenetic (DNA methylation) mechanisms that ensure normal regulation of Ezh2 targets genes in a subset of MYC-transformed B cells. At the same time, the lack of Ezh2, facilitates/ensures the formation of an alternative PRC2 complex consisting of Ezh1, which is recruited to novel, mostly transcriptionally competent, target genes and modulates their expression. Regulation of the latter genes appears to be crucial for tumor growth, as the treatment of type-1 Ezh2 mutant subclones with the Ezh1/2 inhibitor UNC1999 impaired lymphoma expansion *in vitro*. The ability of Ezh1 to be recruited into a non-canonical PRC2 complex in Ezh2 mutant cells, where it contributes to the expression of H3K4me3-marked genes was recently reported in a study addressing the role of Ezh2 in erythroid lineage differentiation (Xu et al., 2015b). Given the limited number of samples so

far analyzed, the epigenomic and transcriptome analysis of a larger series of type-1 Ezh2 mutant lymphomas will be needed to support our conclusions.

The studies on type-1 lymphomas have unveiled the ability of MYC-transformed B cells to circumvent Ezh2 inactivation through the activity of Ezh1. These results have important clinical implications. Treatment of lymphomas and possibly other cancers with Ezh2 inhibitors may indeed unleash the growth of resistant cells that have compensated for the loss of Ezh2 methyltransferase activity through the action of Ezh1. In this context, the ability of the Ezh1/2 inhibitor UNC1999 to interfere with the growth of Ezh2 mutant lymphomas identifies inhibitors of PRC2 function (including UNC1999) as better options for the treatment of GC-derived lymphomas and possibly other cancer types.

Recent evidence showing that lymphomas chronically exposed to low doses of Ezh2 inhibitors lead to the selection of clonal variants acquiring resistance to the treatment (Gibaja et al., 2015), prompted us to investigate whether a similar phenomenon could occur in MYC-transformed B cells subjected to UNC1999 treatment. Chronic exposure of λ-MYC type-1 lymphomas to low doses of UNC1999 resulted in the selection of a pool of resistant cells. The acquired resistance to UNC1999 correlated with the restoration of H3K27me3 activity by resistant tumor B cells. This result is in line with the strict dependence of type-1 lymphomas on PRC2 catalytic activity provided by Ezh2. Future experiments on a representative number of independent clonal variants will indicate whether the reacquired capacity of resistant lymphoma cells to catalyze H3K27me3 results from acquired mutations within the Ezh2 coding sequence, which prevent the binding to UNC1999 (Gibaja et al., 2015). Conversely, in full agreement with our previous findings, type-2 lymphomas resisted to pharmacological PRC2 inhibition without the need to select mechanisms ensuring restoration of H3K27me3. These results identify λ-MYC type-2 lymphomas as a group of highly aggressive (e.g. they grow *in vivo* significantly faster than type-1 lymphomas) tumors that selected genetic mutations allowing tumor cells to grow independently of the PRC2

function. The reconstruction, through whole exome sequencing, of a comprehensive map of genetic mutations selectively found in type-2 lymphomas will contribute to decipher the molecular and genetic bases for primary and acquired resistance of lymphoma cells to the PRC2 inhibition.

8.1 Future plans

8.1.1 Can we employ the molecular signature discriminating λ-MYC type-1 from type-2 lymphomas to stratify B cell NHL?

To address this question, we will initially investigate whether the transcriptional signature identified in λ-MYC lymphomas can help stratify BL cell lines into two separate classes of tumors. Should this be observed, we will test the effects of UNC1999 on representative cases of tumor lines falling in the two categories (responders vs. non responders). A similar approach will be also followed for DLBCL cell lines, including the ones carrying EZH2 g.o.f. mutations. The comparison of the transcriptome profiles of BL (and DLBCL) lines differing in the response to UNC1999 treatment will represent a complementary strategy to ultimately identify a possible molecular signature that can predict the response of highly aggressive B cell tumors to PRC2 inhibition.

8.1.2 Can Cdkn2a status predict the response of B cell lymphomas to PRC2 inhibition?

The preferential inactivation/silencing of Cdkn2a in type-2 lymphomas suggests a possible contribution of this genetic alteration to the failure of lymphomas to response to Ezh2/PRC2 inhibition. To validate these findings, we will follow two strategies:

a) We will test the sensitivity to UNC1999 of Ezh2 mutant subclones derived from Cdkn2a proficient lymphomas that had subsequently lost *Cdkn2a* as a result of the cloning procedure. If Cdkn2a inactivation confers resistance to PRC2

inhibition, we expect to see a clear difference in the response to UNC1999 in Ezh2 mutant subclones that are respectively proficient and deficient for *Cdkn2a;*

b) To establish whether Cdkn2a inactivation, alone, is sufficient to render MYC-transformed B cells resistant to PRC2 inhibition, we will disrupt the *Cdkn2a* locus by Crispr/Cas9 technology in type-1 lymphomas followed by the treatment of mutant cells with UNC1999. The ability to specifically inhibit $p16^{INK4a}$, $p19^{ARF}$ or both genes targeting alternative *Cdkn2a* exons, will allow us to distinguish which gene encoded by the *Cdkn2a* locus is required to confer response of tumor cells to PRC2 inhibition.

8.1.3 The role of Ezh1 in the resistance of MYC lymphomas to Ezh2 inhibition

The data collected so far point to a primary role played by Ezh1 in sustaining the growth of type-1 lymphomas, following Ezh2 inactivation. To corroborate these results, we will employ a genetic approach to inactivate both Ezh1 and Ezh2 in λ-MYC lymphomas of both type-1 and -2 lymphomas. This will be achieved taking advantage of Crispr/Cas9 technology to disrupt the *Ezh1* gene in λ-MYC; $Ezh2^{fl/fl}$ tumor cells, followed by TAT-Cre transduction in order to inactivate Ezh2. The goal of these studies is to confirm the different requirement of type-1 and -2 lymphomas for combined inactivation of Ezh proteins. Should these results confirm our current findings, we will validate the results inhibiting PRC2 function through sequential disruption of the Ezh1 and Ezh2 genes in BL cell lines.

Concerning the mechanism of action of Ezh1, we will consolidate our findings on the genome wide distribution of residual H3K27me3 in Ezh2 mutant subclones, analyzing a larger number of them. We will confirm the existence of H3K27me3 marked genes in Ezh2 mutant subclones by performing by ChIP-qPCR on candidate genes. More importantly, we will test the acute effects of UNC1999 treatment on their expression, to establish which

genes are modulated by H3K27me3. The latter set of genes is expected to include important determinants of lymphoma resistance to Ezh2 inactivation.

8.1.4 Genetics of resistance to PRC2 inhibition

The λ-MYC lymphoma model has provided us with an invaluable source of tumors that display primary resistance to Ezh2 inactivation. This offers the opportunity to reconstruct the genetic map of resistance to Ezh2 inactivation. To this end, we will initially perform whole exome sequencing on three independent type-2 lymphomas, in order to define the spectrum of mutations selected in these tumors. The status of candidate genes will be assessed in type-1 lymphomas to exclude those that are shared between the two types of tumors and hence are likely not responsible for conferring resistance/sensitivity to Ezh2 inhibition.

8.1.5 Can UNC1999 treatment become an effective treatment to cure type-1 MYC-driven B cell lymphomas?

In order to translate into the clinical setting our findings on the efficacy of UNC1999 to inhibit the growth of type-1 lymphomas, we will perform transplantation studies using type-1 lymphomas, followed by the treatment of recipient animals with UNC1999. Goal of these studies is to reveal whether pharmacological Ezh1/2 inhibition in immunoproficient animals delays/impairs *in vivo* growth of λ-MYC type-1 lymphomas.

9 References

- Adams, J.M., Harris, A.W., Pinkert, C.A., Corcoran, L.M., Alexander, W.S., Cory, S., Palmiter, R.D., and Brinster, R.L. (1985). The c-myc oncogene driven by immunoglobulin enhancers induces lymphoid malignancy in transgenic mice. Nature *318*, 533-538.
- Agherbi, H., Gaussmann-Wenger, A., Verthuy, C., Chasson, L., Serrano, M., and Djabali, M. (2009). Polycomb mediated epigenetic silencing and replication timing at the INK4a/ARF locus during senescence. PloS one *4*, e5622.
- Akamine, R., Yamamoto, T., Watanabe, M., Yamazaki, N., Kataoka, M., Ishikawa, M., Ooie, T., Baba, Y., and Shinohara, Y. (2007). Usefulness of the 5' region of the cDNA encoding acidic ribosomal phosphoprotein P0 conserved among rats, mice, and humans as a standard probe for gene expression analysis in different tissues and animal species. Journal of biochemical and biophysical methods *70*, 481-486.
- Alberghini, F., Petrocelli, V., Rahmat, M., and Casola, S. (2015). An epigenetic view of B-cell disorders. Immunology and cell biology *93*, 253-260.
- Allen, C.D., Okada, T., and Cyster, J.G. (2007). Germinal-center organization and cellular dynamics. Immunity *27*, 190-202.
- Attwooll, C., Oddi, S., Cartwright, P., Prosperini, E., Agger, K., Steensgaard, P., Wagener, C., Sardet, C., Moroni, M.C., and Helin, K. (2005). A novel repressive E2F6 complex containing the polycomb group protein, EPC1, that interacts with EZH2 in a proliferation-specific manner. The Journal of biological chemistry *280*, 1199-1208.
- Basso, K., and Dalla-Favera, R. (2015). Germinal centres and B cell lymphomagenesis. Nature reviews. Immunology *15*, 172-184.
- Battey, J., Moulding, C., Taub, R., Murphy, W., Stewart, T., Potter, H., Lenoir, G., and Leder, P. (1983). The human c-myc oncogene: structural consequences of translocation into the IgH locus in Burkitt lymphoma. Cell *34*, 779-787.
- Beck, D.B., Bonasio, R., Kaneko, S., Li, G., Margueron, R., Oda, H., Sarma, K., Sims, R.J., 3rd, Son, J., Trojer, P., and Reinberg, D. (2010). Chromatin in the nuclear landscape. Cold Spring Harbor symposia on quantitative biology *75*, 11-22.
- Beguelin, W., Popovic, R., Teater, M., Jiang, Y., Bunting, K.L., Rosen, M., Shen, H., Yang, S.N., Wang, L., Ezponda, T.*, et al.* (2013). EZH2 is required for germinal center formation and somatic EZH2 mutations promote lymphoid transformation. Cancer cell *23*, 677-692.
- Beisel, C., Buness, A., Roustan-Espinosa, I.M., Koch, B., Schmitt, S., Haas, S.A., Hild, M., Katsuyama, T., and Paro, R. (2007). Comparing active and repressed expression states of genes controlled by the Polycomb/Trithorax group proteins. Proceedings of the National Academy of Sciences of the United States of America *104*, 16615-16620.
- Berg, T., Thoene, S., Yap, D., Wee, T., Schoeler, N., Rosten, P., Lim, E., Bilenky, M., Mungall, A.J., Oellerich, T.*, et al.* (2014). A transgenic mouse model demonstrating the oncogenic role of mutations in the polycomb-group gene EZH2 in lymphomagenesis. Blood *123*, 3914-3924.
- Blum, K.A., Lozanski, G., and Byrd, J.C. (2004). Adult Burkitt leukemia and lymphoma. Blood *104*, 3009-3020.

- Bodor, C., Grossmann, V., Popov, N., Okosun, J., O'Riain, C., Tan, K., Marzec, J., Araf, S., Wang, J., Lee, A.M.*, et al.* (2013). EZH2 mutations are frequent and represent an early event in follicular lymphoma. Blood *122*, 3165-3168.
- Boukarabila, H., Saurin, A.J., Batsche, E., Mossadegh, N., van Lohuizen, M., Otte, A.P., Pradel, J., Muchardt, C., Sieweke, M., and Duprez, E. (2009). The PRC1 Polycomb group complex interacts with PLZF/RARA to mediate leukemic transformation. Genes & development *23*, 1195-1206.
- Boyer, L.A., Plath, K., Zeitlinger, J., Brambrink, T., Medeiros, L.A., Lee, T.I., Levine, S.S., Wernig, M., Tajonar, A., Ray, M.K.*, et al.* (2006). Polycomb complexes repress developmental regulators in murine embryonic stem cells. Nature *441*, 349-353.
- Bracken, A.P., Kleine-Kohlbrecher, D., Dietrich, N., Pasini, D., Gargiulo, G., Beekman, C., Theilgaard-Monch, K., Minucci, S., Porse, B.T., Marine, J.C.*, et al.* (2007). The Polycomb group proteins bind throughout the INK4A-ARF locus and are disassociated in senescent cells. Genes & development *21*, 525-530.
- Bracken, A.P., Pasini, D., Capra, M., Prosperini, E., Colli, E., and Helin, K. (2003). EZH2 is downstream of the pRB-E2F pathway, essential for proliferation and amplified in cancer. The EMBO journal *22*, 5323-5335.
- Burkitt, D. (1958). A sarcoma involving the jaws in African children. The British journal of surgery *46*, 218-223.
- Burkitt, D. (1962). A children's cancer dependent on climatic factors. Nature *194*, 232-234.
- Caganova, M., Carrisi, C., Varano, G., Mainoldi, F., Zanardi, F., Germain, P.L., George, L., Alberghini, F., Ferrarini, L., Talukder, A.K.*, et al.* (2013). Germinal center dysregulation by histone methyltransferase EZH2 promotes lymphomagenesis. The Journal of clinical investigation *123*, 5009-5022.
- Calado, D.P., Sasaki, Y., Godinho, S.A., Pellerin, A., Kochert, K., Sleckman, B.P., de Alboran, I.M., Janz, M., Rodig, S., and Rajewsky, K. (2012). The cell-cycle regulator c-Myc is essential for the formation and maintenance of germinal centers. Nature immunology *13*, 1092-1100.
- Campbell, S., Ismail, I.H., Young, L.C., Poirier, G.G., and Hendzel, M.J. (2013). Polycomb repressive complex 2 contributes to DNA double-strand break repair. Cell cycle *12*, 2675-2683.
- Campisi, J., and d'Adda di Fagagna, F. (2007). Cellular senescence: when bad things happen to good cells. Nature reviews. Molecular cell biology *8*, 729-740.
- Campo, E., Swerdlow, S.H., Harris, N.L., Pileri, S., Stein, H., and Jaffe, E.S. (2011). The 2008 WHO classification of lymphoid neoplasms and beyond: evolving concepts and practical applications. Blood *117*, 5019-5032.
- Campos, E.I., Stafford, J.M., and Reinberg, D. (2014). Epigenetic inheritance: histone bookmarks across generations. Trends in cell biology *24*, 664-674.
- Cao, R., Wang, L., Wang, H., Xia, L., Erdjument-Bromage, H., Tempst, P., Jones, R.S., and Zhang, Y. (2002). Role of histone H3 lysine 27 methylation in Polycomb-group silencing. Science *298*, 1039-1043.

- Cao, R., and Zhang, Y. (2004). SUZ12 is required for both the histone methyltransferase activity and the silencing function of the EED-EZH2 complex. Molecular cell *15*, 57-67.
- Caretti, G., Di Padova, M., Micales, B., Lyons, G.E., and Sartorelli, V. (2004). The Polycomb Ezh2 methyltransferase regulates muscle gene expression and skeletal muscle differentiation. Genes & development *18*, 2627-2638.
- Casola, S. (2007). Control of peripheral B-cell development. Current opinion in immunology *19*, 143-149.
- Chagraoui, J., Hebert, J., Girard, S., and Sauvageau, G. (2011). An anticlastogenic function for the Polycomb Group gene Bmi1. Proceedings of the National Academy of Sciences of the United States of America *108*, 5284-5289.
- Chamberlain, S.J., Yee, D., and Magnuson, T. (2008). Polycomb repressive complex 2 is dispensable for maintenance of embryonic stem cell pluripotency. Stem cells *26*, 1496-1505.
- Chang, S.E.a.Z.B. (2011). Foxo1 is essential for germinal center B cell functions and the development of collagen-induced arthritis The journal of Immunology *186*.
- Chapman, A., Stewart, S.J., Nepom, G.T., Green, W.F., Crowe, D., Thomas, J.W., and Miller, G.G. (1996). CD11b+CD28-CD4+ human T cells: activation requirements and association with HLA-DR alleles. Journal of immunology *157*, 4771-4780.
- Chaudhuri, J., and Alt, F.W. (2004). Class-switch recombination: interplay of transcription, DNA deamination and DNA repair. Nature reviews. Immunology *4*, 541-552.
- Chen, H., Gu, X., Su, I.H., Bottino, R., Contreras, J.L., Tarakhovsky, A., and Kim, S.K. (2009). Polycomb protein Ezh2 regulates pancreatic beta-cell Ink4a/Arf expression and regeneration in diabetes mellitus. Genes & development *23*, 975-985.
- Chou, D.M., Adamson, B., Dephoure, N.E., Tan, X., Nottke, A.C., Hurov, K.E., Gygi, S.P., Colaiacovo, M.P., and Elledge, S.J. (2010). A chromatin localization screen reveals poly (ADP ribose)-regulated recruitment of the repressive polycomb and NuRD complexes to sites of DNA damage. Proceedings of the National Academy of Sciences of the United States of America *107*, 18475-18480.
- Collett, K., Eide, G.E., Arnes, J., Stefansson, I.M., Eide, J., Braaten, A., Aas, T., Otte, A.P., and Akslen, L.A. (2006). Expression of enhancer of zeste homologue 2 is significantly associated with increased tumor cell proliferation and is a marker of aggressive breast cancer. Clinical cancer research : an official journal of the American Association for Cancer Research *12*, 1168-1174.
- Cui, K., Zang, C., Roh, T.Y., Schones, D.E., Childs, R.W., Peng, W., and Zhao, K. (2009). Chromatin signatures in multipotent human hematopoietic stem cells indicate the fate of bivalent genes during differentiation. Cell stem cell *4*, 80-93.
- Dalla-Favera, R., Bregni, M., Erikson, J., Patterson, D., Gallo, R.C., and Croce, C.M. (1982). Human c-myc onc gene is located on the region of chromosome 8 that is translocated in Burkitt lymphoma cells. Proceedings of the National Academy of Sciences of the United States of America *79*, 7824-7827.
- Dhawan, S., Tschen, S.I., and Bhushan, A. (2009). Bmi-1 regulates the Ink4a/Arf locus to control pancreatic beta-cell proliferation. Genes & development *23*, 906-911.

- Di Croce, L., and Helin, K. (2013). Transcriptional regulation by Polycomb group proteins. Nature structural & molecular biology *20*, 1147-1155.
- Di Micco, R., Sulli, G., Dobreva, M., Liontos, M., Botrugno, O.A., Gargiulo, G., dal Zuffo, R., Matti, V., d'Ario, G., Montani, E.*, et al.* (2011). Interplay between oncogene-induced DNA damage response and heterochromatin in senescence and cancer. Nature cell biology *13*, 292-302.
- Dietrich, N., Bracken, A.P., Trinh, E., Schjerling, C.K., Koseki, H., Rappsilber, J., Helin, K., and Hansen, K.H. (2007). Bypass of senescence by the polycomb group protein CBX8 through direct binding to the INK4A-ARF locus. The EMBO journal *26*, 1637-1648.
- Dominguez-Sola, D., Victora, G.D., Ying, C.Y., Phan, R.T., Saito, M., Nussenzweig, M.C., and Dalla-Favera, R. (2012). The proto-oncogene MYC is required for selection in the germinal center and cyclic reentry. Nature immunology *13*, 1083-1091.
- Dorsett, Y., Robbiani, D.F., Jankovic, M., Reina-San-Martin, B., Eisenreich, T.R., and Nussenzweig, M.C. (2007). A role for AID in chromosome translocations between c-myc and the IgH variable region. The Journal of experimental medicine *204*, 2225-2232.
- Dukers, D.F., van Galen, J.C., Giroth, C., Jansen, P., Sewalt, R.G., Otte, A.P., Kluin-Nelemans, H.C., Meijer, C.J., and Raaphorst, F.M. (2004). Unique polycomb gene expression pattern in Hodgkin's lymphoma and Hodgkin's lymphoma-derived cell lines. The American journal of pathology *164*, 873-881.
- Ernst, T., Chase, A.J., Score, J., Hidalgo-Curtis, C.E., Bryant, C., Jones, A.V., Waghorn, K., Zoi, K., Ross, F.M., Reiter, A.*, et al.* (2010). Inactivating mutations of the histone methyltransferase gene EZH2 in myeloid disorders. Nature genetics *42*, 722-726.
- Evan, G.I., Wyllie, A.H., Gilbert, C.S., Littlewood, T.D., Land, H., Brooks, M., Waters, C.M., Penn, L.Z., and Hancock, D.C. (1992). Induction of apoptosis in fibroblasts by c-myc protein. Cell *69*, 119-128.
- Ezhkova, E., Lien, W.H., Stokes, N., Pasolli, H.A., Silva, J.M., and Fuchs, E. (2011). EZH1 and EZH2 cogovern histone H3K27 trimethylation and are essential for hair follicle homeostasis and wound repair. Genes & development *25*, 485-498.
- Ezhkova, E., Pasolli, H.A., Parker, J.S., Stokes, N., Su, I.H., Hannon, G., Tarakhovsky, A., and Fuchs, E. (2009). Ezh2 orchestrates gene expression for the stepwise differentiation of tissue-specific stem cells. Cell *136*, 1122-1135.
- Facchino, S., Abdouh, M., Chatoo, W., and Bernier, G. (2010). BMI1 confers radioresistance to normal and cancerous neural stem cells through recruitment of the DNA damage response machinery. The Journal of neuroscience : the official journal of the Society for Neuroscience *30*, 10096-10111.
- Fan, T., Jiang, S., Chung, N., Alikhan, A., Ni, C., Lee, C.C., and Hornyak, T.J. (2011). EZH2-Dependent Suppression of a Cellular Senescence Phenotype in Melanoma Cells by Inhibition of p21/CDKN1A Expression. Molecular cancer research : MCR *9*, 418-429.
- Fasano, C.A., Dimos, J.T., Ivanova, N.B., Lowry, N., Lemischka, I.R., and Temple, S. (2007). shRNA knockdown of Bmi-1 reveals a critical role for p21-Rb pathway in NSC self-renewal during development. Cell stem cell *1*, 87-99.

- Foon, K.A., Takeshita, K., and Zinzani, P.L. (2012). Novel therapies for aggressive B-cell lymphoma. Advances in hematology *2012*, 302570.
- Fragola, G., Germain, P.L., Laise, P., Cuomo, A., Blasimme, A., Gross, F., Signaroldi, E., Bucci, G., Sommer, C., Pruneri, G.*, et al.* (2013). Cell reprogramming requires silencing of a core subset of polycomb targets. PLoS genetics *9*, e1003292.
- Galante, J.M., Mortenson, M.M., Bowles, T.L., Virudachalam, S., and Bold, R.J. (2009). ERK/BCL-2 pathway in the resistance of pancreatic cancer to anoikis. The Journal of surgical research *152*, 18-25.
- Gao, Z., Zhang, J., Bonasio, R., Strino, F., Sawai, A., Parisi, F., Kluger, Y., and Reinberg, D. (2012). PCGF homologs, CBX proteins, and RYBP define functionally distinct PRC1 family complexes. Molecular cell *45*, 344-356.
- Giacinti, C., and Giordano, A. (2006). RB and cell cycle progression. Oncogene *25*, 5220-5227.
- Gibaja, V., Shen, F., Harari, J., Korn, J., Ruddy, D., Saenz-Vash, V., Zhai, H., Rejtar, T., Paris, C.G., Yu, Z.*, et al.* (2015). Development of secondary mutations in wild-type and mutant EZH2 alleles cooperates to confer resistance to EZH2 inhibitors. Oncogene.
- Ginjala, V., Nacerddine, K., Kulkarni, A., Oza, J., Hill, S.J., Yao, M., Citterio, E., van Lohuizen, M., and Ganesan, S. (2011). BMI1 Is Recruited to DNA Breaks and Contributes to DNA Damage-Induced H2A Ubiquitination and Repair. Molecular and cellular biology *31*, 1972-1982.
- Gunawan, M., Venkatesan, N., Loh, J.T., Wong, J.F., Berger, H., Neo, W.H., Li, L.Y., La Win, M.K., Yau, Y.H., Guo, T.*, et al.* (2015). The methyltransferase Ezh2 controls cell adhesion and migration through direct methylation of the extranuclear regulatory protein talin. Nature immunology *16*, 505-516.
- Guo, J., Cai, J., Yu, L., Tang, H., Chen, C., and Wang, Z. (2011). EZH2 regulates expression of p57 and contributes to progression of ovarian cancer in vitro and in vivo. Cancer science *102*, 530-539.
- Guo, W.J., Datta, S., Band, V., and Dimri, G.P. (2007). Mel-18, a polycomb group protein, regulates cell proliferation and senescence via transcriptional repression of Bmi-1 and c-Myc oncoproteins. Molecular biology of the cell *18*, 536-546.
- Hausmann, M., Leucht, K., Ploner, C., Kiessling, S., Villunger, A., Becker, H., Hofmann, C., Falk, W., Krebs, M., Kellermeier, S.*, et al.* (2011). BCL-2 modifying factor (BMF) is a central regulator of anoikis in human intestinal epithelial cells. The Journal of biological chemistry *286*, 26533-26540.
- Hecht, J.L., and Aster, J.C. (2000). Molecular biology of Burkitt's lymphoma. Journal of clinical oncology : official journal of the American Society of Clinical Oncology *18*, 3707-3721.
- Herranz, N., Pasini, D., Diaz, V.M., Franci, C., Gutierrez, A., Dave, N., Escriva, M., Hernandez-Munoz, I., Di Croce, L., Helin, K.*, et al.* (2008). Polycomb complex 2 is required for E-cadherin repression by the Snail1 transcription factor. Molecular and cellular biology *28*, 4772-4781.
- Hidalgo, I., Herrera-Merchan, A., Ligos, J.M., Carramolino, L., Nunez, J., Martinez, F., Dominguez, O., Torres, M., and Gonzalez, S. (2012). Ezh1 is required for hematopoietic stem cell maintenance and prevents senescence-like cell cycle arrest. Cell stem cell *11*, 649-662.

- Ismail, I.H., Andrin, C., McDonald, D., and Hendzel, M.J. (2010). BMI1-mediated histone ubiquitylation promotes DNA double-strand break repair. The Journal of cell biology *191*, 45-60.
- Itahana, K., Zou, Y., Itahana, Y., Martinez, J.L., Beausejour, C., Jacobs, J.J., Van Lohuizen, M., Band, V., Campisi, J., and Dimri, G.P. (2003). Control of the replicative life span of human fibroblasts by p16 and the polycomb protein Bmi-1. Molecular and cellular biology *23*, 389-401.
- Jacobs, J.J., Kieboom, K., Marino, S., DePinho, R.A., and van Lohuizen, M. (1999). The oncogene and Polycomb-group gene bmi-1 regulates cell proliferation and senescence through the ink4a locus. Nature *397*, 164-168.
- Jung, H.Y., Jun, S., Lee, M., Kim, H.C., Wang, X., Ji, H., McCrea, P.D., and Park, J.I. (2013). PAF and EZH2 induce Wnt/beta-catenin signaling hyperactivation. Molecular cell *52*, 193-205.
- Kanhere, A., Viiri, K., Araujo, C.C., Rasaiyaah, J., Bouwman, R.D., Whyte, W.A., Pereira, C.F., Brookes, E., Walker, K., Bell, G.W.*, et al.* (2010). Short RNAs are transcribed from repressed polycomb target genes and interact with polycomb repressive complex-2. Molecular cell *38*, 675-688.
- Kayagaki, N., Yan, M., Seshasayee, D., Wang, H., Lee, W., French, D.M., Grewal, I.S., Cochran, A.G., Gordon, N.C., Yin, J.*, et al.* (2002). BAFF/BLyS receptor 3 binds the B cell survival factor BAFF ligand through a discrete surface loop and promotes processing of NF-kappaB2. Immunity *17*, 515-524.
- Khan, S.N., Jankowska, A.M., Mahfouz, R., Dunbar, A.J., Sugimoto, Y., Hosono, N., Hu, Z., Cheriyath, V., Vatolin, S., Przychodzen, B.*, et al.* (2013). Multiple mechanisms deregulate EZH2 and histone H3 lysine 27 epigenetic changes in myeloid malignancies. Leukemia *27*, 1301-1309.
- Kim, E., Kim, M., Woo, D.H., Shin, Y., Shin, J., Chang, N., Oh, Y.T., Kim, H., Rheey, J., Nakano, I.*, et al.* (2013a). Phosphorylation of EZH2 activates STAT3 signaling via STAT3 methylation and promotes tumorigenicity of glioblastoma stem-like cells. Cancer cell *23*, 839-852.
- Kim, W., Bird, G.H., Neff, T., Guo, G., Kerenyi, M.A., Walensky, L.D., and Orkin, S.H. (2013b). Targeted disruption of the EZH2-EED complex inhibits EZH2-dependent cancer. Nature chemical biology *9*, 643-650.
- Kim, W.Y., and Sharpless, N.E. (2006). The regulation of INK4/ARF in cancer and aging. Cell *127*, 265-275.
- Kleer, C.G., Cao, Q., Varambally, S., Shen, R., Ota, I., Tomlins, S.A., Ghosh, D., Sewalt, R.G., Otte, A.P., Hayes, D.F.*, et al.* (2003). EZH2 is a marker of aggressive breast cancer and promotes neoplastic transformation of breast epithelial cells. Proceedings of the National Academy of Sciences of the United States of America *100*, 11606-11611.
- Klein, U., and Dalla-Favera, R. (2008). Germinal centres: role in B-cell physiology and malignancy. Nature reviews. Immunology *8*, 22-33.
- Klein, U., Klein, G., Ehlin-Henriksson, B., Rajewsky, K., and Kuppers, R. (1995). Burkitt's lymphoma is a malignancy of mature B cells expressing somatically mutated V region genes. Molecular medicine *1*, 495-505.
- Klein, U., Tu, Y., Stolovitzky, G.A., Keller, J.L., Haddad, J., Jr., Miljkovic, V., Cattoretti, G., Califano, A., and Dalla-Favera, R. (2003). Transcriptional analysis of

the B cell germinal center reaction. Proceedings of the National Academy of Sciences of the United States of America *100*, 2639-2644.

- Knutson, S.K., Wigle, T.J., Warholic, N.M., Sneeringer, C.J., Allain, C.J., Klaus, C.R., Sacks, J.D., Raimondi, A., Majer, C.R., Song, J.*, et al.* (2012). A selective inhibitor of EZH2 blocks H3K27 methylation and kills mutant lymphoma cells. Nature chemical biology *8*, 890-896.
- Konze, K.D., Ma, A., Li, F., Barsyte-Lovejoy, D., Parton, T., Macnevin, C.J., Liu, F., Gao, C., Huang, X.P., Kuznetsova, E.*, et al.* (2013). An orally bioavailable chemical probe of the Lysine Methyltransferases EZH2 and EZH1. ACS chemical biology *8*, 1324-1334.
- Koppens, M., and van Lohuizen, M. (2015). Context-dependent actions of Polycomb repressors in cancer. Oncogene.
- Kornberg, R.D. (1974). Chromatin structure: a repeating unit of histones and DNA. Science *184*, 868-871.
- Kotake, Y., Nakagawa, T., Kitagawa, K., Suzuki, S., Liu, N., Kitagawa, M., and Xiong, Y. (2011). Long non-coding RNA ANRIL is required for the PRC2 recruitment to and silencing of p15(INK4B) tumor suppressor gene. Oncogene *30*, 1956-1962.
- Kovalchuk, A.L., Qi, C.F., Torrey, T.A., Taddesse-Heath, L., Feigenbaum, L., Park, S.S., Gerbitz, A., Klobeck, G., Hoertnagel, K., Polack, A.*, et al.* (2000). Burkitt lymphoma in the mouse. The Journal of experimental medicine *192*, 1183-1190.
- Ku, M., Koche, R.P., Rheinbay, E., Mendenhall, E.M., Endoh, M., Mikkelsen, T.S., Presser, A., Nusbaum, C., Xie, X., Chi, A.S.*, et al.* (2008). Genomewide analysis of PRC1 and PRC2 occupancy identifies two classes of bivalent domains. PLoS genetics *4*, e1000242.
- Kuppers, R., Klein, U., Hansmann, M.L., and Rajewsky, K. (1999). Cellular origin of human B-cell lymphomas. The New England journal of medicine *341*, 1520-1529.
- Kuzyk, A., and Mai, S. (2014). c-MYC-induced genomic instability. Cold Spring Harbor perspectives in medicine *4*, a014373.
- Laborda, J. (1991). 36B4 cDNA used as an estradiol-independent mRNA control is the cDNA for human acidic ribosomal phosphoprotein PO. Nucleic acids research *19*, 3998.
- Landeira, D., Sauer, S., Poot, R., Dvorkina, M., Mazzarella, L., Jorgensen, H.F., Pereira, C.F., Leleu, M., Piccolo, F.M., Spivakov, M.*, et al.* (2010). Jarid2 is a PRC2 component in embryonic stem cells required for multi-lineage differentiation and recruitment of PRC1 and RNA Polymerase II to developmental regulators. Nature cell biology *12*, 618-624.
- Langmead, B., and Salzberg, S.L. (2012). Fast gapped-read alignment with Bowtie 2. Nature methods *9*, 357-359.
- Laugesen, A., and Helin, K. (2014). Chromatin repressive complexes in stem cells, development, and cancer. Cell stem cell *14*, 735-751.
- Lee, J.M., Lee, J.S., Kim, H., Kim, K., Park, H., Kim, J.Y., Lee, S.H., Kim, I.S., Kim, J., Lee, M.*, et al.* (2012). EZH2 generates a methyl degron that is recognized by the DCAF1/DDB1/CUL4 E3 ubiquitin ligase complex. Molecular cell *48*, 572-586.

- Lee, S.C., Phipson, B., Hyland, C.D., Leong, H.S., Allan, R.S., Lun, A., Hilton, D.J., Nutt, S.L., Blewitt, M.E., Smyth, G.K.*, et al.* (2013). Polycomb repressive complex 2 (PRC2) suppresses Emu-myc lymphoma. Blood *122*, 2654-2663.
- Leeb, M., Pasini, D., Novatchkova, M., Jaritz, M., Helin, K., and Wutz, A. (2010). Polycomb complexes act redundantly to repress genomic repeats and genes. Genes & development *24*, 265-276.
- Levine, S.S., Weiss, A., Erdjument-Bromage, H., Shao, Z., Tempst, P., and Kingston, R.E. (2002). The core of the polycomb repressive complex is compositionally and functionally conserved in flies and humans. Molecular and cellular biology *22*, 6070-6078.
- Lewis, E.B. (1978). A gene complex controlling segmentation in Drosophila. Nature *276*, 565-570.
- Lewis, P. (1949). Pc: Polycomb. Drosophila Information Service *21*, 69.
- Lewis, P.W., Muller, M.M., Koletsky, M.S., Cordero, F., Lin, S., Banaszynski, L.A., Garcia, B.A., Muir, T.W., Becher, O.J., and Allis, C.D. (2013). Inhibition of PRC2 activity by a gain-of-function H3 mutation found in pediatric glioblastoma. Science *340*, 857-861.
- Li, G., Margueron, R., Ku, M., Chambon, P., Bernstein, B.E., and Reinberg, D. (2010). Jarid2 and PRC2, partners in regulating gene expression. Genes & development *24*, 368-380.
- Liu, Y., and Mullbacher, A. (1989). Activated B cells can deliver help for the in vitro generation of antiviral cytotoxic T cells. Proceedings of the National Academy of Sciences of the United States of America *86*, 4629-4633.
- Livak, K.J., and Schmittgen, T.D. (2001). Analysis of relative gene expression data using real-time quantitative PCR and the 2(-Delta Delta C(T)) Method. Methods *25*, 402-408.
- Lohr, J.G., Stojanov, P., Lawrence, M.S., Auclair, D., Chapuy, B., Sougnez, C., Cruz-Gordillo, P., Knoechel, B., Asmann, Y.W., Slager, S.L.*, et al.* (2012). Discovery and prioritization of somatic mutations in diffuse large B-cell lymphoma (DLBCL) by whole-exome sequencing. Proceedings of the National Academy of Sciences of the United States of America *109*, 3879-3884.
- Lund, K., Adams, P.D., and Copland, M. (2014). EZH2 in normal and malignant hematopoiesis. Leukemia *28*, 44-49.
- MacLennan, I.C. (1994). Germinal centers. Annual review of immunology *12*, 117-139.
- Margueron, R., Li, G., Sarma, K., Blais, A., Zavadil, J., Woodcock, C.L., Dynlacht, B.D., and Reinberg, D. (2008). Ezh1 and Ezh2 maintain repressive chromatin through different mechanisms. Molecular cell *32*, 503-518.
- Margueron, R., and Reinberg, D. (2011). The Polycomb complex PRC2 and its mark in life. Nature *469*, 343-349.
- Martin, S.S., and Vuori, K. (2004). Regulation of Bcl-2 proteins during anoikis and amorphosis. Biochimica et biophysica acta *1692*, 145-157.
- Martinez-Valdez, H., Guret, C., de Bouteiller, O., Fugier, I., Banchereau, J., and Liu, Y.J. (1996). Human germinal center B cells express the apoptosis-inducing genes

Fas, c-myc, P53, and Bax but not the survival gene bcl-2. The Journal of experimental medicine *183*, 971-977.

- McCabe, M.T., Graves, A.P., Ganji, G., Diaz, E., Halsey, W.S., Jiang, Y., Smitheman, K.N., Ott, H.M., Pappalardi, M.B., Allen, K.E.*, et al.* (2012a). Mutation of A677 in histone methyltransferase EZH2 in human B-cell lymphoma promotes hypertrimethylation of histone H3 on lysine 27 (H3K27). Proceedings of the National Academy of Sciences of the United States of America *109*, 2989-2994.
- McCabe, M.T., Ott, H.M., Ganji, G., Korenchuk, S., Thompson, C., Van Aller, G.S., Liu, Y., Graves, A.P., Della Pietra, A., 3rd, Diaz, E.*, et al.* (2012b). EZH2 inhibition as a therapeutic strategy for lymphoma with EZH2-activating mutations. Nature *492*, 108-112.
- McHeyzer-Williams, L.J., Pelletier, N., Mark, L., Fazilleau, N., and McHeyzer-Williams, M.G. (2009). Follicular helper T cells as cognate regulators of B cell immunity. Current opinion in immunology *21*, 266-273.
- Meyer, N., Kim, S.S., and Penn, L.Z. (2006). The Oscar-worthy role of Myc in apoptosis. Seminars in cancer biology *16*, 275-287.
- Miki, J., Fujimura, Y., Koseki, H., and Kamijo, T. (2007). Polycomb complexes regulate cellular senescence by repression of ARF in cooperation with E2F3. Genes to cells : devoted to molecular & cellular mechanisms *12*, 1371-1382.
- Miltenyi, S., Muller, W., Weichel, W., and Radbruch, A. (1990). High gradient magnetic cell separation with MACS. Cytometry *11*, 231-238.
- Miranda, T.B., Cortez, C.C., Yoo, C.B., Liang, G., Abe, M., Kelly, T.K., Marquez, V.E., and Jones, P.A. (2009). DZNep is a global histone methylation inhibitor that reactivates developmental genes not silenced by DNA methylation. Molecular cancer therapeutics *8*, 1579-1588.
- Miyazaki, M., Miyazaki, K., Itoi, M., Katoh, Y., Guo, Y., Kanno, R., Katoh-Fukui, Y., Honda, H., Amagai, T., van Lohuizen, M.*, et al.* (2008). Thymocyte proliferation induced by pre-T cell receptor signaling is maintained through polycomb gene product Bmi-1-mediated Cdkn2a repression. Immunity *28*, 231-245.
- Mochizuki-Kashio, M., Aoyama, K., Sashida, G., Oshima, M., Tomioka, T., Muto, T., Wang, C., and Iwama, A. (2015). Ezh2 loss in hematopoietic stem cells predisposes mice to develop heterogeneous malignancies in an Ezh1-dependent manner. Blood *126*, 1172-1183.
- Mohn, F., Weber, M., Rebhan, M., Roloff, T.C., Richter, J., Stadler, M.B., Bibel, M., and Schubeler, D. (2008). Lineage-specific polycomb targets and de novo DNA methylation define restriction and potential of neuronal progenitors. Molecular cell *30*, 755-766.
- Molyneux, E.M., Rochford, R., Griffin, B., Newton, R., Jackson, G., Menon, G., Harrison, C.J., Israels, T., and Bailey, S. (2012). Burkitt's lymphoma. Lancet *379*, 1234-1244.
- Mond, J.J., Vos, Q., Lees, A., and Snapper, C.M. (1995). T cell independent antigens. Current opinion in immunology *7*, 349-354.
- Morey, L., and Helin, K. (2010). Polycomb group protein-mediated repression of transcription. Trends in biochemical sciences *35*, 323-332.

- Morin, R.D., Johnson, N.A., Severson, T.M., Mungall, A.J., An, J., Goya, R., Paul, J.E., Boyle, M., Woolcock, B.W., Kuchenbauer, F.*, et al.* (2010). Somatic mutations altering EZH2 (Tyr641) in follicular and diffuse large B-cell lymphomas of germinal-center origin. Nature genetics *42*, 181-185.
- Morin, R.D., Mendez-Lago, M., Mungall, A.J., Goya, R., Mungall, K.L., Corbett, R.D., Johnson, N.A., Severson, T.M., Chiu, R., Field, M.*, et al.* (2011). Frequent mutation of histone-modifying genes in non-Hodgkin lymphoma. Nature *476*, 298-303.
- Mousavi, K., Zare, H., Wang, A.H., and Sartorelli, V. (2012). Polycomb protein Ezh1 promotes RNA polymerase II elongation. Molecular cell *45*, 255-262.
- Muramatsu, M., Sankaranand, V.S., Anant, S., Sugai, M., Kinoshita, K., Davidson, N.O., and Honjo, T. (1999). Specific expression of activation-induced cytidine deaminase (AID), a novel member of the RNA-editing deaminase family in germinal center B cells. The Journal of biological chemistry *274*, 18470-18476.
- Neff, T., Sinha, A.U., Kluk, M.J., Zhu, N., Khattab, M.H., Stein, L., Xie, H., Orkin, S.H., and Armstrong, S.A. (2012). Polycomb repressive complex 2 is required for MLL-AF9 leukemia. Proceedings of the National Academy of Sciences of the United States of America *109*, 5028-5033.
- Nikoloski, G., Langemeijer, S.M., Kuiper, R.P., Knops, R., Massop, M., Tonnissen, E.R., van der Heijden, A., Scheele, T.N., Vandenberghe, P., de Witte, T.*, et al.* (2010). Somatic mutations of the histone methyltransferase gene EZH2 in myelodysplastic syndromes. Nature genetics *42*, 665-667.
- Nolz, J.C., Gomez, T.S., and Billadeau, D.D. (2005). The Ezh2 methyltransferase complex: actin up in the cytosol. Trends in cell biology *15*, 514-517.
- Ntziachristos, P., Tsirigos, A., Van Vlierberghe, P., Nedjic, J., Trimarchi, T., Flaherty, M.S., Ferres-Marco, D., da Ros, V., Tang, Z., Siegle, J.*, et al.* (2012). Genetic inactivation of the polycomb repressive complex 2 in T cell acute lymphoblastic leukemia. Nature medicine *18*, 298-301.
- Oguro, H., Yuan, J., Ichikawa, H., Ikawa, T., Yamazaki, S., Kawamoto, H., Nakauchi, H., and Iwama, A. (2010). Poised lineage specification in multipotential hematopoietic stem and progenitor cells by the polycomb protein Bmi1. Cell stem cell *6*, 279-286.
- Okosun, J., Bodor, C., Wang, J., Araf, S., Yang, C.Y., Pan, C., Boller, S., Cittaro, D., Bozek, M., Iqbal, S.*, et al.* (2014). Integrated genomic analysis identifies recurrent mutations and evolution patterns driving the initiation and progression of follicular lymphoma. Nature genetics *46*, 176-181.
- Pasini, D., Bracken, A.P., Hansen, J.B., Capillo, M., and Helin, K. (2007). The polycomb group protein Suz12 is required for embryonic stem cell differentiation. Molecular and cellular biology *27*, 3769-3779.
- Pasini, D., Bracken, A.P., Jensen, M.R., Lazzerini Denchi, E., and Helin, K. (2004). Suz12 is essential for mouse development and for EZH2 histone methyltransferase activity. The EMBO journal *23*, 4061-4071.
- Pasini, D., Cloos, P.A., Walfridsson, J., Olsson, L., Bukowski, J.P., Johansen, J.V., Bak, M., Tommerup, N., Rappsilber, J., and Helin, K. (2010). JARID2 regulates binding of the Polycomb repressive complex 2 to target genes in ES cells. Nature *464*, 306-310.

- Pasqualucci, L., Bhagat, G., Jankovic, M., Compagno, M., Smith, P., Muramatsu, M., Honjo, T., Morse, H.C., 3rd, Nussenzweig, M.C., and Dalla-Favera, R. (2008). AID is required for germinal center-derived lymphomagenesis. Nature genetics *40*, 108-112.
- Pasqualucci, L., Khiabanian, H., Fangazio, M., Vasishtha, M., Messina, M., Holmes, A.B., Ouillette, P., Trifonov, V., Rossi, D., Tabbo, F.*, et al.* (2014). Genetics of follicular lymphoma transformation. Cell reports *6*, 130-140.
- Peitz, M., Pfannkuche, K., Rajewsky, K., and Edenhofer, F. (2002). Ability of the hydrophobic FGF and basic TAT peptides to promote cellular uptake of recombinant Cre recombinase: a tool for efficient genetic engineering of mammalian genomes. Proceedings of the National Academy of Sciences of the United States of America *99*, 4489-4494.
- Peng, J.C., Valouev, A., Swigut, T., Zhang, J., Zhao, Y., Sidow, A., and Wysocka, J. (2009). Jarid2/Jumonji coordinates control of PRC2 enzymatic activity and target gene occupancy in pluripotent cells. Cell *139*, 1290-1302.
- Peters, A.H., Kubicek, S., Mechtler, K., O'Sullivan, R.J., Derijck, A.A., Perez-Burgos, L., Kohlmaier, A., Opravil, S., Tachibana, M., Shinkai, Y.*, et al.* (2003). Partitioning and plasticity of repressive histone methylation states in mammalian chromatin. Molecular cell *12*, 1577-1589.
- Piunti, A., Rossi, A., Cerutti, A., Albert, M., Jammula, S., Scelfo, A., Cedrone, L., Fragola, G., Olsson, L., Koseki, H.*, et al.* (2014). Polycomb proteins control proliferation and transformation independently of cell cycle checkpoints by regulating DNA replication. Nature communications *5*, 3649.
- Plath, K., Fang, J., Mlynarczyk-Evans, S.K., Cao, R., Worringer, K.A., Wang, H., de la Cruz, C.C., Otte, A.P., Panning, B., and Zhang, Y. (2003). Role of histone H3 lysine 27 methylation in X inactivation. Science *300*, 131-135.
- Puppe, J., Drost, R., Liu, X., Joosse, S.A., Evers, B., Cornelissen-Steijger, P., Nederlof, P., Yu, Q., Jonkers, J., van Lohuizen, M., and Pietersen, A.M. (2009). BRCA1-deficient mammary tumor cells are dependent on EZH2 expression and sensitive to Polycomb Repressive Complex 2-inhibitor 3-deazaneplanocin A. Breast cancer research : BCR *11*, R63.
- Qi, W., Chan, H., Teng, L., Li, L., Chuai, S., Zhang, R., Zeng, J., Li, M., Fan, H., Lin, Y.*, et al.* (2012). Selective inhibition of Ezh2 by a small molecule inhibitor blocks tumor cells proliferation. Proceedings of the National Academy of Sciences of the United States of America *109*, 21360-21365.
- Rajewsky, K. (1996). Clonal selection and learning in the antibody system. Nature *381*, 751-758.
- Rea, S., Eisenhaber, F., O'Carroll, D., Strahl, B.D., Sun, Z.W., Schmid, M., Opravil, S., Mechtler, K., Ponting, C.P., Allis, C.D., and Jenuwein, T. (2000). Regulation of chromatin structure by site-specific histone H3 methyltransferases. Nature *406*, 593-599.
- Richon, V.M., Johnston, D., Sneeringer, C.J., Jin, L., Majer, C.R., Elliston, K., Jerva, L.F., Scott, M.P., and Copeland, R.A. (2011). Chemogenetic analysis of human protein methyltransferases. Chemical biology & drug design *78*, 199-210.
- Rinn, J.L., Kertesz, M., Wang, J.K., Squazzo, S.L., Xu, X., Brugmann, S.A., Goodnough, L.H., Helms, J.A., Farnham, P.J., Segal, E., and Chang, H.Y. (2007).

Functional demarcation of active and silent chromatin domains in human HOX loci by noncoding RNAs. Cell *129*, 1311-1323.

- Sander, S., Bullinger, L., Klapproth, K., Fiedler, K., Kestler, H.A., Barth, T.F., Moller, P., Stilgenbauer, S., Pollack, J.R., and Wirth, T. (2008). MYC stimulates EZH2 expression by repression of its negative regulator miR-26a. Blood *112*, 4202-4212.
- Sander, S., Calado, D.P., Srinivasan, L., Kochert, K., Zhang, B., Rosolowski, M., Rodig, S.J., Holzmann, K., Stilgenbauer, S., Siebert, R.*, et al.* (2012). Synergy between PI3K signaling and MYC in Burkitt lymphomagenesis. Cancer cell *22*, 167-179.
- Sasaki, M., Yamaguchi, J., Ikeda, H., Itatsu, K., and Nakanuma, Y. (2009). Polycomb group protein Bmi1 is overexpressed and essential in anchorage-independent colony formation, cell proliferation and repression of cellular senescence in cholangiocarcinoma: tissue and culture studies. Human pathology *40*, 1723-1730.
- Satijn, D.P., Hamer, K.M., den Blaauwen, J., and Otte, A.P. (2001). The polycomb group protein EED interacts with YY1, and both proteins induce neural tissue in Xenopus embryos. Molecular and cellular biology *21*, 1360-1369.
- Scelfo, A., Piunti, A., and Pasini, D. (2015). The controversial role of the Polycomb group proteins in transcription and cancer: how much do we not understand Polycomb proteins? The FEBS journal *282*, 1703-1722.
- Schmitt, C.A., McCurrach, M.E., de Stanchina, E., Wallace-Brodeur, R.R., and Lowe, S.W. (1999). INK4a/ARF mutations accelerate lymphomagenesis and promote chemoresistance by disabling p53. Genes & development *13*, 2670-2677.
- Schmitz, R., Ceribelli, M., Pittaluga, S., Wright, G., and Staudt, L.M. (2014). Oncogenic mechanisms in Burkitt lymphoma. Cold Spring Harbor perspectives in medicine *4*.
- Schmitz, R., Young, R.M., Ceribelli, M., Jhavar, S., Xiao, W., Zhang, M., Wright, G., Shaffer, A.L., Hodson, D.J., Buras, E.*, et al.* (2012). Burkitt lymphoma pathogenesis and therapeutic targets from structural and functional genomics. Nature *490*, 116-120.
- Schoeftner, S., Sengupta, A.K., Kubicek, S., Mechtler, K., Spahn, L., Koseki, H., Jenuwein, T., and Wutz, A. (2006). Recruitment of PRC1 function at the initiation of X inactivation independent of PRC2 and silencing. The EMBO journal *25*, 3110-3122.
- Schuettengruber, B., and Cavalli, G. (2009). Recruitment of polycomb group complexes and their role in the dynamic regulation of cell fate choice. Development *136*, 3531-3542.
- Schwartzentruber, J., Korshunov, A., Liu, X.Y., Jones, D.T., Pfaff, E., Jacob, K., Sturm, D., Fontebasso, A.M., Quang, D.A., Tonjes, M.*, et al.* (2012). Driver mutations in histone H3.3 and chromatin remodelling genes in paediatric glioblastoma. Nature *482*, 226-231.
- Schwickert, T.A., Lindquist, R.L., Shakhar, G., Livshits, G., Skokos, D., Kosco-Vilbois, M.H., Dustin, M.L., and Nussenzweig, M.C. (2007). In vivo imaging of germinal centres reveals a dynamic open structure. Nature *446*, 83-87.

- Shaffer, A.L., 3rd, Young, R.M., and Staudt, L.M. (2012). Pathogenesis of human B cell lymphomas. Annual review of immunology *30*, 565-610.
- Shao, Z., Raible, F., Mollaaghababa, R., Guyon, J.R., Wu, C.T., Bender, W., and Kingston, R.E. (1999). Stabilization of chromatin structure by PRC1, a Polycomb complex. Cell *98*, 37-46.
- Shen, L., Shao, N., Liu, X., and Nestler, E. (2014). ngs.plot: Quick mining and visualization of next-generation sequencing data by integrating genomic databases. BMC genomics *15*, 284.
- Shen, X., Kim, W., Fujiwara, Y., Simon, M.D., Liu, Y., Mysliwiec, M.R., Yuan, G.C., Lee, Y., and Orkin, S.H. (2009). Jumonji modulates polycomb activity and self-renewal versus differentiation of stem cells. Cell *139*, 1303-1314.
- Shen, X., Liu, Y., Hsu, Y.J., Fujiwara, Y., Kim, J., Mao, X., Yuan, G.C., and Orkin, S.H. (2008). EZH1 mediates methylation on histone H3 lysine 27 and complements EZH2 in maintaining stem cell identity and executing pluripotency. Molecular cell *32*, 491-502.
- Sherr, C.J. (2012). Ink4-Arf locus in cancer and aging. Wiley interdisciplinary reviews. Developmental biology *1*, 731-741.
- Shi, B., Liang, J., Yang, X., Wang, Y., Zhao, Y., Wu, H., Sun, L., Zhang, Y., Chen, Y., Li, R.*, et al.* (2007). Integration of estrogen and Wnt signaling circuits by the polycomb group protein EZH2 in breast cancer cells. Molecular and cellular biology *27*, 5105-5119.
- Simon, C., Chagraoui, J., Krosl, J., Gendron, P., Wilhelm, B., Lemieux, S., Boucher, G., Chagnon, P., Drouin, S., Lambert, R.*, et al.* (2012). A key role for EZH2 and associated genes in mouse and human adult T-cell acute leukemia. Genes & development *26*, 651-656.
- Simon, J.A., and Kingston, R.E. (2009). Mechanisms of polycomb gene silencing: knowns and unknowns. Nature reviews. Molecular cell biology *10*, 697-708.
- Sneeringer, C.J., Scott, M.P., Kuntz, K.W., Knutson, S.K., Pollock, R.M., Richon, V.M., and Copeland, R.A. (2010). Coordinated activities of wild-type plus mutant EZH2 drive tumor-associated hypertrimethylation of lysine 27 on histone H3 (H3K27) in human B-cell lymphomas. Proceedings of the National Academy of Sciences of the United States of America *107*, 20980-20985.
- Stevenson, F.K., Sahota, S.S., Ottensmeier, C.H., Zhu, D., Forconi, F., and Hamblin, T.J. (2001). The occurrence and significance of V gene mutations in B cell-derived human malignancy. Advances in cancer research *83*, 81-116.
- Stock, J.K., Giadrossi, S., Casanova, M., Brookes, E., Vidal, M., Koseki, H., Brockdorff, N., Fisher, A.G., and Pombo, A. (2007). Ring1-mediated ubiquitination of H2A restrains poised RNA polymerase II at bivalent genes in mouse ES cells. Nature cell biology *9*, 1428-1435.
- Su, I.H., Basavaraj, A., Krutchinsky, A.N., Hobert, O., Ullrich, A., Chait, B.T., and Tarakhovsky, A. (2003). Ezh2 controls B cell development through histone H3 methylation and Igh rearrangement. Nature immunology *4*, 124-131.
- Su, I.H., Dobenecker, M.W., Dickinson, E., Oser, M., Basavaraj, A., Marqueron, R., Viale, A., Reinberg, D., Wulfing, C., and Tarakhovsky, A. (2005). Polycomb group protein ezh2 controls actin polymerization and cell signaling. Cell *121*, 425-436.

- Sulli, G., Di Micco, R., and d'Adda di Fagagna, F. (2012). Crosstalk between chromatin state and DNA damage response in cellular senescence and cancer. Nature reviews. Cancer *12*, 709-720.
- Sungalee, S., Mamessier, E., Morgado, E., Gregoire, E., Brohawn, P.Z., Morehouse, C.A., Jouve, N., Monvoisin, C., Menard, C., Debroas, G.*, et al.* (2014). Germinal center reentries of BCL2-overexpressing B cells drive follicular lymphoma progression. The Journal of clinical investigation *124*, 5337-5351.
- Swigut, T., and Wysocka, J. (2007). H3K27 demethylases, at long last. Cell *131*, 29-32.
- Tan, J., Yang, X., Zhuang, L., Jiang, X., Chen, W., Lee, P.L., Karuturi, R.K., Tan, P.B., Liu, E.T., and Yu, Q. (2007). Pharmacologic disruption of Polycomb-repressive complex 2-mediated gene repression selectively induces apoptosis in cancer cells. Genes & development *21*, 1050-1063.
- Tarlinton, D.M., and Smith, K.G. (2000). Dissecting affinity maturation: a model explaining selection of antibody-forming cells and memory B cells in the germinal centre. Immunology today *21*, 436-441.
- Taub, R., Kirsch, I., Morton, C., Lenoir, G., Swan, D., Tronick, S., Aaronson, S., and Leder, P. (1982). Translocation of the c-myc gene into the immunoglobulin heavy chain locus in human Burkitt lymphoma and murine plasmacytoma cells. Proceedings of the National Academy of Sciences of the United States of America *79*, 7837-7841.
- Tovar, C., Rosinski, J., Filipovic, Z., Higgins, B., Kolinsky, K., Hilton, H., Zhao, X., Vu, B.T., Qing, W., Packman, K.*, et al.* (2006). Small-molecule MDM2 antagonists reveal aberrant p53 signaling in cancer: implications for therapy. Proceedings of the National Academy of Sciences of the United States of America *103*, 1888-1893.
- Trapnell, C., Pachter, L., and Salzberg, S.L. (2009). TopHat: discovering splice junctions with RNA-Seq. Bioinformatics *25*, 1105-1111.
- Trimarchi, J.M., Fairchild, B., Wen, J., and Lees, J.A. (2001). The E2F6 transcription factor is a component of the mammalian Bmi1-containing polycomb complex. Proceedings of the National Academy of Sciences of the United States of America *98*, 1519-1524.
- Trojer, P., and Reinberg, D. (2007). Facultative heterochromatin: is there a distinctive molecular signature? Molecular cell *28*, 1-13.
- Tsai, M.C., Manor, O., Wan, Y., Mosammaparast, N., Wang, J.K., Lan, F., Shi, Y., Segal, E., and Chang, H.Y. (2010). Long noncoding RNA as modular scaffold of histone modification complexes. Science *329*, 689-693.
- van den Heuvel, S., and Dyson, N.J. (2008). Conserved functions of the pRB and E2F families. Nature reviews. Molecular cell biology *9*, 713-724.
- van Kemenade, F.J., Raaphorst, F.M., Blokzijl, T., Fieret, E., Hamer, K.M., Satijn, D.P., Otte, A.P., and Meijer, C.J. (2001). Coexpression of BMI-1 and EZH2 polycomb-group proteins is associated with cycling cells and degree of malignancy in B-cell non-Hodgkin lymphoma. Blood *97*, 3896-3901.
- Varambally, S., Dhanasekaran, S.M., Zhou, M., Barrette, T.R., Kumar-Sinha, C., Sanda, M.G., Ghosh, D., Pienta, K.J., Sewalt, R.G., Otte, A.P.*, et al.* (2002). The polycomb group protein EZH2 is involved in progression of prostate cancer. Nature *419*, 624-629.

- Venneti, S., Garimella, M.T., Sullivan, L.M., Martinez, D., Huse, J.T., Heguy, A., Santi, M., Thompson, C.B., and Judkins, A.R. (2013). Evaluation of histone 3 lysine 27 trimethylation (H3K27me3) and enhancer of Zest 2 (EZH2) in pediatric glial and glioneuronal tumors shows decreased H3K27me3 in H3F3A K27M mutant glioblastomas. Brain pathology *23*, 558-564.
- Victora, G.D., Dominguez-Sola, D., Holmes, A.B., Deroubaix, S., Dalla-Favera, R., and Nussenzweig, M.C. (2012). Identification of human germinal center light and dark zone cells and their relationship to human B-cell lymphomas. Blood *120*, 2240-2248.
- Victora, G.D., Schwickert, T.A., Fooksman, D.R., Kamphorst, A.O., Meyer-Hermann, M., Dustin, M.L., and Nussenzweig, M.C. (2010). Germinal center dynamics revealed by multiphoton microscopy with a photoactivatable fluorescent reporter. Cell *143*, 592-605.
- Villa, R., Pasini, D., Gutierrez, A., Morey, L., Occhionorelli, M., Vire, E., Nomdedeu, J.F., Jenuwein, T., Pelicci, P.G., Minucci, S.*, et al.* (2007). Role of the polycomb repressive complex 2 in acute promyelocytic leukemia. Cancer cell *11*, 513-525.
- Volkel, P., Dupret, B., Le Bourhis, X., and Angrand, P.O. (2015). Diverse involvement of EZH2 in cancer epigenetics. American journal of translational research *7*, 175-193.
- Wagner, S.D., and Neuberger, M.S. (1996). Somatic hypermutation of immunoglobulin genes. Annual review of immunology *14*, 441-457.
- Walker, E., Chang, W.Y., Hunkapiller, J., Cagney, G., Garcha, K., Torchia, J., Krogan, N.J., Reiter, J.F., and Stanford, W.L. (2010). Polycomb-like 2 associates with PRC2 and regulates transcriptional networks during mouse embryonic stem cell self-renewal and differentiation. Cell stem cell *6*, 153-166.
- Wang, L., Jin, Q., Lee, J.E., Su, I.H., and Ge, K. (2010). Histone H3K27 methyltransferase Ezh2 represses Wnt genes to facilitate adipogenesis. Proceedings of the National Academy of Sciences of the United States of America *107*, 7317-7322.
- Wee, Z.N., Li, Z., Lee, P.L., Lee, S.T., Lim, Y.P., and Yu, Q. (2014). EZH2-mediated inactivation of IFN-gamma-JAK-STAT1 signaling is an effective therapeutic target in MYC-driven prostate cancer. Cell reports *8*, 204-216.
- Wilkinson, F.H., Park, K., and Atchison, M.L. (2006). Polycomb recruitment to DNA in vivo by the YY1 REPO domain. Proceedings of the National Academy of Sciences of the United States of America *103*, 19296-19301.
- Wilson, B.G., Wang, X., Shen, X., McKenna, E.S., Lemieux, M.E., Cho, Y.J., Koellhoffer, E.C., Pomeroy, S.L., Orkin, S.H., and Roberts, C.W. (2010). Epigenetic antagonism between polycomb and SWI/SNF complexes during oncogenic transformation. Cancer cell *18*, 316-328.
- Workman, P., Aboagye, E.O., Balkwill, F., Balmain, A., Bruder, G., Chaplin, D.J., Double, J.A., Everitt, J., Farningham, D.A., Glennie, M.J.*, et al.* (2010). Guidelines for the welfare and use of animals in cancer research. British journal of cancer *102*, 1555-1577.

- Wu, Z., Lee, S.T., Qiao, Y., Li, Z., Lee, P.L., Lee, Y.J., Jiang, X., Tan, J., Aau, M., Lim, C.Z., and Yu, Q. (2011). Polycomb protein EZH2 regulates cancer cell fate decision in response to DNA damage. Cell death and differentiation.
- Xie, Y., Pittaluga, S., and Jaffe, E.S. (2015). The histological classification of diffuse large B-cell lymphomas. Seminars in hematology *52*, 57-66.
- Xu, B., On, D.M., Ma, A., Parton, T., Konze, K.D., Pattenden, S.G., Allison, D.F., Cai, L., Rockowitz, S., Liu, S.*, et al.* (2015a). Selective inhibition of EZH2 and EZH1 enzymatic activity by a small molecule suppresses MLL-rearranged leukemia. Blood *125*, 346-357.
- Xu, J., Shao, Z., Li, D., Xie, H., Kim, W., Huang, J., Taylor, J.E., Pinello, L., Glass, K., Jaffe, J.D.*, et al.* (2015b). Developmental control of polycomb subunit composition by GATA factors mediates a switch to non-canonical functions. Molecular cell *57*, 304-316.
- Xu, K., Wu, Z.J., Groner, A.C., He, H.H., Cai, C., Lis, R.T., Wu, X., Stack, E.C., Loda, M., Liu, T.*, et al.* (2012). EZH2 oncogenic activity in castration-resistant prostate cancer cells is Polycomb-independent. Science *338*, 1465-1469.
- Yamaguchi, H., and Hung, M.C. (2014). Regulation and Role of EZH2 in Cancer. Cancer research and treatment : official journal of Korean Cancer Association *46*, 209-222.
- Yan, J., Ng, S.B., Tay, J.L., Lin, B., Koh, T.L., Tan, J., Selvarajan, V., Liu, S.C., Bi, C., Wang, S.*, et al.* (2013). EZH2 overexpression in natural killer/T-cell lymphoma confers growth advantage independently of histone methyltransferase activity. Blood *121*, 4512-4520.
- Yang, X., Karuturi, R.K., Sun, F., Aau, M., Yu, K., Shao, R., Miller, L.D., Tan, P.B., and Yu, Q. (2009). CDKN1C (p57) is a direct target of EZH2 and suppressed by multiple epigenetic mechanisms in breast cancer cells. PloS one *4*, e5011.
- Yap, D.B., Chu, J., Berg, T., Schapira, M., Cheng, S.W., Moradian, A., Morin, R.D., Mungall, A.J., Meissner, B., Boyle, M.*, et al.* (2011). Somatic mutations at EZH2 Y641 act dominantly through a mechanism of selectively altered PRC2 catalytic activity, to increase H3K27 trimethylation. Blood *117*, 2451-2459.
- Yap, K.L., Li, S., Munoz-Cabello, A.M., Raguz, S., Zeng, L., Mujtaba, S., Gil, J., Walsh, M.J., and Zhou, M.M. (2010). Molecular interplay of the noncoding RNA ANRIL and methylated histone H3 lysine 27 by polycomb CBX7 in transcriptional silencing of INK4a. Molecular cell *38*, 662-674.
- Zee, B.M., Levin, R.S., Xu, B., LeRoy, G., Wingreen, N.S., and Garcia, B.A. (2010). In vivo residue-specific histone methylation dynamics. The Journal of biological chemistry *285*, 3341-3350.
- Zhang, X., Zhao, X., Fiskus, W., Lin, J., Lwin, T., Rao, R., Zhang, Y., Chan, J.C., Fu, K., Marquez, V.E.*, et al.* (2012). Coordinated silencing of MYC-mediated miR-29 by HDAC3 and EZH2 as a therapeutic target of histone modification in aggressive B-Cell lymphomas. Cancer cell *22*, 506-523.
- Zhang, Y., Liu, T., Meyer, C.A., Eeckhoute, J., Johnson, D.S., Bernstein, B.E., Nusbaum, C., Myers, R.M., Brown, M., Li, W., and Liu, X.S. (2008). Model-based analysis of ChIP-Seq (MACS). Genome biology *9*, R137.

Acknowledgments

This work has been possible thanks to the collaboration of many people. First, I would like to thank my supervisor Stefano Casola, who gave me the opportunity to join his lab and to run this challenging, but interesting project. His mentorship contributed to my professional and personal growth and to develop critical thinking skills for the evaluation of my project.

I would also like to show my gratitude to all SCA's members, current and past members, for scientific discussions and suggestions and for their help in the everyday life in the lab.

A special thank to Gabriele Varano. I was incredibly lucky to share with him this project. He is always available for scientific advices and personal support.

I am grateful to all collaborators, which contribute to this work, providing precious reagents and helpful discussions.

I am also thankful to all IFOM facilities, which support our research, making each experiment easier to manage and providing their technical expertise.

An important thank to Lara Sicouri and Valentina Buttiglione, who started with me the PhD 4 years ago and are always by my side, sharing not only joyful moments, but also the difficult moments of this experience.

I would like to thank my friends for being with me even from different places. They have been always updated to my professional adventure and available to spend time for long and supportive discussions.

I kindly thank my family, which always believe in me and support my passion for the research. They are my strength and I am always grateful to them for what they do for me.

The most important thank to Antonio, who encouraged me to start this experience, pushing me to desire and do the best for myself. He was patient during stressful periods, supportive during moments of fragility and happy, during successful events.